Diss. ETH No. 19385

On Security and Economy Enhancements in Power Systems by Decision Support

A dissertation submitted to the
ETH Zürich

for the degree of
Doctor of Sciences ETH Zürich

presented by
MARIJA ZIMA-BOČKARJOVA
Master of Science, Riga Technical University
born January 17th, 1978
citizen of Latvia

accepted on the recommendation of
Prof. Dr. Göran Andersson, examiner
Prof. Dr. Ali Abur, co-examiner

2010

Acknowledgments

I would like sincerely thank prof. Göran Andersson for creating an outstanding opportunity for me to join his group, first as a guest researcher and later as a PhD student. I am very grateful for the guidance, support and encouragement of researchers' individuality and maturity. In these years, I met not only enriching and encouraging research atmosphere, but also many friends.

I would like to thank prof. Ali Abur for accepting to co-examining this thesis and very valuable comments.

I highly acknowledge ABB contribution to this work. Apart from financial support of the research I have received many precious inputs and valuable practical insights. I would like especially thank Mats Larsson, Ernst Sholtz, Reynaldo Nuqui, Magnus Johansson, Inger Segerquist for all the inputs and discussions. I would like to thank also John Finney and Otto Preis, who recognized potential behind the topic of state estimation, which sometimes referred as "classical" and trusted with the work on it.

My gratitude to Swiss Federal Scholarship Commission for Scholarships for Foreign Students, with this support I could come to ETH Zürich as a guest researcher that, eventually, encouraged me for the further work with the group. I thank Elizabeth Schniderlin for the first introduction to Swiss culture and help.

Collaboration with my oldest friend Julija Matevosyan and prof. Lennart Söder on wind-hydro operation planning was another sparkle for me during these years. It was not only a new and very fun topic of hydro systems and stochastic programming, but also scientific argues, creative brainstorming and the results - all I greatly enjoyed. I would like to

Abstract

Modern power system is a complex interaction of various actors in an established (market) framework. Nowadays, power system experiences an increasing pressure to improved efficiency and asset utilization, preserving security at least existing level as the life of the present society is almost unimaginable without electric power supply.

Information and the control means available to the actors have changed in past decades. In overall, they are now exposed to higher uncertainty. On the other hand, consequences of the uninformed actions may be dramatic and frequently, particularly in the power system operation, affecting not only decision maker, but also other entities.

New technology, faster high-bandwidth communications, more computational power and development of the mathematical methods adjusted to present conditions shall support entities, which are involved in power system planning, operation, control and also use, to make better decisions in term of economical and secure exploitation. A vision of contribution to the development of such decision tools motivated the work presented in this thesis. Although the most parts of the thesis consider problems faced by the TSO both in real time and offline analysis, for except the last chapter dealing with the planning of operation and bidding by a power producer, it is almost indisputable that any entity could improve their decisions with the right tools.

Present thesis addresses several sample problems and proposes new approaches that shall either better quantify, diminish uncertainties involved in power system operation or suggest a robust decision. Extended mathematical models of the processes and suitable methods are essential for this development.

All the proposals are supported by the illustrative examples and numerical simulations. The advantages and practicality of the proposed techniques support an optimism of the author that this work contributes to power systems research and, thus, to another step towards enhancement of the security and economy.

Kurzfassung

Das moderne Übertragungsnetz weist komplexe Zusammenhänge und Beziehungen zwischen den Teilnehmern im etablierten Rahmen der Strommärkte auf. Übertragungsnetze sind heute mit dem steigenden Druck konfrontiert den Nutzungsgrad von Anlagen zu verbessern und gleichzeitig Versorgungssicherheit zu gewährleisten, da das Leben der modernen Gesellschaft ohne Stromversorgung nicht vorstellbar ist.

Die den Teilnehmern verfügbaren Informationen und Steuerungsmöglichkeiten haben sich in den letzten Dekaden verändert, jedoch die Informationen sind mit höheren Unsicherheiten belastet. Anderseits können ohne Informationen getroffene Entscheidungen dramatische Folgen haben, die auch andere Teilnehmer betreffen, vor allem im Systembetrieb.

Die in der Systembetrieb, die Systemplanung und Regelung involvierten Teilnehmer sollten von neuen Technologien, schnelleren Kommunikationssystemen, höheren Rechnerleistungen und der Entwicklung von mathematischen Methoden sowohl für technische wie auch wirtschaftliche Fragestellungen unterstützt werden. Die Entwicklung der "decision support tools" in diesem Kontext war die Motivation für diese Dissertation. Obwohl sich die Dissertation auf die Probleme von Übertragungsnetzbetreibern konzentriert (mit der Ausnahme der letzten Kapitel, wo das Interesse eines Erzeugers oder Händlers im Vordergrund steht), können auch andere Teilnehmer von der erforschten Methodik für "decision support tools" profitieren.

Die Dissertation präsentiert ausgewählte Probleme und schlägt neue Ansätze für Quantifizierung und Minderung der Unsicherheiten und Methodik für robuste Entscheidungen vor. Die Erweiterung von mathematischen Modellen und Methoden sind für diese Entwicklung zentral.

Alle entwickelten Konzepte und Ansätze werden auch anhand von Beispielen erläutert, und es kann gezeigt werden, dass die vorgeschlagenen Methoden messbaren Nutzen bringen und praktisch umsetzbar sind. Die Autorin hofft, dass diese Dissertation einen nützlichen Beitrag zur Forschung im Bereich der Übertragungsnetze und Systeme und insbesondere Verbesserung der Wirtschaftlichkeit und Sicherheit leistet.

Contents

Notation

AC	Alternative Current
ACSR	Aluminum Conductor, Steel Reinforced
BG	Balancing Group
CIM	Common Information Model
DC	Direct Current
DSO	Distribution System Operator
EMS	Energy Management System
GPS	Global Positioning System
HE	an Hour Equivalent is a water flow $1m^3/s$ for 1 hour or $3600m^3$
HPP	Hydro Power Plant
HVDC	High Voltage Direct Current (transmission)
IEEE	Institute of Electrical and Electronics Engineers
ISO	Independent System Operator
IEC	International Electrotechnical Commission
LMS	Least Median of Squares (estimator)
nrv	normal random variable
OTC	Over the Counter
OMU	Optical Measurement Unit
PMU	Phasor Measurement Unit
pdf	Probability Density Function
RTU	Remote Terminal Unit
RMS	Root Mean Square
SCADA	Supervisory Control and Data Acquisition
SE	State Estimation
TSO	Transmission System Operator
WF	Wind farm
WLAV	Weighted Least Absolute Value (estimator)
WLS	Weighted Least Square (estimator)

The notation used throughout the thesis is listed below for a quick reference.

in Chapter 6, Influence of Topology

Sets, Graphs, Matrices

$G(\mathcal{N}, \mathcal{E})$	network graph
$G_{\setminus We}$	network graph excluding W_e
$\mathcal{E}$	set of edges
$\mathcal{N}$	set of nodes
$\mathcal{N}_e$	set of erroneous nodes
$\mathcal{N}_{PMU}$	set of verified PMU path nodes
$\mathcal{N}_T$	terminal, i.e. start and end nodes of a path
$\mathcal{V}_N(V, N_V)$	set of pairs - voltage and visitors of node N
$\mathcal{V}$	set of $\mathcal{V}_N$
$\mathcal{V}_{F\mathcal{N}e}$	forward profile of the voltages in $\mathcal{N}_e$
$\mathcal{V}_{B\mathcal{N}e}$	backward profile of the voltages in $\mathcal{N}_e$
$C(\mathcal{N}, \mathcal{E})$	a simple cycle
$P(\mathcal{N}, \mathcal{E})$	a simple path
$P_a(\mathcal{N}_a, \mathcal{E}_a)$	an alternative path
$P_{PMU}(\mathcal{N}_{PMU}, \mathcal{E}_{PMU})$	an PMU path
$W(\mathcal{N}, \mathcal{E})$	a walk
$W_e(\mathcal{N}_e, \mathcal{E}_e)$	an erroneous walk
$P_W(\mathcal{N}_W, \mathcal{E}_W)$	withhold path
e	vector of edges' labels
$\mathbb{R}$	real numbers
$\mathbb{C}$	complex numbers

Indices, Superscripts

i, j, n	number of the set element
$\square^{(k)}$	variable at k-th iteration
$\square^{(k+)}$	changed variable at k-th iteration
$\square_{\cdot, k}$	k-th value of a set
$\square$	complex variable

Constants

C^N number of nodes in the network

Variables

k	iteration number
$V_{N,k}$	k-th value of voltage assigned to node N
$V_N(M)$	value of voltage assigned to node N by visitor M
V_N^{PMU}	voltage measurement in node N

Functions, Operation

$\lvert \cdot \rvert$	Cardinality of a some set
$\lvert \cdot \rvert_1$	First or Euclidian norm
$\star$	cross correlation operator
$\deg(N)$	degree of node (vertex) N
$\otimes$	bit-wise multiplication, operation "and"
$\oplus$	bit-wise addition, operation "or"
$\setminus$	set substraction
$\cup$	union of sets
$\cap$	intersection of sets
$\subseteq$	subset
$\subsetneq$	proper subset
$\varnothing$	empty set
$\downarrow$	adjacency
$N_{Gk}(\cdot)$	set of open k-degree neighbors
$N_{Gk}[\cdot]$	set of closed k-degree neighbours
$I(\cdot)$	set of elements corresponding to indexes of nonzero entries in a binary vetor
$A(\cdot)$	edges adjacent to the node
$N_T(W)$	extract terminal node of a walk
$N_s(W)$	extract start node of a walk
$N_f(W)$	extract end node of a walk
$max(\cdot)$	maximal value of a set
$\{\cdot\}$	a set
$(\cdot)$	a sequence

Special Nodes (Vertices)

N_c	conflict node
N_V	visitor
N_s	start node of a walk
N_f	end node of a walk

in Chapter 7, Slow Model Variations

Functions

A'	projected area of conductor, ft^2 per lineal ft
D	conductor diameter, in
H_c	altitude of the sun, deg
H_e	elevation of conductor above the sea level, ft
I	line currents, A
k_f	air thermal conductivity coefficient, W/ft
K_ϕ	coefficient in convection heat computation
q_c	the heat losses due to convection, W
q_r	the heat losses due to radiation, W
q_s	the solar heat gain, W
Q_s	total solar and sky radiated heat flux, W/ft^2
R_{T_c}	resistance per lineal foot of conductor at T_c, Ω/ft
R_{ac}	conductor resistance to AC current, Ω
R_{dc}	conductor resistance to DC current, Ω
T_a	ambient temperature, $°C$
T_{film}	air film temperature, $°C$
T_c	conductor temperature, $°C$
V_w	velocity of the air stream, ft/h
Z_c	azimuth, deg
Z_l	azimuth of line , deg
α	solar absorptivity
α_a	the temperature coefficient for aluminium, C^{-1}
ϵ	emissivity
θ	coefficient in solar heat gain computation
μ_f	absolute viscosity of air, $lb/(ft \cdot h)$
ϕ	angle between conductor axis and the air stream, deg
ρ_f	air density, lb/ft^3

in Chapter 8, Performance During Transients

Functions

f	differential equations
g	algebraic equations
h	matrix
h_s	measurement function
J	objective function

Variables

o	observation, measurement
t	time
x	differential state variables
y	algebraic state variables
v	bus voltage angles and magnitudes
$\hat{v}$	estimated voltage variables
y_d	auxiliary variables defining changes in g
y_e	auxiliary variables defining switching of the z
z	discrete state variables
x^- , y^-, z^-	state variables prior to the event
x^+ , y^+, z^+	state variables after the event
x_0, y_0, z_0	value at the initial time instant

Constants

a	contingency scenario
A_{sc}	number of scenarios
b	upgrade candidate
λ_0	initial parameters
λ	parameters
d	number of structural changes
e	number of switchings of discrete variables
m	dimensions of the algebraic states
l	dimensions of parameters space

k	dimensions of discrete states
n	dimensions of dynamic states
T	considered time interval
C_{budget}	upgrade budget
S	measurement number

Sets, Vectors

B	set of candidate upgrades
C	upgrade cost
D	matrix
E	matrix
L	set of parameters
U	binary decision vector for optimal upgrades
X	set of dynamic state variables
Y	set of algebraic states
Z	set of discrete states
$\mathbf{R}$	space of real numbers
W_s	measurement weights
W_{sc}	scenario weights

in Chapter 9, Allocation in Game Theory

$\mathcal{A}$	set of all players
$\phi_l(c)$	profit share of the entity l, Shapley value, EUR
c	coalition profit, EUR
C	subset of players
l	considered player
$n_{\mathcal{A}}$	number of players
n_C	cardinality of subset C

in Chapter 10, Allocation of Losses

In addition to notation from Chapter 9:

$\mathbb{C}_{n_C}^{n_{\mathcal{A}}}$	combination of n_C from $n_{\mathcal{A}}$
Δc_l	incremental costs
P_{loss}	network loss
N_G	set of generation busses
N_D	set of demand busses

Pf_l penalty factor for demand l
P_{Gg} power injection in the generation bus g
P_{Dd} power injection in the demand bus d

in Chapter 11, Operation Planning

Terms of the objective function and constraints

g_h^{hb}	hydraulical balance constraints, HE
g_h^{rt}	targets of the hydro reservoirs' content, HE
g_w^{imb}	wind imbalance equality constraints, MW
h_h^d	discharge limitations, HE
h_h^{rl}	hydro reservoir constraints, HE
h_w^{imb}	wind imbalance inequality constraints, MW
h_h^t	transmission capacity constraints for the uncoordinated hydro, MW
h_{h+w}^t	coalition transmission capacity constraints, MW
h_w^t	transmission capacity constraints for the uncoordinated wind, MW
z_h^s	profit from the hydro production accepted at the spot, EUR
z_w^s	profit from the wind production accepted at the spot, EUR
z_w^{imb}	profit from the wind imbalance, EUR

Sets

Ω_i	index set of HPPs upstream from plant i
$\mathcal{A}$	all the entities
C	formed coalition
I	index set of HPPs
K	hours of the total planning horizon
K^{day}	hours of the next planning day
M	set of wind scenarios
N	set of price scenarios
S_i	index set of units at HPP i

Indices, Superscripts

i	hydro power plant
j	hydro power plant directly upstream from i
k	hour
l	entity joining the coalition
m	wind scenario
n	price scenario
s	hydro unit at power plant
$\Box^{imb}$	imbalance related quantity
$\Box^{s}$	spot related quantity
$\Box^{sc}$	quantity related to realized scenario
$\Box_{h}$	hydro related quantity
$\Box_{is}$	unit s, plant i related quantity
$\Box_{w}$	wind related quantity

Variables

$\phi_l(c)$	profit share of the entity l, Shapley value, EUR
b	continuous variable
c	coalition profit, EUR
c^s	spot price, EUR
c_{pos}^{imb}	overproduction price, EUR
c_{neg}^{imb}	underproduction price, EUR
P_w^s	production of wind submitted to spot, MW
$\bar{P}_w^{sc}$	power equivalent of available wind, MW
P_w^{sc}	actual power production of wind, MW
P_{is}^s	production of hydro unit submitted to spot, MW
P_{is}^{sc}	actual production of hydro unit, MW
u_{is}	water discharge from unit s, plant i, HE
x_i	reservoir content of i-th HPP, HE
y_i	water spillage from plant i, HE

Constants

p	success probability of a price scenario
q	success probability of a wind scenario

μ_{is}	production equivalent of unit s HPP i, MWh/HE
τ_{ij}	time delay for water inflow from HPP j
	and the reservoir downstream i
n_C	number of entities in coalition C
$n_{\mathcal{A}}$	number of entities
$\bar{P}_{12}$	capacity of transmission corridor , MW
P_{av}	power equivalent of monthly average
	available wind, MW
$\bar{P}_w$	installed capacity of wind farm, MW
$\bar{u}_{is}$	maximal water discharge from unit s, plant i, HE
$\bar{x}_i$	maximum reservoir content, HE
x_i^o	initial reservoir content of i-th HPP, HE
x_i^{last}	final reservoir content of i-th HPP, HE
w_i	water inflow into the reservoir i
D	large number

Introduction

Chapter 1

Positioning of the Work

This chapter briefly reviews modern power system, its actors and oper-
ation. The relevance of the work described in this dissertation is also
discussed.

1.1 The Playground:
Power System and Electricity Market

1.1.1 Actors

The purpose of power systems is to supply electric energy to consumers,
i.e. industry, commercial and residential entities. Nowadays, electricity
supply typically involves interactions among the following entities (or
actors):

- Consumers

- Producers

- Traders

- System Operator

- Distribution System Operator

- Regulator

- Nature[1].

A brief description of the role of each market participant is provided below [63]:

Consumers use and pay separately for the electric energy, balancing energy, transmission and distribution network usage, losses and network security (the ancillary services - control and reactive power, which are necessary for system operator to maintain quality and security of the supply) or alternatively, an all inclusive tariff.

Producers offer and provide energy and the ancillary services. From the organizational prospective, producer can own or share an ownership of a single power plant or the portfolio of several plants.

Traders purchase and sell electricity products and transmission capacities. One could distinguish between *wholesale* and *retail* trading activities based on the customer and targeted market type.

System Operator comprises two entities, which can also be separated:

- Market Operator provides trading platform, clearing services and settlements for the ahead of real-time markets.

- Independent System Operator (ISO) is responsible for the power system security, including load and generation balancing in real time and balance settlements.

A transmission company owns the transmission assets and operates those in accordance with the instructions from ISO. If the ownership and the operation responsibility are merged in one entity, it is referred to as transmission system operator (TSO).

For the simplification and, since that is a more common organization in Europe, let us further address the TSO tasks. Let us structure the tasks of the TSO by the time scale:

- short-term planning: verifies system state, confirms unit commitment, by necessity employing congestion management schemes, acquires ancillary services

- real-time operation: employs ancillary services to keep the balance and preserve security of the system, congestion management, resistance. Following the operation - settlements.

---

[1]this is a standard term in game theory, see an explanation later in this section

- long-term planning: grants access to network in a non- discriminatory way, ensuring economy and reliability of the system

The TSO bears responsibility for open network access and system security. In *short-term* planning, TSO receives production schedules from the market participants and checks the forecasted system state. If the market situation results in congestion, then the TSO applies an approved congestion management scheme. Besides, TSO carries out cross border capacity auctions and coordinates the system operation and development with the other interconnected TSOs, both in real-time and planning stages. Based on the balancing group schedules, in-post operation TSO also determines the imbalances.

To assure its independent role, TSO is not allowed to own any generation. However, TSO must have access to the control resources provided by generators that are necessary for a secure system operation. In the network operation planning stage, when there is a sufficient time to act typically from several hours to days, TSOs use market based mechanisms for the acquisition of these ancillary services, which by necessity should be able to activate in *real-time*. In emergency situations, if the system security is violated and the time to act is typically in the order of minutes, TSO has a legal right to interfere into the generators' production.

In long-term planning, TSO evaluates the adequacy and reliability of the network and the control reserves as well as conducts necessary measures.

The transmission capacity is allocated to the existing market participants. When a new market participant requests network access, the TSO shall issue the requirements to be fulfilled that may include the necessity for the grid reinforcements to avoid frequent congestion. Although, there are no uniformly accepted rules among all the systems for the reinforcement cost allocation, it is likely that the new producer will have to accept one of the following options:

- bearing costs of the reinforcements,

- reduction of the generation capacity to be installed.

There are several possible approaches to asset developments in long-term, when it is not related to particular new player. These approaches can be divided into cost- and value-based expansion.

Distribution System Operator usually owns the distribution network. It bears responsibility for the operation, planning and maintenance of the assets. The sale of the energy to the consumers shall be fully decoupled from these activities, yet frequently, retail division can be a subsidiary of the distribution company.

Regulator ensures through the regulatory framework fair competition and efficient electricity market, economy, environmental friendliness, quality and reliability of the supply.

Nature denotes an impersonal background, which does not follow any particular objective, yet influences the actions of all the players. Some examples of the nature's impacts are weather, outages of the equipment, unintentional mistakes of personnel.

Every actor, except, perhaps, nature is trying to maximize his utility (e.g. profit). In order to achieve their objective, they have to make decisions in changing conditions and with incomplete information.

1.1.2   The Products

The most laconic summary of the electricity markets specifics, to my opinion, is the following: *"... electrical energy is inextricably linked with a physical system that functions faster than any market"* [63].

These specifics can be translated in commonly mentioned properties, such as non-storability of electricity, necessity for exact matching of supply and demand at all times, non-tractability of the transactions etc. It reflects subsequently in different types of the traded products, as in Fig. 1.1.

Forward market products can be classified in the physical delivery products or forwards, and financial products, such as futures and options. Financial products are mostly used for risk management.

Spot day-ahead market takes place day ahead of the actual day of the electricity delivery. It usually takes the form of a pool or exchange. This means that all following activities take place day ahead: market actors submit their bid in the morning, the spot market clearing entity clears the market, i.e. determines which bids are accepted based on the merit-order principle and informs market actors, which bids were accepted and which are rejected.

Intra-day market is usually based on bilateral agreements.
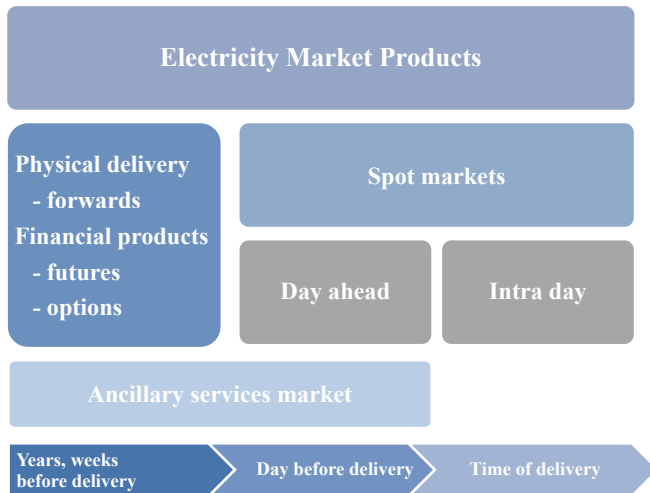
Figure 1.1: Categories of the electricity market and products.

The ancillary services, which are necessary for the TSO to maintain systems security include:

- primary frequency control

- secondary frequency control

- tertiary frequency control

- voltage control

- active power losses coverage

- blackstart capability.

A typical market mechanism for provision of an ancillary service is tender for a longer time period, e.g. one month. A comprehensive overview of ancillary services is given in [103].

1.1.3   Settlements and Allocation

Another specific of the electricity market, which requires centralized settlement system is: *"..electric energy cannot be directed to a specific customer"* [63].

The financial settlements between the market participants include two major components: energy and transportation.

Energy settlements

The **energy** settlements conditions are part of the bilateral contracts. At the spot market, the market operator usually forwards payments between the buyers and sellers. However, settlements for the balancing energy are more complex, and require computations by the central entity.

Balancing energy settlements cover secondary and tertiary control energy, while primary control is accounted only per available power. The balancing rules as follows might be not fully precise for the particular market, but yet reflects general principles common to many markets. The TSO keeps the control reserves and when needed, activates them. If a control zone is "short"[2], the TSO activates positive control reserves to produce missing energy. When a control zone is "long", the TSO activates negative control reserves, i.e. reduces production of generators providing control reserves. Use of the control reserves implies financial costs for the TSO. These costs are allocated to the consumers and producers causing the imbalances.

All the consumers and producers are structured in the balance groups in order to simplify registering of the schedules to TSO and billing of real time balancing. Balance groups are pure billing/accounting units without any geographical correlation except belonging to same control zone, frequently meaning same country. They register day ahead the aggregated schedules to the TSO (i.e. not the schedules of individual consumers or producers) which should reflect balance between produced and consumed energy inside of the group, plus imported and exported energy of of the group.

The TSO determines the deviations by comparing metering data depicting actual production or consumption with the schedules. Metering

---

[2]A control zone (system) or a market actor is said to be "short", if it lacks energy as compared to the prediction. If it has an excess of energy, it is said to be "long".
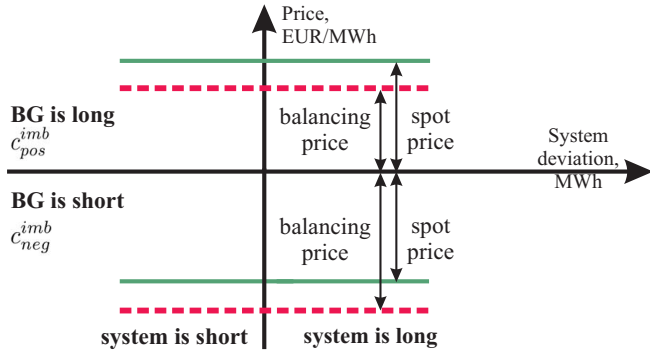
Figure 1.2: Balancing energy payment scheme from the perspective of a power producer.

devices measure energy without distinguishing how this energy was redistributed during the time interval of the measurement, which is usually 15 minutes, or one hour, depending on the power system. Note that from the perspective of a producer or a consumer, only energy deviations are penalized, while the instantaneous power deviations are not.

Let us consider this principle from the balance group point of view, which comprises several producers and consumers. The payment scheme is shown in Fig. 1.2. If this balance group is short, it receives balancing energy. The cost of this balancing energy should be higher than a spot price, so that the balance group would be penalized for its imbalance and would have an incentive to make more accurate predictions. Similarly, if a balance group is long, it "overproduces" energy. This energy is "bought" by the TSO, however, for a lower price than the spot price, so the balance group would again have an incentive for a better prediction. Therefore, this can be seen as a penalization: if the balance group would predict its produced energy better, it could sell it to the spot market for a full spot market price.

The mechanism or rules for the balancing energy cost sharing within the balancing group is an internal policy of that balancing group.
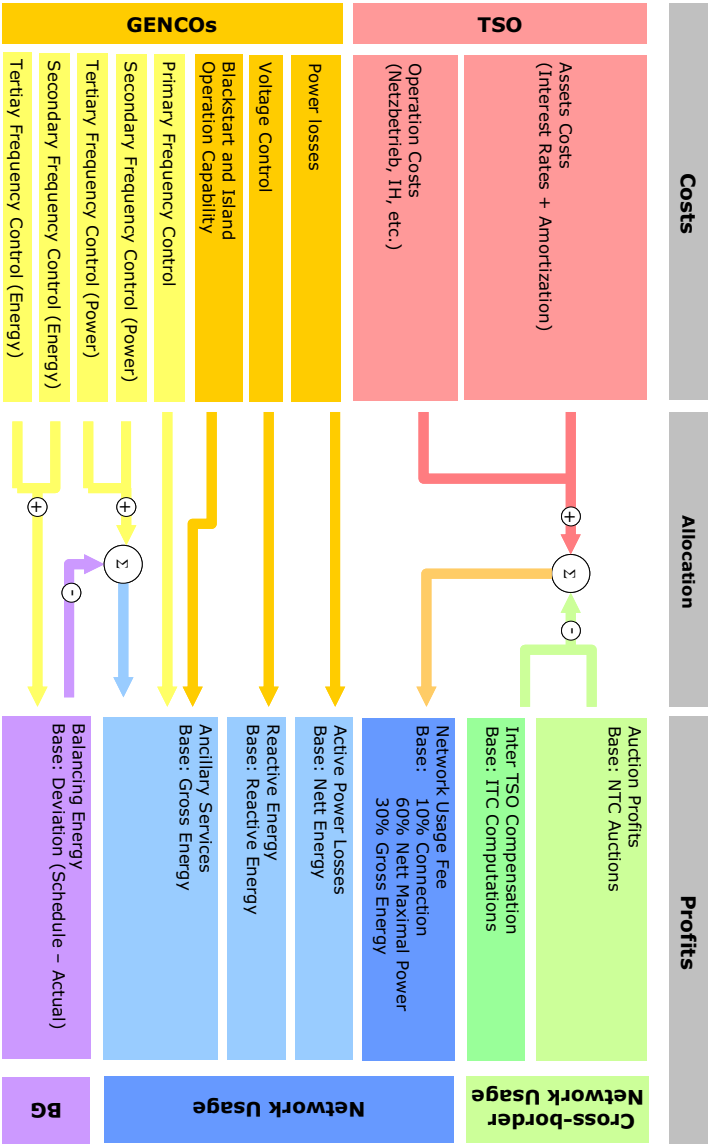
Figure 1.3: Financial balance of the TSO [145]
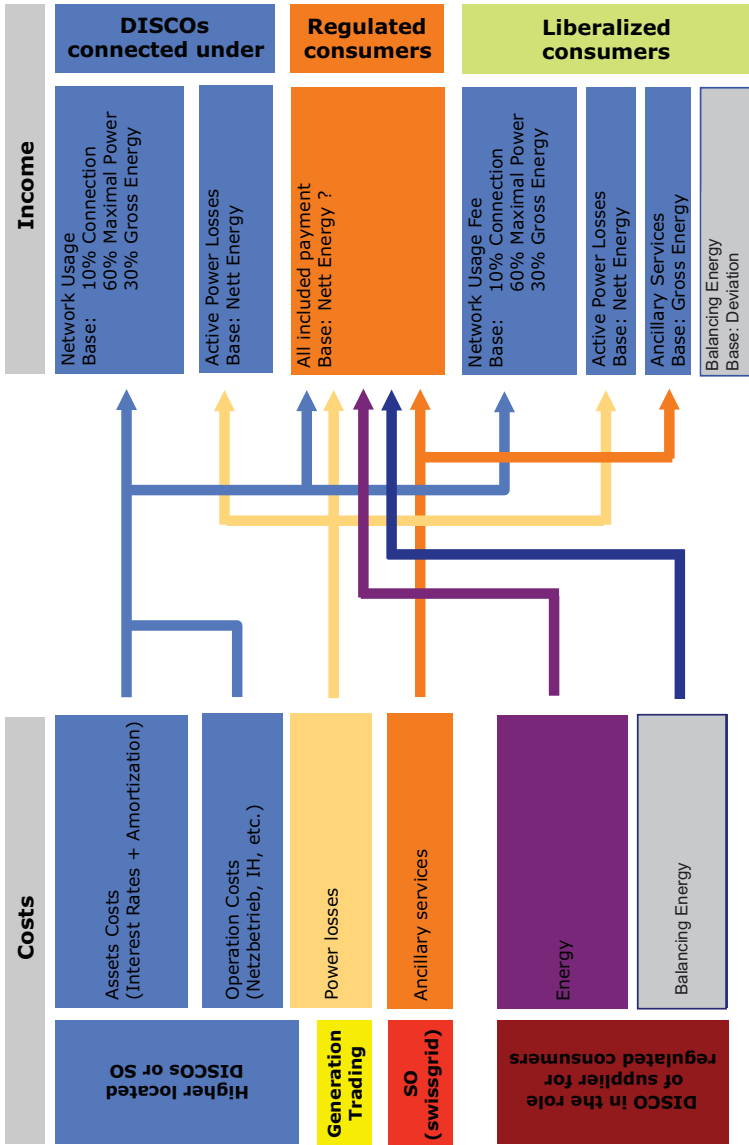
Figure 1.4: Financial balance of the DSO.

Transportation

The transportation or delivery **network** costs and income structure is shown for the TSO and DSO in Fig. 1.3 and Fig. 1.4.

For the consumer, the tariff most commonly is charged proportionally to the consumed energy and includes three components:

- Network usage

- Losses

- Ancillary services fee

Ancillary services fee covers costs related to keeping transmission system security at desired level. This fee does not include balancing energy costs, which are accounted for in energy settlements.

For the network usage, in Switzerland, similarly to other European countries, so called "post stamp" model has been adopted. As the network structure is hierarchical, divided into voltage levels, costs are determined for each of them. The location of a consumer determines how many network layers are included in his network usage fee, e.g. a consumer connected to network layer 5 pays his share of costs on top network layer - transmission and the 2-5 network layers belonging to distribution. The network usage fee for a consumer is determined based on his number of connection points (weighting factor 10 %), consumed energy (30 %) and peak of consumed power (60 %). According to this model, network usage costs are allocated only to consumers; producers, including consumption in the case of pumped storage, do not pay for the network usage.

Such model of the cost split, as a specific example, is a decision that has to be justified by the computations. In general, the existing organization and all the rules discussed previously in this chapter and beyond have to be rationally chosen, i.e. these are results of the decisions based on the considerations and/or computations.

1.1.4   Summarizing Remarks

The description above leads us to the following summarizing statements:

- The economy, efficiency, reliability and environmental impact of the power system, as well as long the term sustainability depend on the decisions taken by all the actors on the market.

- In a long term prospective, the regulator holds responsibility for the decisions in the strategic power system planning by determining the market rules and rules for the interactions among the actors.

- Main responsibility for the secure and reliable power system operation is allocated to TSO.

- Decisions, and thus, control actions influencing power system operation are made by several actors seeking for the utility (profit) maximization. The objectives of the actors might be conflicting.

- Decisions have to be taken with incomplete information, high uncertainty and under the influence of the stochastic factors.

The decision making under uncertainty can be improved by diminishing or decreasing the influence of the uncertainty, i.e. by eliminating the source of errors - better weather forecasts, more accurate state estimation etc. Besides, the improvement can be achieved by developing more advanced models and decision making algorithms, e.g. adopting stochastic approach, decision and game theory.

1.2 Power Systems and Decision Theory

1.2.1 Decisions and Games

Game theory mathematically describes rational behavior of the players in strategic situations, or games, when a success of an individual depends also on the decisions of others. Game and decision theory is concerned with identifying the values, uncertainties and other relevant issues for the rationality and optimality of a decision.

First works on game theory are dated back to Cournot (1838), Bertrand (1883) and Edgeworth (1925), who studied oligopolistic pricing and production. However, the idea of general game theory came first in 1944 from John von Neumann and Oskar Morgenstern with their book "Theory of Games and Economic behavior", in which the authors formulated

several forms of games and proposed that it is how economic problems should be analyzed.

Nowadays, game theory is a broad branch of applied mathematics that is used in many areas apart from the economics, e.g. social sciences, engineering, biology and computer science. According to Aumann (1987), today game theory is an umbrella field to study the rational side of the social science, where social interactions shall be perceived broadly to include human and non-human players.

Such interactions are classified according to several criteria, for example, as one player games studied by the decision theory and many player games - subject of the game theory. Yet, some of the tools used by both fields are quite similar [69], [92].

The many player game theory classifies the interactions as:

- antagonistic - when the players are competing with each other;

- neutral - when players are not concerned about each other profits;

- cooperative - when players are helping each other.

Other categories of games include perfect information and imperfect information, simultaneous and sequential, infinitely long games, discrete and continuous games.

In power systems one can find example of each of the game categories. In the game theory terms, power system is a complex interaction between each player and the nature, or interactions of either competing, neutral or collaborating decision makers.

1.2.2   Necessity for Decisions

Whether an engineer is designing a cable, runs contingency screening, builds up a load forecast or computes network usage costs, he or she has to make a decision. What shall the conductor cross section for a given load be? Is the system secure under given contingency? What are the electrical loads in the new industrial district? What are the losses created by the particular consumer? The game theory provides tools to formalize such decision problems in a mathematical framework and is concerned with identifying and quantifying the issues relevant for a general decision.

In power system industry, frequently decisions are evaluated intuitively, partially due to the multi-dimensional complexity of the problems and difficulties to find particular quantification indices. However in the last decades with the development of the computational technology and the game theory itself, many works, whether or not these are formulated in decision theory terms, stress the beneficial use of the game theory [10] and stochastic decision support indices in addition to classical deterministic criteria.

1.2.3 Uncertainty and Risk

Statistics and decision theory, distinguishes between risk and uncertainty [74]. If the probability of nature (or system) states can be quantified, then the decision is to be made in *risk* conditions. Otherwise, if the conditions are unknown and there is only partial statistical information available to describe possible states, then it is about decisions under *uncertainty*. An *ignorance* denotes complete lack of information on the nature states.

Power systems involve very complex technical and economical interactions of the players, who are exposed to different types of risks and uncertainties. Consumers are exposed, for example, to electricity price risks and regulatory uncertainty. Producers do not posses exact knowledge on the costs structure and offers of other companies, technical condition of the power plant, power system development plans, prices for the fuels, emissions, regulations. Transmission systems operator does not know exactly evolution of the electricity demand, technical conditions of power plants and their profits, new players, changes in regulations and even presents physical conditions of the system[3]. The regulator has to consider the risk or uncertainty of the economical and technological development, response of the market actors to regulations and policies etc.

The decision support in power systems is even more complicated, since some of the considerations are very subjective and are problematic to quantify. Perhaps, one of the most classical examples is how to valuate the security of supply. Speaking in terms of game theory, it is difficult to formulate state space and utility, loss, regret loss, risk or other decision

---

[3]in power systems operation and planning it is more common to talk about uncertainty or risk conditions using complementary term 'security'.

functions for the game outcomes. Hence, in order to make a decision, some state space, decision space and requirements must be formulated.

1.2.4   Optimality and Risk Management

The optimal strategy can vary depending on the decision-maker preferences - the considerations that can be formulated into particular optimality criteria.

Let us define the decisions a of the player on the decision space $\mathcal{A}$ and the natures' states w on the state space Ω, with some probability distribution $p(w)$. The function L mapping $\mathcal{A}$ and Ω to the corresponding loss values $L(w, a)$ is the *loss function*:

$$L : \Omega \times \mathcal{A} \to \bar{\mathbb{P}}, \tag{1.1}$$

where $\bar{\mathbb{P}} = [0, \infty]$ set of nonnegative extended real numbers, Ω also corresponds to the space of strategies of an opponent in two-players game.

If L_a is a function on $\mathcal{A}$, as follows: $L_a(w) = L(w, a) \; \forall w \in \Omega$, a shall be preferred to a', if $L_a < L'_a$. On the contrary, *utility* function denotes satisfaction of the player with the decision outcome:

$$U : \Omega \times \mathcal{A} \to \bar{\mathbb{P}} \tag{1.2}$$

and is complementary to the loss function, if $U_a \leq U'_a$ then a' shall be preferred to a.

We can formulate a decision game [69], as follows:

$$G = (\Omega, \mathcal{A}, q), \tag{1.3}$$

where q is some optimality criterion, for example minimal loss.

The solution of the decision problem is then:

$$\min_a \quad q(a, w). \tag{1.4}$$

Decision theory formalizes the requirements to optimal decision in criteria.

Today, the advantages of the risk considerations in decision are obvious, though might be difficult to implement in practice. Once risks have been identified and assessed, all techniques to manage the risk fall into one or more of these four major categories [31]:

- Avoidance (eliminate)

- Reduction (mitigate)

- Transfer (outsource or insure)

- Retention (accept and budget)

The approaches discussed in this thesis dominantly fall under the category of risk reduction. For the TSO tasks this could be achieved for example, by increasing security margins. The thesis discusses algorithms that use additional information about the random processes and parameters to mitigate the risk, as well as, the necessary organizational measures.

1.3 Objective of the Work

Main objective of the given work is enhancement of the methods and algorithms in power systems by stochastic approach, application of decision and game theory. This way the influence of the random and uncertain factors is taken into account in decision making and power systems security and economy is improved.

In a modern power system environment one should clearly identify a user of the proposed method, thus a decision maker. This work argues for the advantageous use of the statistical approach, game theory and decision support tools in several areas of power systems, as follows:

- In the first part of the thesis power system state estimation is extensively discussed. The designed algorithms shall lead to increased reliability of the topology determination and state estimation. Thus, the probability of taking the wrong decision is decreased - the cause of the wide emergencies and blackouts, technical and economic losses. This falls under the responsibility and, thus decisions of a TSO.

  This problem corresponds to the class of games with experiments - a statistician is trying to learn about nature's state from experiments. The outcomes z of the experiment are available, as well as the some knowledge on probabilities $p(z \mid w)$ of the outcomes of the experiments under the state w. The operation with the a posterior probabilities $p(z \mid w)$ allows to estimate the state with the

maximum likelihood principle, i.e the estimated state is the most likely according to the outcome of the experiment. This principle is the basis for the power system state estimation;

- The second part of thesis discusses two applications of the cooperative games theory:

  - A new method is justified for allocation of the electric loss in the transmission lines to network users. This shall long term contribute to the increase of the network operation efficiency. The decision makers and users of the algorithm in this case are the Regulator and the TSO.

  - A new strategy for the efficient coordinated operation of the hydro and wind production is developed, which shall be used by Producers or BG responsible.

  In contrast to the non-cooperative games discussed earlier, the cooperative games theory studies outcomes of the game, if the players form different coalitions, as well as loss (or profit) allocations among them. Two applications of the *Shapley value*, a well known concept in the game theory, are presented in this work.

Besides, I was involved previously in the work on statistical approach to power system protection algorithms [17]. In that work, several distance protection and fault location algorithms for high voltage transmission lines were developed, which determine and operate in addition to the classical expectation of the distance to the fault, with the probability distribution of the distance to the fault. Both algorithm design [15], [13], [110] and equipment testing stages [109] were dealt with.

I would like to mention this work, since the ideas and results fit very well with the current objective, namely improvement of power systems security and economy by application of stochastic approach and the game theory.

Chapter 2

Contributions

The main contributions of the presented work to decision support in real time operation include:

- A systematic summary of the sources of the uncertainty associated with the real time model of power system;

- A new method for topology error detection and topology identification;

  The method satisfies the requirement of performance even in case, when state estimation is not converging. The proposed method is based on network search techniques, uses statistical methods to evaluate measurement error propagation and benefits from, but not necessarily requires, phasor measurements.

- A new approach to the reduction of the system model uncertainty used for the state estimation. This approach involves correction of the overhead transmission line resistance using meteorological data and information on the operating conditions;

- Proposal for systematic analysis of the performance of traditional state estimator, which is based on the static model, during system dynamics; In addition to the general concept, an approach based on trajectory sensitivities is proposed to efficiently analyze the influence of parameter changes on the state estimator performance.

We believe that assessment of dynamic performance of a state estimator should be considered and even become a standard procedure in the stage of engineering and parametrization of the state estimator.

- An approach for improvement of state estimation performance during dynamic conditions by upgrading the SCADA infrastructure;

Contributions to development of the decision support tools in off-line analysis are:

- A new allocation method of electric loss in transmission lines to the network users, supported by the implications from the game theory;

  The proposed loss allocation method can also be used to justify fairness of the locational marginal pricing. The method is based on the Shapley value that considers incremental impact of the individual members of the coalition on the total profit/loss.

- A new operation planning and bidding scheme for the coalition of wind-hydro producers.

  The coordination scheme considers wind uncertainty and employs stochastic optimization to maximize total expected profit including the imbalance penalties.

- A proposal for splitting of the profit from coordinated operation of hydro and wind producers with the Shapley value, i.e a fair and transparent method justified by coalitional game theory.

All the proposed methods and concepts are verified by simulations using realistic power system models and operating conditions. The proposed methods are suitable for practical implementation using technology available today.

Chapter 3

List of Publications

The work reported in this dissertation has been partially covered by the following publications:

1. M. Zima-Bockarjova, M. Zima and G. Andersson, "Analysis of the State Estimation Performance in Transient Conditions" in *IEEE Transactions on Power Systems*, *to appear 2011* doi: 10.1109/TPWRS.2011.2124476.

2. M. Zima-Bockarjova, J. Matevosyan, M. Zima, and L. Söder, "Sharing of Profit From Coordinated Operation Planning and Bidding of Hydro and Wind Power," in *IEEE Transactions on Power Systems*, vol.25, no.3, pp.1663-1673, August 2010, doi: 10.1109/TPWRS.2010.2040636

3. M. Zima, M. Zima-Bockarjova, and G. Andersson, "Liberalization of the electricity sector in Switzerland" in *Proceedings, 8th International Conference on Control of Power Systems 08*, June 11-13, Štrbské Pleso, High Tatras, Slovak Republic, 2008.

4. M. Zima-Bockarjova, M. Larsson, E. Scholtz, and G. Andersson, "Critical consideration of the suitability of randomized optimization methods: Power system topology estimation problem,", Paper ♯78, in *PowerTech 2009*, IEEE. Bucharest, Romania, 2009.

5. M. Bockarjova, M. Zima, and G. Andersson, "On allocation of the transmission network losses using game theory," in *Electric-*

ity Market, 2008. EEM 2008. 5th International Conference on European, 2008, pp. 1–6. **Best PhD student Paper award**

6. M. Bockarjova and G. Andersson, "Transmission line conductor temperature impact on state estimation accuracy," in *Power Tech, 2007 IEEE Lausanne*, 2007, pp. 701–706.

Besides the papers above, several other publications were authored and co-authored, which are not within the scope of this dissertation, but address related topics. The list of the selected publications is below:

1. R. Baltensperger, A. Loosli, H. Sauvain, M. Zima-Bockarjova, R. Nuqui, G. Andersson, 'An Implementation of Two-Stage Hybrid State Estimation with Limited Number of PMUs', in *The 10th IET International Conference on Developments in Power System Protection, Manchester, UK*, 2010.

2. M. Bockarjova, A. Dolgicers, and A. Sauhats, "Enhancing fault location performance on power transmission lines," in *Power Tech, 2007 IEEE Lausanne*, 2007, pp. 1123–1128.

3. M. Bockarjova, G. Andersson, and A. Sauhats, "Statistical algorithm for power transmission lines distance protection," in *Probabilistic Methods Applied to Power Systems, 2006. PMAPS 2006. International Conference on*, 2006, pp. 1–7. **Best Paper award in Track 1**

4. M. Bockarjova, A. Sauhats, and G. Andersson, "Statistical algorithms for fault location on power transmission lines," in *Power Tech, 2005 IEEE Russia*, 2005, pp. 1–7.

5. A. Sauhats, M. Bockarjova, A. Dolgicers, and M. Silarajs, "New method for complicated automation systems simulation test," in *Developments in Power System Protection, 2004. Eighth IEE International Conference on*, vol. 1, 2004, pp. 280–283 Vol.1.

6. A. Sauhats and M. Danilova, "Fault location algorithms for super high voltage power transmission lines," in *Power Tech Conference Proceedings, 2003 IEEE Bologna*, vol. 3, 2003, p. 6 pp. Vol.3. **Best Paper award**

Chapter 4

Dissertation Outline

This thesis deals with several aspects related to power systems state estimation, loss allocation and profit allocation.

The Introduction part provides general overview of the power system environment, shows necessity and challenges with decisions and positions the proposed contributions in the power systems context.

Part I of the thesis comprises proposals to reduce uncertainty associated with the real time model, explicitly enhancements of state estimation. This part directly targets at improvements of security and indirectly also the economy, since many settlements are based on the information from the real time model.

Chapter 5 reviews the problems in real time modeling. Chapter 6 proposes a new method to identify power system topology. Chapter 7 evaluates the impact and accounts for slow variations of one model parameter, namely the transmission line resistance. Chapter 8 studies performance of the state estimator during dynamic conditions, and proposes a method for the evaluation of the impact of measurement chain upgrade on dynamic performance.

Part II applies the Shapley value, a well known concept in game theory for profit allocation, to two cases in power system: electric loss allocation in transmission systems to network users and profit allocation among collaborating hydro and wind producers in the area with limited transmission capacity.

Chapter 9 reviews the Shapley value concept. Chapter 10 discusses allocation by existing methods and the proposed method of the electric loss in the transmission system to the users. Chapter 11 describes a possible organizational framework of the hydro-wind producers' collaboration, quantifies advantages of the collaboration and applies the Shapley value to profit sharing.

The Closure summarizes the work presented in the thesis and outlines further research directions.

Part I

Real Time Operation: State and Topology Estimation

Chapter 5

Problem Formulation

This chapter discusses the role and necessity of a real time model of power system. The uncertainties associated with the measurements and the model are briefly described, as well as their causes. Further, the methods to reduce uncertainty, namely state estimation and technological developments are reviewed. A summary of the problems to be addressed in the thesis finalizes this chapter.

5.1 Real Time Model

Reliable electric power supply is a result of a careful design and control of the power system. The power system is a highly complex dynamic system experiencing both continuous and discrete changes of the loads, generation, structure (switching of the lines). The system states or voltages are determined by these quantities via nonlinear equations.

State control objectives must be continuously satisfied: states determined power flows have to be within allowable ranges [71]. To maintain this objective a number of sensors and actuators were designed during the evolution of power systems that can be classified based on the time constants of the controlled process. Figure 5.1 shows the processes in power system, time constants and the devoted controls [32].

Nowadays, thanks to the availability of powerful computers and broadband communications many of the control algorithms are being reviewed to insure optimal performance under uncertainty. In the previous work

[112], [110], [13], [14] we proposed novel algorithms of the transmission line protection for fault location and distance protection, which evaluate an impact of measurement and parameters errors. Thus, based on the determined probability distribution of the distance or impedance to the fault, more efficient decisions can be taken.
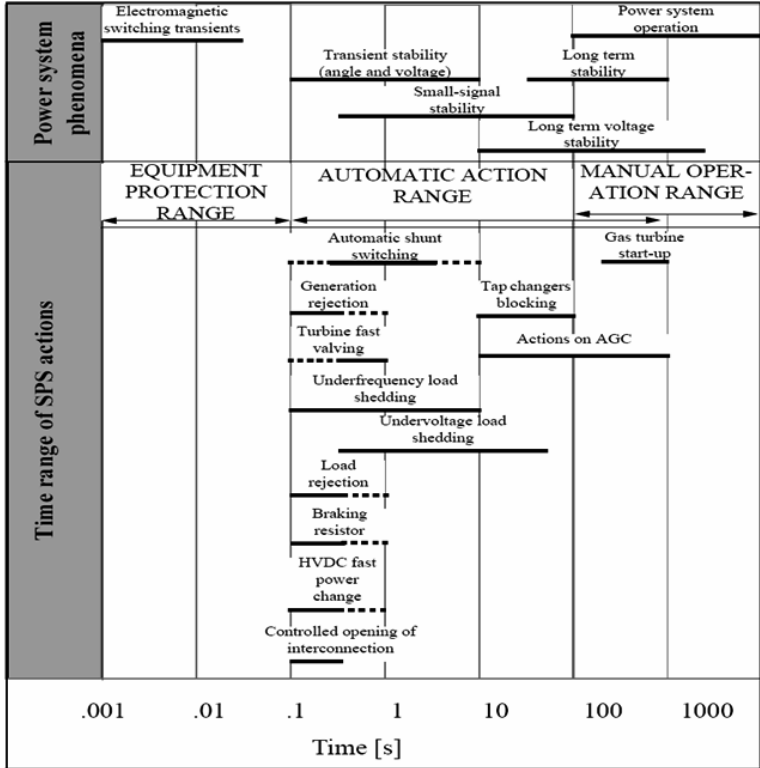
Figure 5.1: Power System Control [32].

The scope of this part is focused on manual (operation range) controls or, more precisely, on obtaining the necessary information in order to perform these controls. The manual or dispatcher control is normally accomplished at the power system control center, based on the data that the control center application, such as Supervisory Control and Data Acquisition System (SCADA), receive via the communication channels
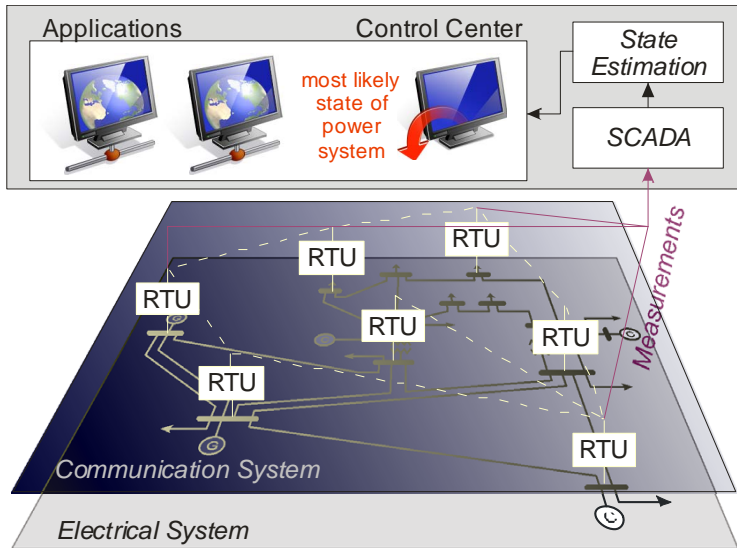
Figure 5.2: Supervisory Control and Data Acquisition system.

from the remote sensors - measurements of the processes and statuses of the switches determining the system structure, as in Fig. 5.2.

These observations are excessive but are subjected to uncertainty in both measurements and power system model. Therefore, the application of the state estimation theory to determine most likely system state from redundant measurements [119], [118], [115] is beneficial. State estimators shall improve quality of real time system model on which basis system operator may decide on preventive or corrective actions [2].

The role of real time model in modern control center is not limited, nevertheless, to more accurate monitoring. All the analysis activities both in real time and pre/post operation are based on these models. Security, settlements, network usage billing, load forecasting, models verification etc, all use real time model as an input. Thus, development of robust and accurate real time model is of great importance [2].

5.2   Uncertainties in Measurements

The centralized supervision and control of power system is possible due
to a number of the measurements performed in the substations and
transferred through the communication channels to the control center,
Fig. 5.2. However, each of the stages of the measurement acquisition in-
troduces an error. In the following, we briefly review the causes of errors
in the substation measurement chain equipment, centralized acquisition
and various modeling discrepancies.

5.2.1   Substation Measurement Infrastructure

Measurements of the electrical quantities at the substation pass through
several stages, as shown in Fig. 5.3. The evaluation of the introduced
inaccuracies at each stage at nominal system frequency (50 or 60 Hz) is
provided in Table 5.3.
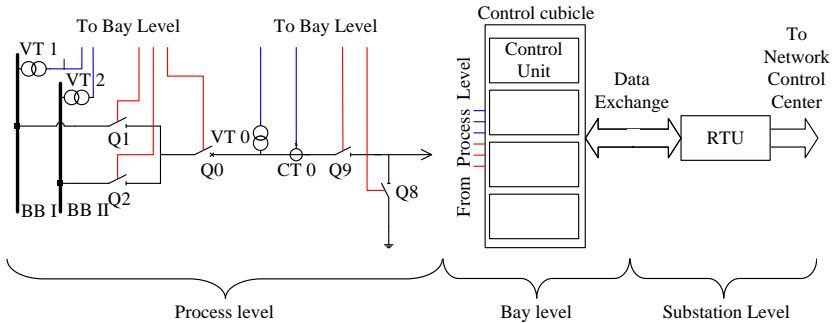
Figure 5.3: Measurement acquisition chain within a substation.

CT / VT measurements The measurements are performed at the
process level of the substation. The instrument current and volt-
age transformers transform high voltage and current values to low
power values, typically $1A$, $5A$, $100V$, $200V$ that can be measured
without inducing high losses and are safe for humans.

The accuracy of instrument transformers is standardized by the
ANSI and IEEE accuracy classes [52]. For current transformers,

Table 5.1: Maximum Magnitude and Phase Error for ANSI class type current transformers

ANSI CT Type	Type	Max Magnitude Error, σ in pu	Max Phase Error, σ in degrees
Metering	1.2	0.024	2.08
		0.012	1.04
Metering	0.6	0.012	1.04
		0.006	0.52
Metering	0.3	0.006	0.52
		0.003	0.26

the allowable error range is given at 10% and 100% of the rated primary current, where both the magnitude and the angle errors are specified. For the voltage transformers, the specified accuracy will be kept, when the voltage at primary side is being within $\pm 10\%$ of the rated voltage.

Such a performance should be guaranteed at specified conditions, namely, frequency, altitude, ambient temperature and burden, i.e. equivalent impedance of the secondary circuit that is mostly determined by the resistance of the conductors connected to the transformer at the process level and the meter at the bay level. Table 5.1 and 5.2 list ANSI standard values for metering instrument transformers.

Some manufacturers pursue a philosophy of remote input-output terminals, which are placed in a marshaling kiosk - can be imagined as a small box next to the switchyard and are hardwired to sensors and actuators and connected via fibre optics to the bay level, in order to minimize potential electromagnetic compatibility problems. However, recent trends supported by the introduction of the communication standard IEC 61850, aims at the introduction of sensors possessing a transducer and a direct communication interface. An example of new technology is optical metering unit (OMU) [120] providing combined optical current and voltage measurements with increased accuracy. These units contain magneto optic current transducer and electro optic voltage transducer (might include analog-digital converter, digital filtering) and can directly communicate with the bay level electronic devices.

Table 5.2: Maximum Magnitude and Phase Error for ANSI class type
potential transformers

ANSI PT Type	Type	Max Magnitude Error, σ in pu	Max Phase Error, σ in degrees
Metering	1.2	0.012	2.08
Metering	0.6	0.006	1.04
Metering	0.3	0.003	0.52

Transducer is sometimes used for the control systems. Dedicated
   transducer preprocess and convert the sinusoidal signal into RMS
   values of voltage, current and power and deliver these quantities
   via serial link of as mA or V signals.

Interposing signal transformer provides galvanic isolation between
   process level and the electronic equipment to protect electronics
   from electromagnetic disturbances and transforms the signal to
   mA and V range.

Filtering The signals are passed trough anti-aliasing filter.

A/D conversion Signal is converted to digital form by means of an
   analog-digital (A/D) converter. A/D converter shall be charac-
   terized by the bit number and the clock that determines sampling
   frequency. After this conversion the digital filtering may be per-
   formed.

Scaling Measurand from A/D are integers that must be converted to
   engineering units. Phasors of the signals shall be formed and
   might be compared with values at other phase. This requires the
   synchronization accuracy in the order of some microseconds.

Data Transfer The measurements are transferred from the control
   unit to substation level upon the request by the Remote Terminal
   Unit (RTU). More novel substation design implies that substation
   automation receives the measurements at the bay level as well
   transmits the measurements to the control center [21]. Lastly, the
   data from RTU is collected by the central unit.

Filtering, A/D conversion and scaling are usually performed by a mi-
croprocessor based device at bay level - protection or control unit. It
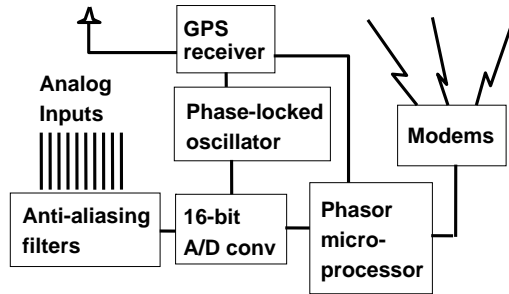
Figure 5.4: Phasor measurement unit structure [93]

may include an additional input from GPS receiver as shown in Fig. 5.4. Such a device called phasor measurment unit (PMU) allows signal sampling and stamping with a highly precise GPS time reference, thus, it allows the comparison of the signal phases at distant locations of power system. PMUs have a separate high speed communication link going directly to the Control center.

GPS devices are also common in substation automation, but only to tag discrete states - events. Besides, a new generation of RTU may have GPS input to time stamp collected measurands [101].

5.2.2 Centralized Data Acquisition

Most of the SCADA systems acquire data on the polled basis [40] - RTU transmits data upon the request from the master station. RTU may respond to the request in two ways:

- by sending the actual values or statuses

- by sending only the changed values or exceeding certain pre-defined value since the last request - reporting by exception to avoid unnecessary communication overload. Compared with the data transmission to higher level, RTU scans the measurements at higher rates, therefore the transfer may be processed directly from RTU memory.

Table 5.3: Table I. Measurement acquisition stages [21].

Function / Device	Accuracy	Comments
Instrument Transformer: from kV to $+/-200V$	Relative accuracy at nominal value 0.5% (IEC standard 0.5, ANSI standard 0.6)	
Interposing Transformer from $200V$ to $10V$	Relative accuracy at nominal value 0.1%	Barrier against disturbances as well
Filter	Influences frequency range only; no influence on RMS value	
A / D converter (16 bit)	Conversion inaccuracy can normally be neglected. The inaccuracy depends on the bit range that is used for the measurand range (e.g. full 16 bit signed used for needed range $\rightarrow$ accuracy is $2^{-14} \rightarrow 0.006\%$	An 8 bit measurand for transmission, or from A/D conversion leads to an accuracy of 2.5%, a 12 bit measurand (11 bit and sign) to 0.25 %
Scaling	Can be neglected, if the result is a 32 bit floating point (accuracy better then 16 bit integer)	32 bit floating point has a mantissa of 24 bit
Communication Oscillation suppression delta (deadband)	Depending on the delta: to get a sufficient communication load reduction, often around 0.1 % of the measurand normal/nominal value is needed	[72] suggests that dead bands may reach 3σ

There are two common ways of polling the data: *fixed period polling and round robin approach* . With fixed period polling the information is transmitted at certain time intervals, implemented taking into account necessity for the information update frequency. In the round robin approach the RTU message contains end of message (EOM) indicator - as soon as the EOM is received, the next RTU on the same communication channel is polled.

[40] provides a extensive overview on SCADA structure and details of technical functionalities.

The error introduced by the centralized data acquisition may vary significantly depending on the available communication infrastructure. Modern fiber optic communication links have a high bandwidth for the data transfer, on the other hand the size of the system is growing as well as the amount of information exchanged between the substations and the control center. In [21] a frequent value given for the deadband is 0.1% of measurand.

5.2.3 Further Measurement Errors

Besides the causes mentioned in table 5.3, degradation of the measurement quality may occur [144] due to:

- age, temperature and other ambient effects related to drift and deterioration of the instrument over the time

- changes in gains, zero offsets and nonlinear characteristics of the instruments involved in the measurement process

- inadvertently introduced gross errors due to wrong modeling and scaling used at the control center, such as wrong point of reference (in the database measurement is assigned to a different location than in reality) and sign errors [124].

- errors in transducer parameters, instrument transformer ratios transformer ratings and scaling coefficients.

Measurement calibration in field conditions is a very expensive task. Several publication suggest remote measurement calibration [144]. However, [72] emphasizes the difficulty of such calibration due the several factors such as time skews, deadbands and the varying accuracy of the

measurement equipment with the value of the measured signal, for example the accuracy of the current transformer is higher around its nominal value and decreases for smaller currents or deteriorates at high currents.

5.3   Uncertainties in the Network Model

Many types of system studies rely on known model parameters. Usually, the parameters can be specified with good accuracy: as the length of the transmission lines is known quite accurately together with the line design, type and characteristics of conductors one can determine the line parameters. Transformer data is provided by the manufacturer, parameters of generators are accurately known as well.

However, parameters are varying during the operation of power system due to the loading, for example changes in position of tap changers of the transformers, resistance of the line and position of switches to modify the topology. Weather conditions impact susceptance and series impedance of the lines. Data may be incorrectly provided in the manufacturer data sheets or not updated in the system database. Other impacts, such as aging may contribute to deviations of the parameters in the long term.

Several approaches have been developed addressing the parameter estimation of transmission lines and transformers, such as inclusion of the relevant parameter in the state estimation, sensitivity analysis and use of Kalman filter. An overview of the methods is provided in [141].

Assumptions and viable simplifications in modeling of the physical processes are necessary when addressing such complex systems as power networks, yet these may also result in inaccuracies. Examples of such assumptions are symmetrical and steady state conditions in power flow and state estimation, neglecting the load current in short circuit analysis etc.

Naturally, the impacts mentioned above are evaluated by the engineer to conclude on the validity of the results in particular studies.

5.4   Uncertainty Reduction with State Estimation

Determination of the real time model of the power system usually includes several stages [2]:

Topology processor determines the structure of power system and connectivity of the parts of the system from the logical statuses of the switches.

Observability analysis determines whether the system state can be determined from the obtained analog measurement set.

State estimation solution determines the most likely state of the system, composed of complex bus voltages in the entire power system as well as best estimates for line flows, loads, generation outputs. It is based on the system model and the measurements.

Bad data processing Detects presence of the gross measurement errors and compensates for them.

Parameter and structural error processing estimates network parameters and structure, and eliminates the errors.

If the knowledge about system parameters and the measurements would be complete and perfect, bad data and parameter error processing would be unnecessary activities. Yet, state estimation, or in that case solution of the set of power flow equations, still would be necessary to reconstruct the unmeasured values.

State estimation is an efficient technique that reduces the influence of uncertainty. This section provides brief classification and overview of the state estimation methods, following the structure in figure 5.5. The topology processing and topology errors are in focus of Chapter 6. Discussion of other techniques for this purpose can be found in [89], [2] including references to the recent research papers.

5.4.1   Static State estimation

State estimation in power systems was first formulated by F. Schweppe [119], [118], [115], in the early 70-ties. It involves several assumptions
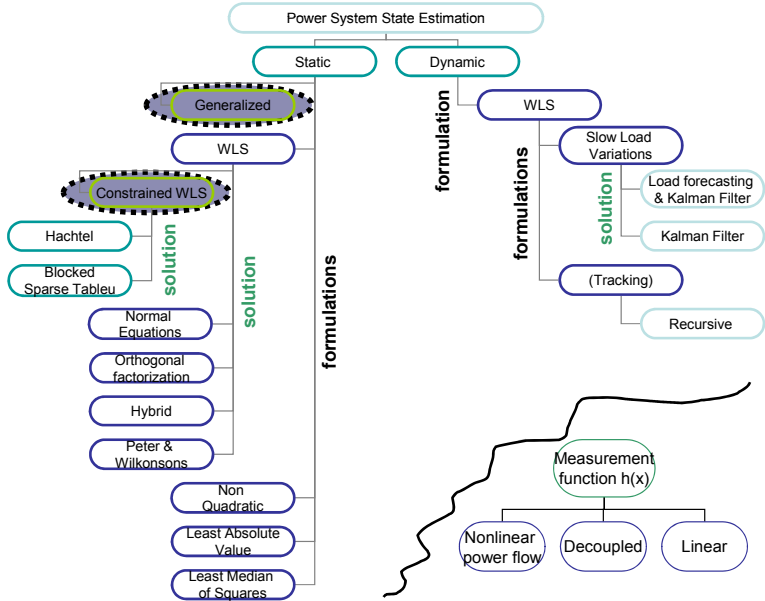
Figure 5.5: State estimation methods.

concerning steady state balanced conditions, namely that loads and powers flows are three phase and balanced, transmission lines are fully transposed and other devices are symmetrical. Thus, the power system is modeled with single phase positive sequence representation. Ref. [72] suggests use of the positive sequence instead of phase voltages for better accuracy and robustness in case of unbalanced operation. Ref. [84] argues for three phase state estimation. However, nowadays a majority of the SE are based on the single phase modeling.

Weighted Least Square formulation

Vector x of bus voltage magnitudes and voltage angles:

$$x^T = (\theta_1 \ldots \theta_N, V_1 V_2 \ldots V_N) \tag{5.1}$$

uniquely determines the state of the power system [119], [2]. However, mapping the states x to measurements z or vice versa is biased by the

measurement errors e:

$$z - h(x) = e, \tag{5.2}$$

where $h(x)$, known as *measurement function*, relates the system state vector x to the measured quantities, such as voltage magnitudes V, bus power injections P, Q, branch power flows P_f, Q_f, see Appendix B.

The errors in (5.2) are modeled as stochastic and are assumed to have the following properties:

- expectation value of the measurement error is zero:
  $E(e_i) = \mu_i = 0, \forall i = 1 \dots M$.

- Gaussian probability distribution $N(\mu, \sigma)$ with the mean value μ and the standard deviation σ:
  $f(e) = \frac{1}{\sigma \sqrt{2\pi}} \exp(-\frac{1}{2} \frac{z - \mu}{\sigma})$.

  Standard deviation σ_i refers to the complete measurement signal chain accuracy of the measurement z_i, e.g. CT and VT, amplifier, RTU.

- measurement errors are independent, i.e.
  $E[e_i e_j] = 0$, thus $Cov(e) = E[e \ e^T] = R = diag\{\sigma_1^2, \sigma_2^2 \dots \sigma_M^2\}$.

The equation (5.2) involves stochastic variables, therefore the most likely rather than exact values of the state variables can be determined.

The joint probability density function of obtaining the set of m measurements with the particular independent errors, can be written as:

$$f_m(e) = f(e_1) \cdot f(e_2) \cdots f(e_m). \tag{5.3}$$

By maximizing the value of this function, called joint maximum likelihood function, or its logarithm, we say that the obtained set of measurements should have the most likely errors:

$$\max \ \log f_m(e) = \sum_{i=1}^{m} \log f(e_i) = \tag{5.4}$$

$$= -\frac{1}{2} \sum_{i=1}^{m} \left(\frac{e_i}{\sigma_i} \right)^2 - \frac{m}{2} \log 2\pi - \sum_{i=1}^{m} \log \sigma_i, \tag{5.5}$$

or sequentially:

$$\min \ \sum_{i=1}^{m} \left(\frac{e_i}{\sigma_i} \right)^2. \tag{5.6}$$
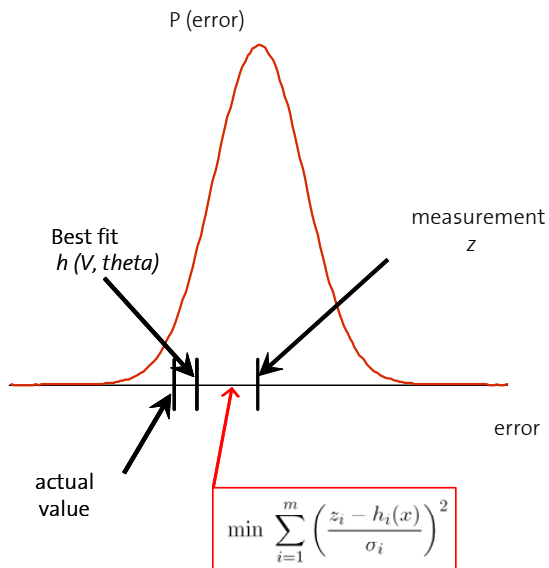
Figure 5.6: Formulation of the state estimation problem.

In accordance with (5.2) it can be rewritten:

$$\min \sum_{i=1}^{m} \left(\frac{z_i - h_i(\hat{x})}{\sigma_i} \right)^2, \tag{5.7}$$

where $\hat{x}$ is the estimated state vector.

Introducing residuals, $r_i = \Delta z_i = z_i - h_i(\hat{x})$, and choosing the weights (assigned to the square of the residuals r_i^2) as $W_{ii} = \frac{1}{\sigma_i^2}$, the residual formulation Weighted Least Square estimator (WLS) for $\hat{x}$ becomes:

$$\min \sum_{i=1}^{m} W_{ii} \cdot r_i^2$$
$$\text{s.t. } z_i = h_i(\hat{x}) + r_i, \quad i = 1 \ldots M. \tag{5.8}$$

The solution of this optimization problem is the weighted least squares estimation. Figure 5.6 shows the principle of the most likely state estimation.

In formulation (5.8) the measurement function $h(x)$ is nonlinear which, however, can be simplified by the following assumptions at the initialization stage: $\theta_i - \theta_j \approx 0$ and $V_i \approx 1$. Thus, $P = h(\theta)$ and $Q = h(V)$ leads to **decoupled estimator**. This usually allows to preserve high degree of accuracy and to increase performance, i.e. computational speed, significantly. This type of estimator is most widely used in practice. Further simplification leading to **linear or DC** estimator is achieved by neglecting line resistances and shunts.

Normal Equations and Solution of WLS

The WLS estimator will, thus, minimize the following objective function $J(x)$:

$$J(x) = [z - h(x)]^T \cdot W \cdot [z - h(x)]. \tag{5.9}$$

As a minimum the first order optimality conditions should be met:

$$g(x) = \frac{\partial J(x)}{\partial x} = -H^T(x) \cdot W \cdot [z - h(x)] = 0, \tag{5.10}$$

where $H(x) = \frac{\partial h(x)}{\partial x}$ is the measurement Jacobian.

Expanding the non-linear function $g(x)$ in Taylor series around state vector x^k, and neglecting second and higher order terms:

$$g(x^k) + \frac{\partial g(x^k)}{\partial x}(x - x^k) = 0, \qquad (5.11)$$

where $\frac{\partial g(x^k)}{\partial x}$ is called the gain matrix $G(x^k) = H^T(x^k) \cdot W \cdot H(x^k)$.

This leads to an iterative solution scheme known as Gauss-Newton method, with the updates of $\Delta x^{k+1} = x^{k+1} - x^k$ for the next iteration $k + 1$ being obtained as following:

$$G(x^k)\Delta x^{k+1} = -g(x^k). \qquad (5.12)$$

Transforming (5.12) and substituting $g(x^k)$ in (5.10) the following equations are obtained known as Normal equations:

$$G(x^k)\Delta x^{k+1} = H^T(x^k) \cdot W \cdot [z - h(x^k)]. \qquad (5.13)$$

Solving this equation for the updates Δx^{k+1} and iterating until the required accuracy ε is reached, i.e. $\Delta x < \varepsilon$, will provide the solution of SE.

Usually, for the solution of (5.13) the gain matrix $G(x^k)$ is not inverted, as it is very sparse and frequently, ill-conditioned due to near zero impedance branches, high number of injection measurements and highly different weights [90]. Instead matrix decomposition techniques are used, followed by the back/forward substitution.

Some of the methods avoiding numerical difficulties are summarized in Table 5.4, where:

- $\Delta\widetilde{z} = W^{1/2}\,\Delta z$, z is residual vector $\Delta z = z - h(x)$

- $\widetilde{H} = W^{1/2}H$

- $\widetilde{H} = QR = \left[\begin{array}{cc} Q_n & Q_0 \end{array}\right]\left[\begin{array}{c} U \\ 0 \end{array}\right]$, such as R is an $m \cdot n$ upper trapezoidal matrix, Q is $m \cdot m$ orthogonal matrix ($Q^T = Q^{-1}$), U is $n \cdot n$ triangular matrix. For the efficient QR decomposition the Givens rotations can be applied [133].

- $\widetilde{H} = LU$, L is lower trapezoidal matrix and U is upper triangular

All these methods will result in triangular matrices and thus, forward/back substitution methods can be used to obtain the solution.

Table 5.4: Solution methods for Normal equations

Method	Basis Equation	Description
Normal Equation	$G\Delta x^{k+1} = H^T W \Delta z$	inversion of matrix G
Cholesky decomposition $G = L^T L$	$L^T L \Delta x^{k+1} = H^T W \Delta z$	solving first for $L\Delta x^{k+1}$ then for Δx^{k+1}
Orthogonal factorization $\tilde{H} = QR$	$U\Delta x^{k+1} = Q_n^T \Delta \tilde{z}$	Qn, U obtained by QR decomposition
Hybrid method $G = U^T U$	$U^T U \Delta x = \tilde{H}^T \Delta \tilde{z}$	instead of Cholesky QR decomposition
Peters and Wilkinson $\tilde{H} = LU$	$(L^T L)\Delta y = L^T \Delta \tilde{z}$ $U\Delta x = \Delta y$	LU decomposition, Cholesky of $(L^T L)$ to solve for Δy, then for Δx

Constrained WLS

Formulation (5.8) may include additional equality and inequality constraints representing for example target values and operating limits in unobservable part of the network:

$$\min \sum_{i=1}^{m} W_{ii} \cdot r_i^2$$
$$\text{s.t. } c_i(x) = 0, \quad i = 1 \ldots n_c,$$
$$q_i(x) \leq 0, \quad i = 1 \ldots n_q. \qquad (5.14)$$

Besides, the equality constraints may be used to model zero or small injections and impedance branches, to which branch equations cannot be applied.

The equality constrains may be treated explicitly - the optimization problem is expressed by a Lagrangian function. Karush-Kuhn-Tucker first order necessary conditions are formulated and the Gauss-Newton method is used to solve the equations.

Thus,

$$\begin{pmatrix} \tilde{H}' \tilde{H} & -C' \\ -C & 0 \end{pmatrix} \begin{pmatrix} \Delta x^\nu \\ \Lambda^{\nu+1} \end{pmatrix} = \begin{pmatrix} \tilde{H}' \tilde{r}(x^\nu) \\ c(x^\nu) \end{pmatrix}, \qquad (5.15)$$

where

- Λ is the Lagrangian multiplier

- $C(x) = \partial c / \partial x$ is the partial derivative of the constraints

- $\tilde{H} = W \cdot \partial h / \partial x$ is the weighted partial derivative of the measurement function.

The coefficient matrix in (5.15) is indefinite and special sparse factorization is required, due to occurrence of zero pivots. Delayed pivoting, blocked sparse matrices and mixed pivoting have been used [90]. Another approach is to include constraints in the objective function - pseudomeasurements with relatively high weights, which requires numerically robust state estimation.

Inequality constraints can be initially relaxed, while approaching the solution, the violated ones are enforced on the corresponding limits by one of the methods above. Ref. [27] suggests to apply the interior point algorithm.

Hachtel state estimator solves the equality constrained state estimation, when the regular measurements are included in the constraints. **Blocked sparse tableau** method improves sparsity of factors in Hachtel tableau [90].

Alternative Formulations

In contrast to *quadratic* objective function used in (5.8),in the optimization problem of state estimation, alternative formulations may be used:

Non-quadratic optimizes some nonquadratic scalar function of the weighted residual.

Least Absolute Value (LAV) minimizes absolute value of the weighted residuals. This formulation has been applied to topology estimation [129].

Least Median of Squares (LMS) minimizes median of the squared residual.

LAV estimator is considered to give an advantage in estimation robustness in the presence of leverage points. However, it has been shown in [90] that it is not always the case. LMS provides less accurate results but more robust towards leverage points.

5.4.2 Dynamic State estimation

Several papers have been published introducing what is called dynamic state estimation, where however, due to historic evolution, the term dynamic was used in different contexts. Before proceeding, we find it appropriate to review the use of this term.

- dynamic in sense of being fast static state estimation;

  Several publications refer to static state estimation algorithm that solves the problem in a shorter computational time as dynamic.

- Multi-snapshot recursive processing of the measurements with no dynamics in the states - *tracking* SE [117];

- Multi-snapshot SE of slow dynamics due to load variations;

  These methods process sequential measurement snapshots and are combined [107], [122] with various short-term, in the order of several minutes, load forecasting techniques to consider slow algebraic states variation. An extensive review of the multi-snapshot state estimation techniques based mostly on the Kalman filter is provided in [107]. Hierarchical decomposition of the estimation problem is proposed to ensure performance in real time applications.

- Very few works can be found that are dealing with estimation of power system dynamics - state estimators for the swing states estimation, which involve observer-based techniques [88], [25], [114].

  The objective of the dynamic state estimation is to determine the state from few non-redundant measurements and predict system evolution several seconds ahead. In [113] a model based filter application for detection of the disturbance and estimation of the voltage phases is presented.

In this thesis dynamic state estimation is defined according to the last item above. In recent discussions and publications dynamic state estimation gains more and more attention of the research community, largely encouraged by the availability of the phasor measurement units (PMUs) [96], [18], [97]. Furthermore, there is a growing need for the fast flexible control systems.

However, to our knowledge no dynamic state estimators have been implemented in real power systems. Despite new attractive features, dynamic state estimators are associated with high computational complexity and necessity of adequate dynamic models of the power system.

5.4.3 Results Evaluation and Visualization

The accuracy evaluation of the SE results is an important aspect. Even though the provided results are rarely inaccurate, control center engineer may loose trust in SE if too large inaccuracies occur. Particularly, unusual and, thus, most dangerous situations may be perceived by the dispatcher rather as SE failure. Providing additional indications and criteria on the algorithm performance are, thus very helpful.

One such performance index could be $J(\hat{x})$ originating from the bad data detection. It can be shown [90] that sum of m normally distributed squared independent random variables $N(0, \sigma_i^2)$ results in a chi-square distribution with m degrees of freedom λ_m^2. Then, hypothesis testing can be applied to verify if the random variable follows chi-square distribution with different levels of significance. Another class of approaches would be based in the analysis of residuals. In [59], [22] various performance metrics are summarized and the Shannon entropy of estimated states has been proposed as an uncertainty measure for the evaluation of PMU impact on SE performance.

Sensitivity analysis of SE objective function and estimates to model inaccuracies, measurements and other parameters were proposed in [86]. These sensitivities can indicate credibility and stability of the results.

An interesting concept of bus credibility index was introduced in [3]. It is defined as a probability measure that quantifies estimation reliability or ability to detect bad data on the particular bus within specific system taking into account probability of bad data in the measurement. Although it has been proposed for the measurement system evaluation for the distributed SE, it is rather a *local indication*. Similar ideas can be applied to SE evaluation.

Good visualization techniques of the system state as well as reliability of the estimates that could be easily perceived by the power system operator is another important development direction. Some approaches to state estimation visualization are presented in [85], [138]. An extensive report on general power system visualization techniques is provided in [94].

5.4.4 Experience with SE

Historical Development

State estimation has found an interest and recognition among utilities almost from the very beginning. The formulations and solution techniques of the core algorithm have developed with the growing expectations from the users.

Several development stages can be observed:

- 70ties: the normal equations

- 80ties: the fast decoupled formulation

- 90ties: extended plausibility checks for topology processing, matrix pivoting, orthogonal transformations to improve speed and robustness of SE. First installation of estimator using PMU measurements.

- 2000: visualization, constrained estimators, measurement quality statistics, multi-area SE with the PMU.

Despite all the improvements achieved, power industry has still growing expectations, prompted partially by the market conditions.

Surveys

An extensive bibliography on power systems state estimation literature (1968 - 1989) can be found in [35]. Several surveys were conducted starting from 70ties on various aspects of state estimation and the associated algorithms.

1974 The pioneering set of papers by Schweppe established the basis of several aspects of SE [119], [118], [115]. It was followed soon by the first overview of the alternatives and developments by Schweppe and Handschin [116].

1983 Van Cutsem and Pavella presented a critical survey of hierarchical methods for state estimation of electric power systems [29].

1987 Bose and Clements published a summary on real time modelling [20].

1988 Comparison of methods for state estimation was provided by Holten et all [47].

1987 CIGRE Task Force on analytical topics of power system and analysis committee published results of the conducted questionnaire that included SE [36].

1989 A survey on static state estimation was conducted by Wu [137].

1990 Comprehensive discussion of state estimation techniques that are based on several sequential snapshots was provided by Rosseaux, Van Cutsem and Dy Liacco in "Whither dynamic state estimation" [107].

2000 A survey on parameter estimation Zarco and Exposito [141].

2000 The latest detailed review by Monticelli, which includes generalized state estimation, was published [90].

2005 A book covering main aspects of SE and including expensive references to the recent papers published by Abur and Exposito [2].

Utility Survey by CIGRE

In 1985 the CIGRE task Force conducted a questionnaire on analytical techniques in power systems including SE [36]. SE was indicated to be of strong interest for almost all the utilities that were participating in the questionnaire. At that moment weighted least square SE was the dominating technique in operation. Motivation for existing or planned installations was a need for more consistent and reliable basis for the real time operating, post incidence and predictive analysis, defined as activities related to short term operation planning, i.e. economic dispatch, interactive load flow, contingency analysis.

Improvements were suggested in the methodology and schemes. The main proposed R&D areas:

- Increase of the solution speed and computational stability, particularly for large systems

- Improve methods of detecting/rejecting bad data, including differentiation between metering, structural and parameter errors

- Improve modeling of external systems, including definition and interchange of related essential data

- Use of dynamic methods during changes in network topology and if the metering failures occur.

One participant mentioned that SE should indicate a confidence error in each measurement based on historical and and present data. Others mention necessity for developments in measurement placement algorithms.

Industrial Experience

1972-2006 One of the first implementations was conducted in Switzerland [125] by Elektrizitaets-Gesellschaft Laufenburg (EGL) in 1972 . In 1978 it was upgraded first time and [8] describes the implementation of a third generation that uses plausibility checks, limit verification after SE execution. Topology processor run only in the tracking mode using graph techniques. Decoupled Newtop-Raphson SE algorithm was implemented with the small R/X, G/B ratios correction of line impedance to prevent the divergence. Later overview of the problems experienced with SE is provided in [124]. It is mentioned that SE involves a significant effort for the initial installation and a permanent maintenance.

1983 In 1983 Harris corporation and Atlantic Electric reported an installation of the new control center required to operate as a satellite control area of the PJM power pool [78]. Topology processor, which is referred in publication as network configurator, was based on the status information from real time database. Tag and quality information was summarized for the dispatcher in order to ensure the data quality awareness. Topology processor provided a model for the online load flow and contingency analysis. Fast Decoupled weighted least square SE was used together with the residual or normalized residual analysis for bad data identification. Observability analysis identified observable regions and splits. For unobservable islands, online load flow (LF) program used results of state estimation, generator schedules and load distributions to provide a complete solution consistent with SE. Jacobian formed by the SE and LF was used to calculate penalty factors that account for transmission losses caused by the generation units. Another installation in Ohio Edisson is described in [79].

1983 TRW Controls reports on five installation of SE in SEGBA Argentina, E de C Venezuela, AyEE Argentina, Iberduero Spain, ENDESA Chile [53]. At the moment of publication three installations were operating successfully: SEGBA, E de C, Iberduero. An example of Iberduero is discussed. Details on the SE algorithm are not provided. Aspects of the external system modeling are addressed as system has many interconnections. Slow SE convergence was experienced in the areas with high line impedance and simultaneously low measurement redundancy. Another cause of disturbance in SE operation was the presence of nonconforming loads, in this example a $35MW$ load was fluctuating every minute. The installation and tuning took approximately two month and the measurement error was improved by a factor of three during the tuning.

1983 A PJM implementation of advanced monitoring project driven by the voltage stability is described in [38]. The network connectivity was determined by the algorithm in [42]. Observability analysis of the subnetworks and fast decoupled formulation of SE was used.

1983 An practical work targeting at measurement placement optimization is provided in [1]. State estimation algorithm used in this paper was based on normal equations and the transformations of normal equations.

1983 Westinghouse Electric has developed a WLS based SE installed at Orange and Rockland Utilities [132]. Normalized residual test was used for bad data identification. The results of SE were used for online load flow and contingency analysis. Common sources of errors discovered during the installation in measurements and model, were summarized.

1991 An installation of the Westinghouse Electric SCADA and AGC software in Northeast China power system was reported in [143]. The software was accomplished with the in house SE. Fast Decoupled method with sparsity based ordering of Gain matrix was used. Topology preprocessor and plausibility checks were implemented. A linearized bad data identification method is proposed for multiple interacting bad data processing [142].

1994 Pacific Gas and electricity company shares the experience with an SE installation from EMPROS systems in [9]. Symbolic observability routine [126] was used. State estimation was formulated as the equality constrained problem [47]. Since the changes in substation topology were frequently not reported by personnel this resulted in weakened SE performance, the plausibility checks were implemented in a topology

processor. This measure helped to resolve status errors in substations. Bad data identification used Chi-squared and the normalized residual techniques. The results were used for penalty factor calculation, security analysis and transmission constrained economic dispatch. The sources of inaccuracies were described in this publication.

1995 First phasor measurement implementation in industrial state estimation is presented in [128]. SE used enhanced Givens method [133] for SE and partial or full system solution. Partial solution was used to increase the update rate of results. Bad data identification was based on linear residual calculation and measurement compensation, thereof it is able to identify multiple interacting and conforming bad data [127]. Besides, a "hot-start" feature that uses predicted states, is introduced. Observability analysis is conducted by symbolic Jacobian reduction [126]. Tests showed a significant positive impact of PMU on the SE performance.

2006 Some of Siemens SE capabilities are presented in [41]. A Huber M-estimator for topology error identification is applied, enhanced Givens state estimation method, linear residual calculation for bad data analysis are mentioned. Emphasis is put on the remote calibration technique that estimates calibration parameters for the RTUs using pre-calibrated ones. An experience with SE enhancement by PMUs in NYPA is reported. Further work is targeting the use of PMU to identify the abrupt change in system state and to block SE till reaching steady state conditions, when RTUs provide consistent measurements.

2006 Areva reported in [77] on the ongoing project with one of the largest utilities in North America on evaluation of the new approach to topology error problem. Presumably, combinatorial solutions were investigated. The publication also provides a general overview of trends with SE, among the other the importance of metrics is emphasized.

2006 WLS SE used in Sweden and Finland is described in [43]. These form the basis for grid loss computation and verification of the planned outages, as well as for voltage level optimization and contingency screening in Finland and voltage collapse supervision system in Sweden. Both systems were initially from GE Network Solutions (ex. Harris Controls) and were later upgraded. It is not clear, however, if the upgraded solution comes from the same vendor. Finland used SE as a source for corona losses estimation, but the technique seems to be vulnerable: it seems to incorrectly identify corona losses as measurement errors. The correction of the line resistances to the ambient temperature to be im-

plemented is mentioned. Thus, a more accurate resistive loss determination is targeted. Further plans on PMU measurements installations are mentioned as well.

2006 The work sponsored by the Brazilian South State Electric Utility on the implementation of Schweppe type Huber Givens estimator is presented in [98]. An iterative weights refining method is chosen to handle the equality constraints. Examples from real operation are provided.

2006 Transenergie [72] reports on its experience with decoupled WLS estimator with equality constraints to model zero injections. In-house software for the preprocessing of branch topology errors is added based on the similar techniques as [19]. No further details are provided on the developed algorithm. SE results are used for online contingency screening and for off-line dynamic security assessment. Measurement bias statistics and load distribution factors are calculated and updated through exponential filtering. An interesting and important observation is made that the standard deviation of the measurement error is nearly linearly dependent on the measured value.

5.5   Technological Developments and Standards

An alternative or additional approach to reduce uncertainty of the power system model is to use new devices, e.g. sensors, which provide more accurate information.

Indeed, optical measurement units have higher accuracy and provide immediate transformation of the signal into digital form, so it is not further distorted by electromagnetic interference. Yet, installations of such sensors are still relatively rare.

The introduction of semiconductor devices in 20th century and subsequent development of computers had major impact in many industrial areas. It brought control and protection devices based on microprocessors, intelligent electronic devices, substation automation systems in power systems. Besides, creation of the global positioning system (GPS) led to development of PMUs and RTUs with accurate time stamp. Many developments were achieved also on the primary equipment side, for example HVDC, FACTS, gas isolated substations etc.

Trends in control system development go along with standardization, integration and interoperability. Thus, IEC 61850 standard "Communication networks and systems in substations" was adopted by a majority of the equipment manufacturers. This standard guarantees the devices from the different suppliers and substation automation system will have possibility for the data exchange.

With the Common Information Model (CIM) a standard of data representation has been developed by the industry. The goal of CIM is to let all EMS applications refer to a common (same) model. This way discrepancies can be avoided and the robustness of data should be improved.

Also, communication networks are increasingly based on fiber-optic cables, having much higher bandwidth and the costs for the information transfer have significantly decreased.

Undoubtedly, in the future these technologies will contribute to the improvements of the accuracy and robustness of real time models. New technologies will appear and even replace some functions in power systems control. Could in the future state estimation become an obsolete technique? Probably not, since it not only reduces the uncertainty but also enables such features as estimation of the non-measured quantities and bad data filtering.

Moreover, introduction of almost all new technologies in power system operation is associated with a high inertia. Replacement of equipment or software involves intensive work, is time consuming and expensive. Besides, it may require extensive testing. The number of devices to be replaced is huge. Therefore, for the next few decades, one can hardly foresee such changes that would make state estimation obsolete. On the contrary, new methods shall directly use advantages offered by, for example, PMU devices, while other technologies, such as common information model, can be explored and applied with respect to the proposed methods in the course of industrial development.

5.6 Summary

The real time model is essential for the actions of the TSO. The reliability of this model affects decisions concerning both security and economy of the power systems operation.

Uncertainties associated with both model and measurements cannot and will not be fully eliminated by advances of the metering and communication technology.

Since the very first installations the benefits of using state estimators were undisputable and significant progress has been achieved over the last decades. Still improvements in robustness and accuracy of the estimators are expected, such as operability in rapidly changing conditions, they are still prone to fail due to topology errors - a problem particularly difficult if the SE does not converge, discrepancies due to time skews in measurements etc. Some of these issues can be improved with the computational power available nowadays and further enhanced in the future, PMUs and communication systems. The following chapters give contributions to several aspects related to reliability of real time system model.

Chapter 6

Influence of Topology

This chapter discusses problem of erroneous topology in state estimation. If the errors stay uncorrected, operators' decisions will be based on wrong information and may endanger power system security. A brief overview of the existing approaches to topology error identification is provided. A new method is proposed and illustrated by a numerical example.

6.1 Introduction

6.1.1 Topology Processor

Power system structure is far more complicated than the model used for power flow calculation or state estimation studies. It contains busbars, switching devices and circuit breakers and switching the latter might change the status of the particular equipment and the topology of the entire system.

A network topology processor analyzes the status of the switching devices and determines interconnections of the physical nodes and transmission elements. It reduces the number of nodes in the model by transforming the *bus-section/switch model* into a *bus/branch model* and assigns the measurements to branches and busses, a simple example is shown in Fig. 6.2. It also identifies energized, de-energized and grounded parts of the network.
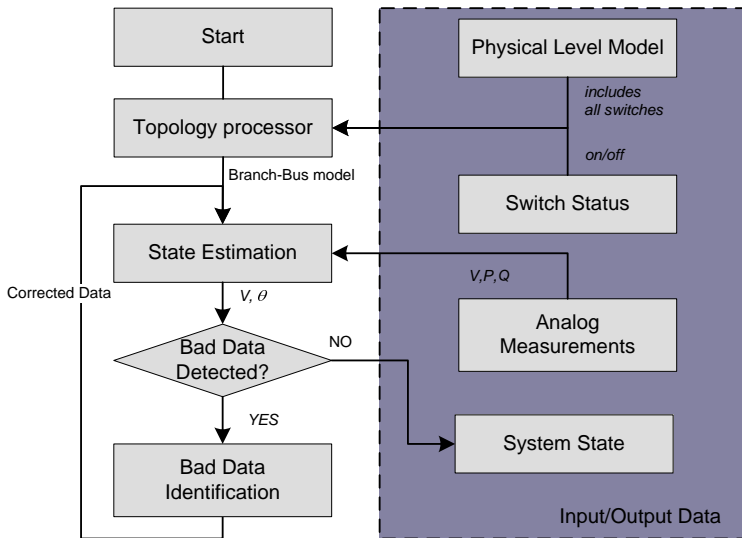
Figure 6.1: State estimation and auxiliary algorithms.

The steps of the network topology processor can be summarized, as follows:

1. Converting raw measurements in appropriate units and verify operating limits, rate of change of operating variables, the zero flows in opened switches, zero voltage difference across closed switches;

2. Processing the bus sections to determine connectivity in bus groups and form the network busses;

3. Building the data structures (pointers and links) to associate busses with branch and shunt devices: transmission lines, phase shifters, capacitors, reactors etc, as well as measurement devices;

4. Analyzing network connectivity for islands.

The location of the switching and metering devices is assumed to be available from the database (static data). Conventional SE rely only on the logical signals about the switch position (dynamic data).

A rule based power system topology processing algorithm is described [108]. In [20] it is pointed out that [108] is basically the only algorithm
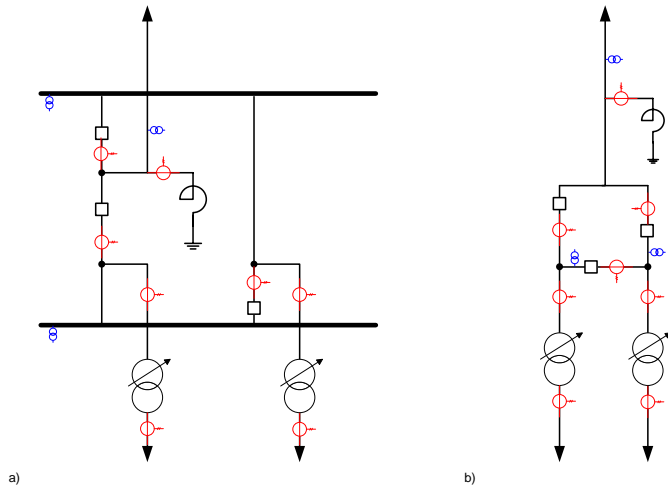
Figure 6.2: Simple substation diagram, including measurement devices location

used in practice. Several sources mention simple tree search being applied to *substation* graph for bus section connectivity construction. Similarly, *the network* connectivity is determined by a simple tree search algorithm [108] and depth first search method [11], [105].

The border between topology processing and topology errors identification is vague in some methods, such as plausibility checks - the error identification is a natural feature of the processing algorithm. In [123] a plausibility check method was developed - an expert system was created that verifies breaker status information with the analog measurements creating rules to topology detection. Practical experience with such a detector is described in [125].

In the *tracking mode* only the changes of the status are considered and the corresponding parts of the network are updated [100]. Then, plausibility checks are performed using the Kirchhoff's laws.

One may notice that topology processing is in a way close to the observability determination. In fact, a class of methods for observability determination is referred to as topological observability. Similarly for both tasks, the topology of the network is traced by some method. The difference is in the objective, namely, in topology processing the mea-

surements are used only for plausibility checks or confirmation of the correct switch status signal, while observability follows the topological tree to check the sufficiency of the available measurements.

Network connectivity determination for islands by the local updates was addressed in [140]. An elegant solution to *island and connectivity detection* can be found in [42]. The bus incident matrix is boolean, and when boolean multiplied by itself a second degree (two nodes away) incident matrix being obtained. Repeating the multiplication procedure for the connected network would eventually result in a matrix of ones[1]. Thus, network islands and corresponding busses can be determined easily. Besides, a decomposition of the systems is suggested: the connectivity is determined within each part and later, the connectivity between the parts. Another attractive algorithm presented in [102] also involves incident matrix and sequential trace and elimination of the incident entries. The algorithm stops, if all the entries were covered or no more eliminations are possible. Both these methods operate with the already obtained incident matrix.

6.1.2   Approaches to Topology Error Identification

If the status of the circuit breaker(s) is determined incorrectly, it results in locally incorrect bus/branch model giving a topological error. It usually causes SE to be significantly biased and the bad data processing would eliminate several measurements, consequently resulting in convergence problems or in an unacceptable state. Thus, detection of topology errors is an important problem in state estimation.

Topology errors identification methods can be classified in two categories: **a priori** processing - plausibility checks as discussed before and **a posteriori** processing - as the SE has converged, an analysis of the identification of topology errors can be performed.

Besides, different approaches are required for two types of topology errors:

Branch status error - error in status of the network branch, non-zero impedance element.

---

[1]it seems to the author of this thesis that boolean addition of the original matrix to the result is necessary at each step. This description is missing in the referenced paper.

The approaches to overcome this type of error are similar to parameter estimation techniques. The impedances of the branches are explicitly presented in SE, therefore there is no need for a special model. Essentially, two posteriori methods are used for the branch status errors identification: by the means of normalized residuals or state vector augmentation of the suspected branch status.

Substation configuration error - errors affecting circuit breakers that link busbars, zero impedance elements. Two types of errors may be encountered: error in the static model of the substation - configuration of the substation and interconnection between the elements or the dynamic status determined by the status of the switches.

This error type requires a specific procedure, when the affected CB appear explicitly in SE model.

The most outstanding techniques, according to the opinion of the author of this thesis, can be listed, as follows:

- Network search techniques;

- Mini-network;

- Generalized SE;

- Implicit SE;

- Two stage SE techniques.

Substation data validation based on linear programming state estimator was first proposed in [54]. Besides, one should mention branch and bound, tabu search algorithms, which were applied to topology error identification [89]. ANN application was suggested in [131].

Some of these techniques are discussed in more details below.

Network search

A graph search based algorithm for network state estimation verification was developed in [19]. This work addresses state verification and assigns bad data labels to contradicting values in accordance with Kirchhoff's

laws. Although, the authors mention that in case of discrepancy in bus flows, one should suspect a topological error the primarily focus is the state and bad data.

Other works [146] and [104] were addressing state estimation and verification with network search and the use of PMUs.

I mention these work here, since similar ideas were used as a basis for the topological error method development to be proposed.

Mini-network

In [65], [64] developed method for suspicious substation identification based on ordered list "black marks" assigned to bad measurements measurements as identified by state estimation and applies χ^2-test to confirm the error in substation. Then, substation topology variants are evaluated based on a mini-network - the substation and the neighboring bus estimates, which were obtained from the "remaining network". A method to disregard a-priori some topologies is described as well. The main disadvantage of the approach is relying that an SE solution must be available.

Generalized State estimation

Conventional SE techniques are based on the branch-bus model of power system and corresponding analogous measurements. The topology of the branch-bus model is determined from the received logical status signals.

In [89] the concept of generalized state estimation is proposed - estimation of states, network topology and parameters that may partially include physical level models, i.e bus-section/switching device. This formulation allows the inclusion of measurements on zero-impedance branches and switching devices, which is advantageous for the topology errors identification.

Specific types of pseudomeasurements are included in state estimation, for example for zero impedance branches, voltage drop and angle differences between the busses equal to zero:

$$V_k - V_m = 0 \text{ and } \theta_{km} = \theta_k - \theta_m = 0. \tag{6.1}$$

and the actual flow measurements P_f, Q_f are added as state variables.
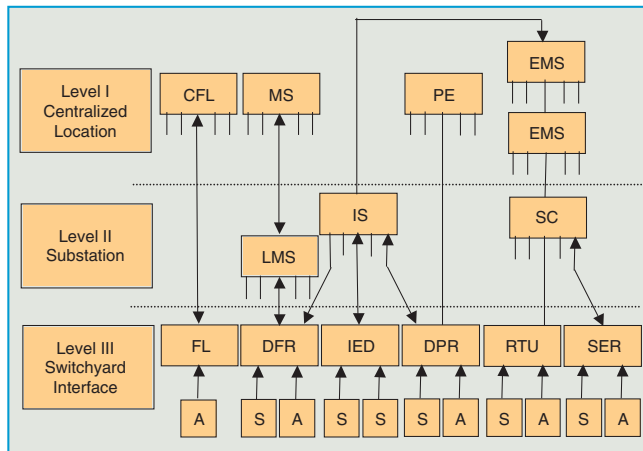
Figure 6.3: Hierarchical Separation of Information (monitoring, control, and protection) [62].

Implicit Substation model

The generalized formulation [89] was a step forward in SE. However, the proposed formulation was suffering from drastically increasing dimensionality of the problem.

First, the suspected substation was identified and the the second stage estimation carried out. The development of this method by considering Kirchhoff's laws and topological constraints decreases the substation model. As a result, an implicit substation model [33] is obtained that is insignificantly larger then the classical branch/bus model. Thus, the entire system can be modeled providing advantages in bad data and topology error analysis.

Two-Stage State estimation

Two-stage state estimation concept was proposed by Abur [5]. First, WLAV estimation is performed for the considered power system and the suspected substation is identified. Then, full bus section / switch representation is modeled for this substation. Next, the second stage

SE is performed involving additional information from the substation. The detailed study results are covered in a PSERC report [4].

Concept of close monitoring of the circuit breaker to avoid topology errors is proposed in [60], as well as topology consistency check based on the measurements from intelligent electronic devices in the substation as in Fig. 6.3 [61], [62].

6.1.3   Rationale for the Chosen Direction

The algorithm developed in this thesis shall fulfill several requirement stated by the project partner: it should be feasible even if SE does not converge and not rely on the availability of the physical level model, i.e. explicit substation layout may be unavailable. Limited number of PMUs might be installed in the network and the measurements available on the common platform with SE.

Substation topology error was a primary focus of the thesis, since it is the most challenging one, although the proposed method can be applied to other types of errors as well.

The chosen approach, therefore, involves network search techniques, uses bus-branch model and, optionally, measurements from PMUs. The proposed algorithm can be used in the cases, when SE does not converge at all. Besides, network search based techniques are transparent and intuitive methods, which can be easily distributed and scaled.

6.2   Topological Error Location

6.2.1   Definitions

The following section of the chapter uses some terms, which are defined below:

Node - a busbar or several busbars directly connected by zero impedance lines and, thus, having the same voltage, magnitude and phase.

Neighbor - a node being directly connected by a transmission line or a transformer to the considered node.

Visitor - a neighbor that was used to compute the voltage on the node under consideration.

Walk - a sequence of the connected nodes.

Path - a sequence of the connected nodes, where no nodes and connections are repeated.

Cycle - a walk that starts and ends at the same node(s), but otherwise has no repeated nodes or connections.

Conflict node - a node, in which the difference of the voltages determined by two different visitors exceeds given threshold.

Erroneous path - (shortest) path that contains nodes leading to voltage discrepancy in conflict node.

Erroneous node - any node on the erroneous path.

PMU path - a path between two installed in the system PMU confirmed by the PMU measurements.

Alternative path - (shortest) path between two nodes on erroneous path or between node on erroneous path and PMU path.

6.2.2   Outline of the Proposed Method

The proposed algorithm for the topological error location shall determine the node or possible minimal set of nodes, which contain topological error. It consists of two major stages:

- Detection of the discrepancy in computed voltage
- Localization of the topology error

Proposed algorithm is based on bus-branch model of the network and sequential or chain computation of the node voltages. The first reference bus is an arbitrary PMU node (or if no PMU is installed, an arbitrary node). At every step, the proposed algorithm determines first degree neighbors with breadth-first search and computes voltage in those. To compute the voltage algorithm requires a pair of the line flow measurements at the current bus or local line end or remote end measurements. The standard mathematical models for the transmission branch and expression for the voltage computation are provided in Appendix B. In addition, if the measurements are available at both branch ends, one
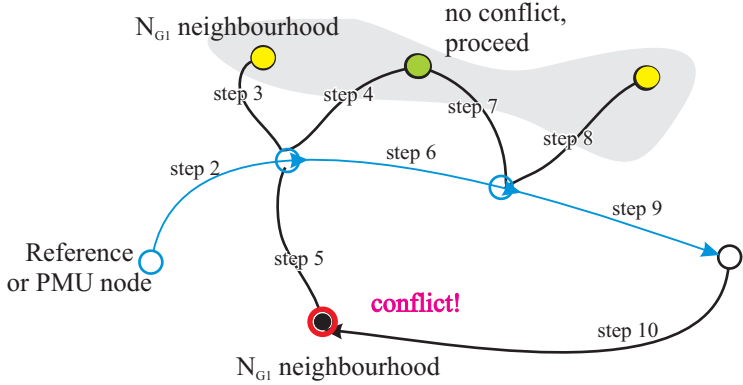
Figure 6.4: Illustration of the algorithm steps for the error detection.

could perform local SE for just two buses and one branch system. That should further contribute to the accuracy improvements.

For each node, all the visitors of the node and the values of the computed voltage are recorded. As the search progresses, each node will be visited as many times as there are connected branches. In a the case of a topological error in the network, at some node there will be encountered a mismatch between two voltage values determined by two different visitors of the node. Using the information on visitors and the voltage records for each node, an erroneous path can be identified. This path will contain a node with a topological error that led to voltage discrepancy. Fig. 6.4 illustrates these steps of the algorithm.

The discrepancy in voltage must exceed measurement noise level, i.e. certain detection threshold shall be employed. This threshold should be sufficiently high to ensure that measurement noise is not mistaken for topology error - detection security requirement. Simultaneously, it should provide sufficient dependability for the error detection. The approach to evaluation of proper threshold value is further discussed in Section 6.2.5.

Once the error has been detected and the erroneous path identified, it is necessary to identify the node or possibly minimal set of nodes that resulted in the discrepancy. This principle is outlined in Fig. 6.5. The voltage in the erroneous nodes is consequently verified through
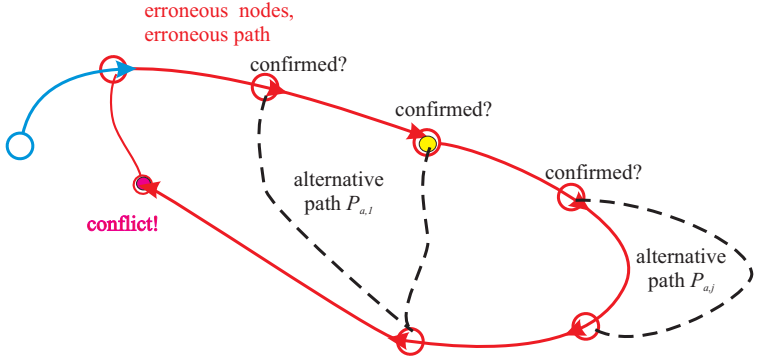
Figure 6.5: Illustration of the algorithm steps for the error localization.

the alternative pathes. Once there is a confirmation of the voltage value, the node can be discriminated from the erroneous path. This localization routine stops, if no more alternative pathes can be found or the erroneous path contains only two nodes.

These algorithms are discussed in details in the following Sections 6.2.3 - 6.2.4. The details on the network search algorithms to determine in which sequence the node voltages have to be computed, as well as how to find the alternative path are provided in Appendix D.2.2.

To speed up the matrix operations and reduce dimensionality of the problem, the network can be split into several overlapping regions. In addition, all the radially connected nodes can be eliminated from the considered network, since it will not be possible to distinguish between bad data and topological errors for such nodes.

6.2.3 Error Detection and Localization on the PMU Path

PMUs provide both voltage magnitude and, perhaps, more importantly for the topological error detection, the voltage angle measurements. Thus, if two or more PMUs are installed in the network, we can re-compute voltages along the PMU path $P_{PMU}(\mathcal{N}_{PMU}, \mathcal{E}_{PMU})$ and compare it with the measurements V_{Nf}^{PMU}. The shortest path between

PMUs P_{PMU} is found employing breadth-first search algorithm Appendix D.2.2. The flow chart of the algorithm is shown in Fig. 6.6.

The discrepancy between the phasor measurement and computed value exceeding the defined threshold ϵ, indicates presence of a topological error on the considered path. Should an error have been detected, it has to be localized. Here for every non-terminal node, i.e $\forall N \in (\mathcal{N}_{PMU} \setminus \mathcal{N}_{PMU,T})$, the following routine is performed:

1. Set $j = 0$;

2. Set $j = j + 1$;

3. Modify network topology: erase adjacent branches of the current node $N_{PMU,j}$ from the network graph:

$$G^{(j)}(\mathcal{N}^{(j)}, \mathcal{E}^{(j)}) = G^{(j-1)}(\mathcal{N}^{(j-1)} \setminus N_{PMU,j}, \mathcal{E}^{(j-1)} \setminus A(N_{PMU,j}));$$

4. Find the shortest path between the PMUs $P_{a,PMU}(G^{(j)})$ for the modified network topology;

5. Verify voltage along the new PMU path $P_{a,PMU}$;

6. If $V_{N_f(P_{a,PMU})} \neq V_{Nf}^{PMU}$ the voltage discrepancy is preserved between measured and computed values, go to the step 2. Otherwise assign error nodes $\mathcal{N}_e = N_{G1}[N_{PMU,j}] \cap \mathcal{N}_{PMU}$ - current node and its first-degree neighbors on the original PMU path and stop.

In case, when an error could not be assigned to the any of the nodes between PMUs, it should be concluded that one of PMUs nodes has an error. If three or more PMUs are available, the set of erroneous nodes can be narrowed down to one by the algorithm analogous to the one described above.

If the difference between computed voltage value $V_{N_f(P_{PMU})}$ and the measurement V_{Nf}^{PMU} was within expected limits, all the nodes $\mathcal{N}_{PMU}$ on the PMU path are considered verified reference nodes. The algorithm for error detection outside the PMU path is then initiated.
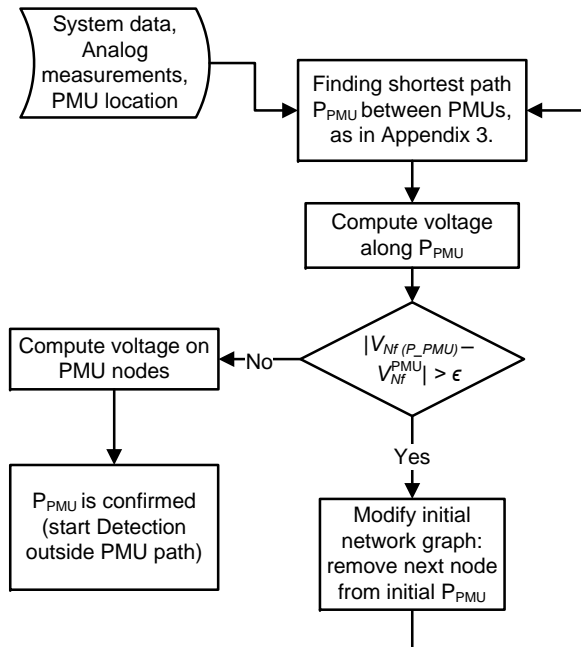
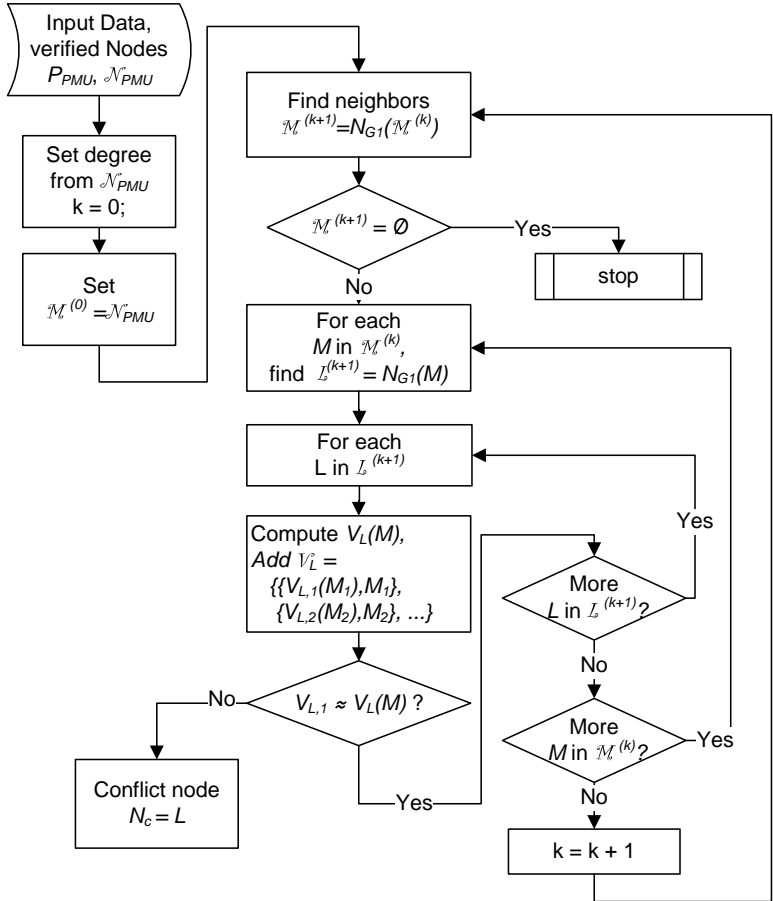Figure 6.6: Algorithm of the topological error identification on the PMU path.

Figure 6.7: Algorithm of the topological error detection outside of the PMU path.

6.2.4 Error Detection and Localization Outside of the PMU Path

Error Detection

If no error has been detected on the PMU path, we propose to proceed with the search till the discrepancy is encountered, as follows. These steps of the error detection are also depicted in the diagram in Fig. 6.6:

1. $k = 0$ - a degree of neighborhood from the PMU path;

2. Set $\mathcal{M}^0 = \mathcal{N}_{PMU}$ a set of PMU path nodes;

3. Determine set $\mathcal{M}^{(k+1)} = N_{G1}(\mathcal{M}^{(k)})$ - as first degree neighbors by the breadth-first search algorithm, Appendix D.2.2;

4. If $\mathcal{M}^{(k+1)} = \emptyset$ is empty, **stop**;

5. For each node $\forall M \in \mathcal{M}^{(k)}$ and $\forall L \in \mathcal{L}^{(k+1)}$, where $\mathcal{L}^{(k+1)} = N_{G1}(M)$ a first degree neighbors of M:

   - Compute voltage $V_L(M)$. Use branch model, branch flow measurements as in Appendix B.3 and $V_{M,1}$ - the first value of the voltage assigned to M;
   - Store computation results $\mathcal{V}_L = \mathcal{V}_L \cup \{V_L(M), M\}$ a pair of voltage value and a visitor (variable `NODE`);
   - Compare determined voltage value $V_L(M)$ to a previously computed voltages in this node $V_{L,1}$;
   - If voltage difference exceed threshold ϵ or voltage value is not within physically feasible range - assign conflict node $N_c = L$, **stop**;

6. Set $k = k + 1$ and go to step 3.

If the exit from the computation loop was at step 5, the discrepancy was detected at N_c and the error back-tracking is initiated to establish the erroneous walk $W_e(\mathcal{N}_e, \mathcal{E}_e)$. Proposed back-tracking algorithm, which is inspired by breadth-first search, is described in Appendix D.2.1.

Determined erroneous walk can be a cycle. The cycle should then be transformed into a simple cycle, i.e. all the common nodes but one shall be disregarded. Indeed, if an error would be on common walk segment, the voltage mismatch would be detected earlier instead of the conflict node N_c.

Error Localization: Preprocessing

When a cardinality of the erroneous nodes set $|\mathcal{N}_e| > 2$, analysis is continued further to narrow down the number of possibly erroneous nodes.

First, the erroneous walk $W_e(\mathcal{N}_e, \mathcal{E}_e)$ is subtracted from the network graph $G_{\backslash W_e} = G \setminus W_e$, and subsequently all the isolated nodes are deleted as these cannot contribute to the verification of the node voltages. For the same reason all the radial connections are removed to decrease dimensionality of the problem.

Assign voltage value $\mathcal{V}_{F\mathcal{N}e,1} = V_{Ns(We)}$ for the start node $N_s \in \mathcal{N}_e$, a voltage profile $\mathcal{V}_{F\mathcal{N}e}$ is recomputed along the erroneous walk - a "forward" profile. Then, in the opposite direction a "backward" profile $\mathcal{V}_{B\mathcal{N}e}$ is computed from the end node $N_f \in \mathcal{N}_e$ towards the start node, $\mathcal{V}_{B\mathcal{N}e,1} = V_{Nf(We)}$. These operations are further clarified in Fig. 6.8.

If any of the voltages $V \in \mathcal{V}_{F\mathcal{N}}$ is out of the feasibility range $\{V_m, V_M\}$ implied by the physical properties of power systems, the subsequent nodes can be excluded from the erroneous set:

$$\forall V_j \in \mathcal{V}_{F\mathcal{N}}, \tag{6.2}$$

$$\text{if } \exists \quad |V_j|_1 < V_m \text{ or } |V_j|_1 > V_M \tag{6.3}$$

$$\text{then} \quad \mathcal{N}_e = \mathcal{N}_e \setminus (\bigcup_{l>j} N_l), \tag{6.4}$$

Similarly, for the $\mathcal{V}_{\mathcal{N}B}$:

$$\forall V_j \in \mathcal{V}_{B\mathcal{N}}, \tag{6.5}$$

$$\text{if } \exists \quad |V_j|_1 < V_m \text{ or } |V_j|_1 > V_M \tag{6.6}$$

$$\text{then} \quad \mathcal{N}_e = \mathcal{N}_e \setminus (\bigcup_{l<j} N_l) \tag{6.7}$$

where $||_1$ is a first norm.

Thus, pre-processing help to reduce erroneous path.

Error Localization: Core Algorithm

Proceeding with the error localization, initialize withhold path $P_W = \varnothing$ as empty (variable `WithholdPath`). Besides, initialize e as zero vector

$e \in \mathbb{R}^{|\mathcal{N}_e|-1}$ (variable `Edges`). In the following iterations, e shall contain 0 if an edge was not verified by the checks. A numeric value is assigned to e_j, if it was verified that the corresponding segment does contain an error. Different numeric values (or labels) will identify particular checked segments. This approach is similar to coloring in graph theory.

Performing the following steps shall determine possibly minimal set of the nodes, including one containing topological error:

1. Iteration number $k = 0$;

2. Iteration number $k = k + 1$;

(a) initial erroneous path $W_e(\mathcal{N}_e, \mathcal{E}_e)$

forward computation of the voltage

(b) feasible voltages N_1-N_4

backward computation of the voltage

(c) feasible voltages N_3-N_6
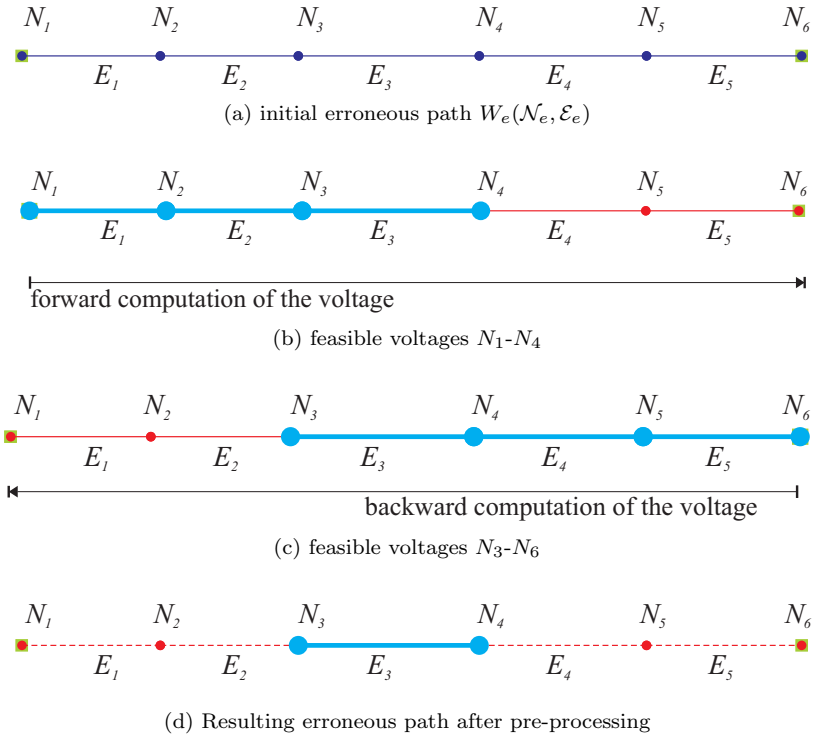

(d) Resulting erroneous path after pre-processing

Figure 6.8: Computation of the forward and backward profile and discrimination of the erroneous path.

3. Find alternative pathes $P_a^{(k)} \supset P_{a,j}^{(k)}$ of next minimal distance, according to algorithm in Appendix D.2.2. Here $P_{a,j}^{(k)}(\mathcal{N}_{a,j}^{(k)}, \mathcal{E}_{a,j}^{(k)}) \subset G_{\setminus We}$ is a subgraph of a network graph after erroneous path was excluded;

4. Analyze obtained $P_{a,j}^{(k)} \subset P_a^{(k)}$, as shown in diagram 6.7:

   If erroneous walk $W_e^{(k)}$ is a cycle:

   - If $P_a^{(k)} = \varnothing$ and withheld path $P_W \neq \varnothing$, then set $P_a^{(k)} = P_W$.
   - If $P_a^{(k)} \neq \varnothing$, withhold all alternative pathes, which include terminal nodes: for all $P_{a,j}^{(k)} \in P_a^{(k)}$, $\forall j \in J$, such that terminal nodes are superset to the start node of erroneous path $N_T(P_{a,j}^{(k)}) \supset N_s(W_e)$, assign $P_W = P_W \cup (\bigcup_J P_{a,j}^{(k)})$;

   else (when $W_e^{(k)}$ is not a cycle), when $P_W \neq \varnothing$, add withhold pathes P_W to the set of new alternative pathes $P_a^{(k)} = P_a^{(k)} \cup P_W$, and erase withhold pathes $P_W = \varnothing$.

   This part of code helps to prevent misclassification of the erroneous nodes, in case when erroneous walk is a cycle and error is in a terminal node.

5. If $P_a^{(k)} \neq \varnothing$, start the verification algorithm for each alternative path in $\forall P_{a,j}^{(k)} \in P_a^{(k)}$:
   Verify if the next path to be checked is internal, i.e. connecting two nodes from the current erroneous path $N_T(P_{a,j}^{(k)}) \subset \mathcal{N}_e^{(k+)}$, or external, i.e. connecting a node on the erroneous path and a previously verified node such as a PMU path node $N_T(P_{a,j}^{(k)}) \cap \mathcal{N}_{PMU} \neq \varnothing$;

   If considered path is external, check that the erroneous walk still contains this node $N_T(P_{a,j}^{(k)}) \cap \mathcal{N}_e^{(k+)} \neq \varnothing$, which is not a terminal node $N_T(P_{a,j}^{(k)}) \cap N_T(W_e^{(k+)}) = \varnothing$ as such verification is not informative. Start procedure **"Verification by the external nodes"** as described in the following subsection;

   else (if considered path is internal), check that terminals of internal path to verify are not the erroneous terminal nodes

$N_T(P_{a,j}^{(k)}) \neq N_T(W_e^{(k+)})$ as such verification is not informative. Start procedure **"Verification by internal nodes"** as described in the following subsection.

6. If a degree for all non-terminal nodes:

$$\deg |N| \leq 2, \quad \forall N \in \quad (\mathcal{N}_e^{(k+)} \setminus N_T(W_e^{(k+)})), \qquad (6.8)$$

or $|\mathcal{N}_e^{(k+)}| < 2$, or $P_a^{(k)} = \varnothing$ and $P_W = \varnothing$ - **stop**, otherwise go to step 2.

In the end, erroneous nodes having adjacent edges with the same label (color) can be excluded from the erroneous path.

Shortest path and computational efficiency is guaranteed by the use of breadth-first inspired algorithms as in Appendix D.2.2. The following two subsection provide more detail on verification algorithms.

Error Localization: Verification by external nodes

This procedure shall recompute the voltage $V_{a,\mathcal{N}e}$ on the erroneous node $N_{e,n}$ along the alternative path from the external node with the reference voltage. Depending on the result, i.e whether or not the erroneous node voltage is confirmed, the erroneous walk can be reduced differently. Thus, verification procedure is as follows:

1. Recompute voltage $V_{\mathcal{N}e,n}$ through $P_{a,j}$;

2. If $|V_{\mathcal{N}e,n} - V_{F\mathcal{N}e,n}|_1 \leq \epsilon$ computed voltage differs from the corresponding one in a "forward" profile $V_{F\ N_{e,n}} \in \mathcal{V}_{F\mathcal{N}_e}$ by less than expected noise impact, proceed as in Fig. 6.9:

   - If, as shown in Fig. 6.9d, the edge E preceding the verified node $N_{e,j}$ was already marked "safe" by the internal checks, i.e. $e_{j-1} > 0$, remove all edges having the same "safe" mark $e_l = \varnothing \quad \forall l \in L$, such that $e_l = e_{j-1}$ and remove corresponding nodes $\mathcal{N}_e = \mathcal{N}_e \setminus (\bigcup_L N_l)$ as in Fig. 6.9e;

   - Remove all nodes preceding the verified node from the erroneous path $\mathcal{N}_e = \mathcal{N}_e \setminus (\bigcup_{l<j} N_l)$, remove corresponding edges $e_l = \varnothing \quad \forall l < j$, as shown in Fig. 6.9c ;

(a) Initial erroneous path.

External
alternative path

(b) connection from an external node

(c) exclusion of nodes N_1-N_2 with positive check result

previous check - ok

(d) exclusion of nodes with positive check and previously labeled edges - decision making

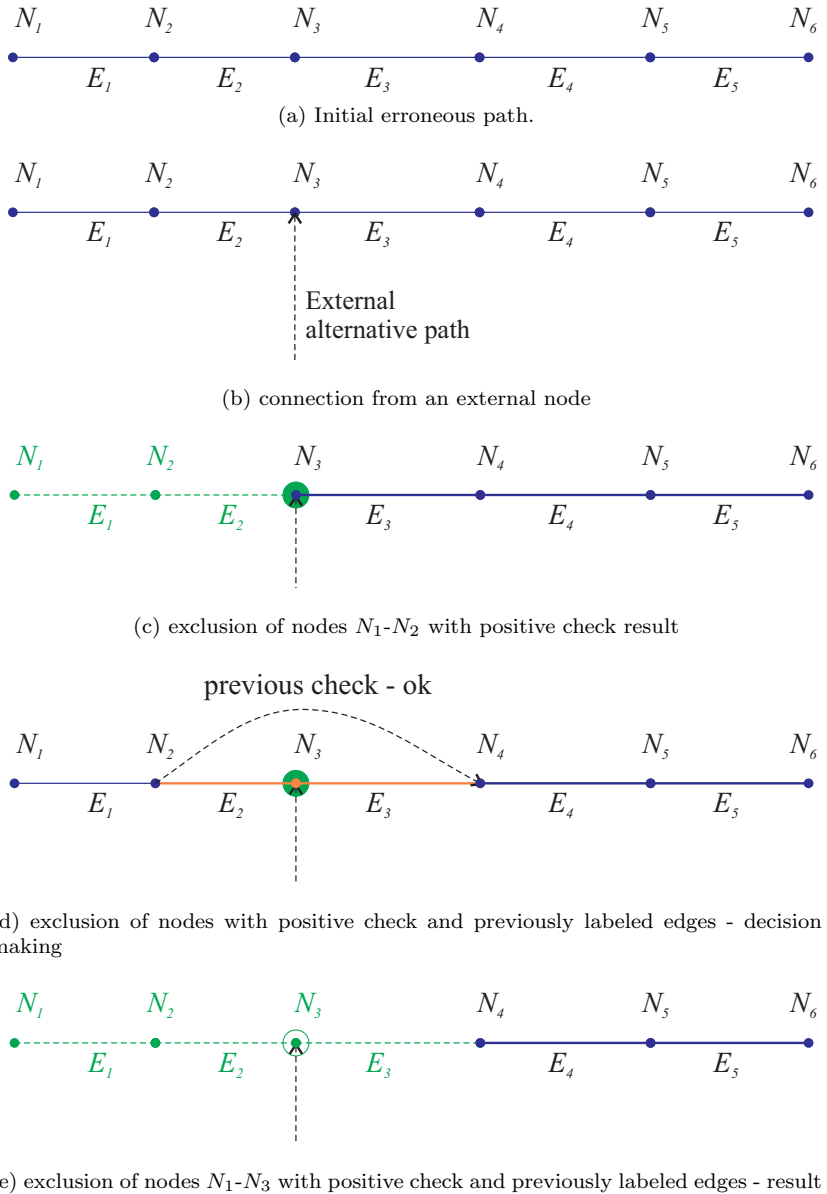(e) exclusion of nodes N_1-N_3 with positive check and previously labeled edges - result

Figure 6.9: Verification of the erroneous path by the external reference nodes and discrimination of the erroneous path in case of positive check.

(a) initial erroneous path

(b) connection from the external node

(c) exclusion of nodes N_4-N_6 with check failure

(d) exclusion of nodes with check failure and previously labeled edges - decision making

(e) exclusion of nodes N_3-N_6 with check failure and previously labeled edges - result
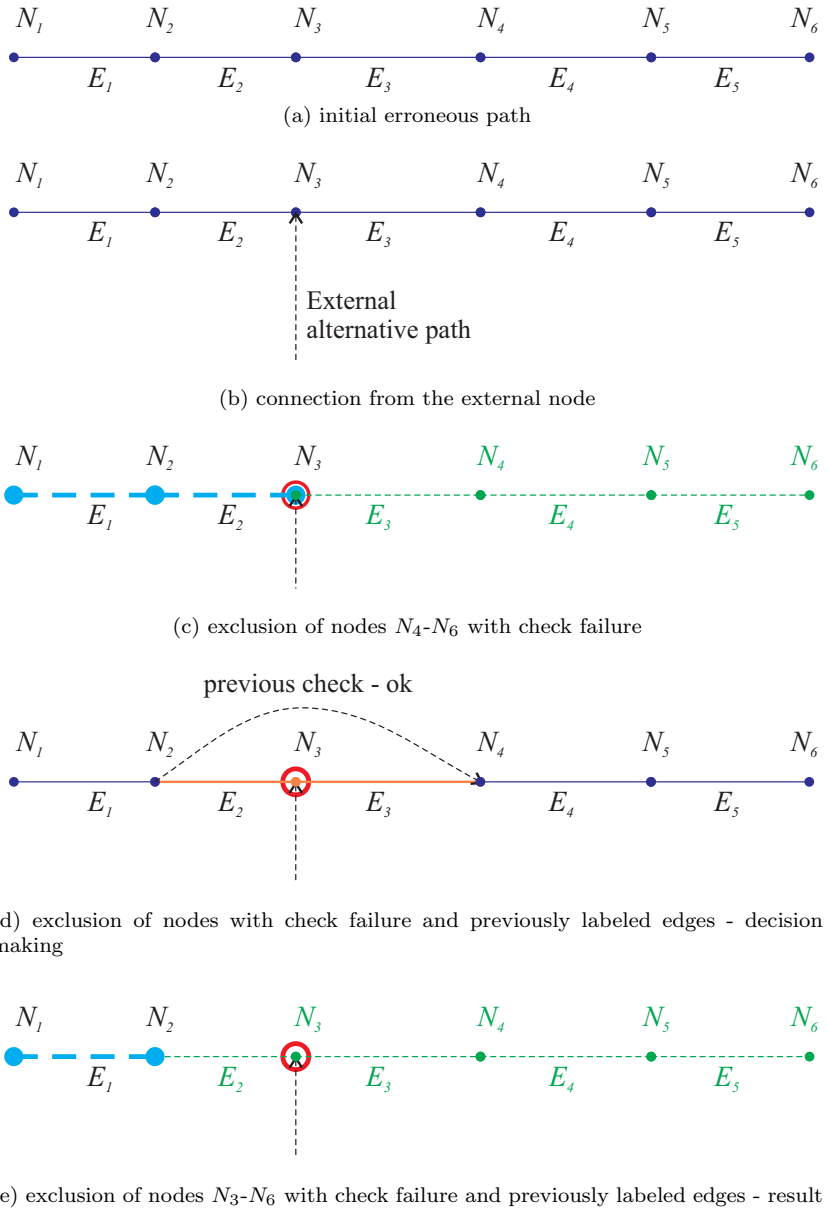
Figure 6.10: Verification of the erroneous path by the external reference nodes and discrimination of the erroneous path in case of check failure.

3. else $|V_{\mathcal{N}e,j} - V_{F\mathcal{N}e,j}|_1 > \epsilon$ computed voltage difference exceeds the expected noise impact, see Fig. 6.10:

If considered erroneous node is not a start node $N_{e,j} \neq N_s(W_e)$ and both edges connected to this node are marked "safe" $e(A(\mathcal{N}_e, n) \cap \mathcal{E}_e) > 0$, then

$$\forall l \in L, \text{ such that } e_l = e(A(N_e) \cap \mathcal{E}_e)$$

and $\forall i \in I, i > j$, remove all the nodes $\mathcal{N}_e = \mathcal{N}_e \setminus (\bigcup_L N_e, l) \setminus (\bigcup_I N_e, i)$ and erase corresponding edges from $\mathcal{E}_e$ and $e_{L \cup I} = \varnothing$, see Fig. 6.10d - Fig. 6.10e;

otherwise remove all the nodes following the considered $N_{e,j}$: $\mathcal{N}_e = \mathcal{N}_e \setminus (\cup_I N_i) \; \forall i \in I, i > j$ and the corresponding edges from $\mathcal{E}_e$, $e_I = \varnothing$, see Fig. 6.10c.

After verification, return values e and $W_e(\mathcal{N}_e, \mathcal{E}_e)$ to main error localization loop.

Error Localization: Verification by Internal Nodes

The following verification procedure is performed with alternative path $P_{a,j}(\mathcal{N}_{a,j}, \mathcal{E}_{a,j})$, unless same segment has already been confirmed according to information in e (variable `Edges`):

1. Recompute voltage $V_{Nf(Pa,j)}$ starting with the node $V_{Ns(Pa)}$ along $P_{a,j}$. An index n is such that $\mathcal{N}_{e,n} = N_{as}$ and i is such that $\mathcal{N}_{e,i} = N_f(P_{a,j})$;

   If during computations in step 1, voltage exceeds feasible range it is considered to be equivalent to exceeding tolerance ϵ - step 3.

2. If $|V_{Nf(Pa,j)} - V_{F\mathcal{N}e,i}|_1 \leq \epsilon$, as in Fig. 6.11:

If any edges were labeled on the current segment $\exists e_l > 0, \forall l \in L, s.t. \quad n \leq l < i$, find $s = \max(e_l)$, then:

- if $e_n > 0$ the first edge on considered segment is "safe", assign

$$e_k = s \quad \forall k, \text{ s.t. } e_k = e_n,$$

to all the edges with same label a new label s.

- if $e_{i-1} > 0$ the last edge of the considered segment is "safe", assign

$$e_k = s \quad \forall k, \text{ s.t. } e_k = e_{i-1},$$

  to all the edges with the same label a new label s.
- assign s to all the edges on the considered segment
$$e_k = s \quad \forall n < k < i.$$

else (if none of the edges on this segment has been verified), mark edges of the current segment "safe" by assigning a higher value than on any other edge: $e_l = \max(e) + 1 \forall l \in L, s.t.n \leq l \leq i$;

3. else, when $|V_{Nf(Pa,j)} - V_{F\mathcal{N}e,i}|_1 > \epsilon$, proceed with current erroneous walk $W_e^{(k+)}$ as in Fig. 6.12.

   - if the edges adjacent to the first considered node had the same label, remove all the edges with that label:

   $$\mathcal{N}_e^{(k+)} = \mathcal{N}_e^+ \setminus (\cup_L N_l) \qquad \forall l \in L, \text{ s.t.} e_l = e_{j-1} = e_j;$$
   $$\mathcal{E}_e^{(k+)} = \mathcal{E}_e^+ \setminus (\cup_L E_l) \qquad \forall l \in L, \text{ s.t.} e_l = e_{j-1} = e_j;$$

   - if the edges adjacent to the last considered node had the same label, remove all the edges with that label:

   $$\mathcal{N}_e^{(k+)} = \mathcal{N}_e^{(k+)} \setminus (\cup_L N_l) \qquad \forall l \in L, \text{ s.t.} e_l = e_{i-1} = e_i;$$
   $$\mathcal{E}_e^{(k+)} = \mathcal{E}_e^{(k+)} \setminus (\cup_L E_l) \qquad \forall l \in L, \text{ s.t.} e_l = e_{i-1} = e_i;$$

   - remove from erroneous nodes all the nodes except considered segment

   $$\mathcal{N}_e^{(k+)} = \cup_L N_l \qquad \forall l \in L, s.t.n \leq l \leq i;$$
   $$\mathcal{E}_e^{(k+)} = \cup_L E_l \qquad \forall l \in L, s.t.n \leq l < i;$$

After verification, return e and $W_e^{(k+)}$ to the main error localization loop.

Several supplementary algorithms inspired by breadth-first search from the graph theory was developed and tuned to the specifics of the addressed problem, namely fast identification of the shortest alternative

(a) initial erroneous path

(b) connection with internal nodes

(c) coloring of safe edges, E_2-E_4 if check is positive

(d) coloring of safe edges, with previous check - decision making

(e) coloring of safe edges E_1-E_4 , with previous check - result
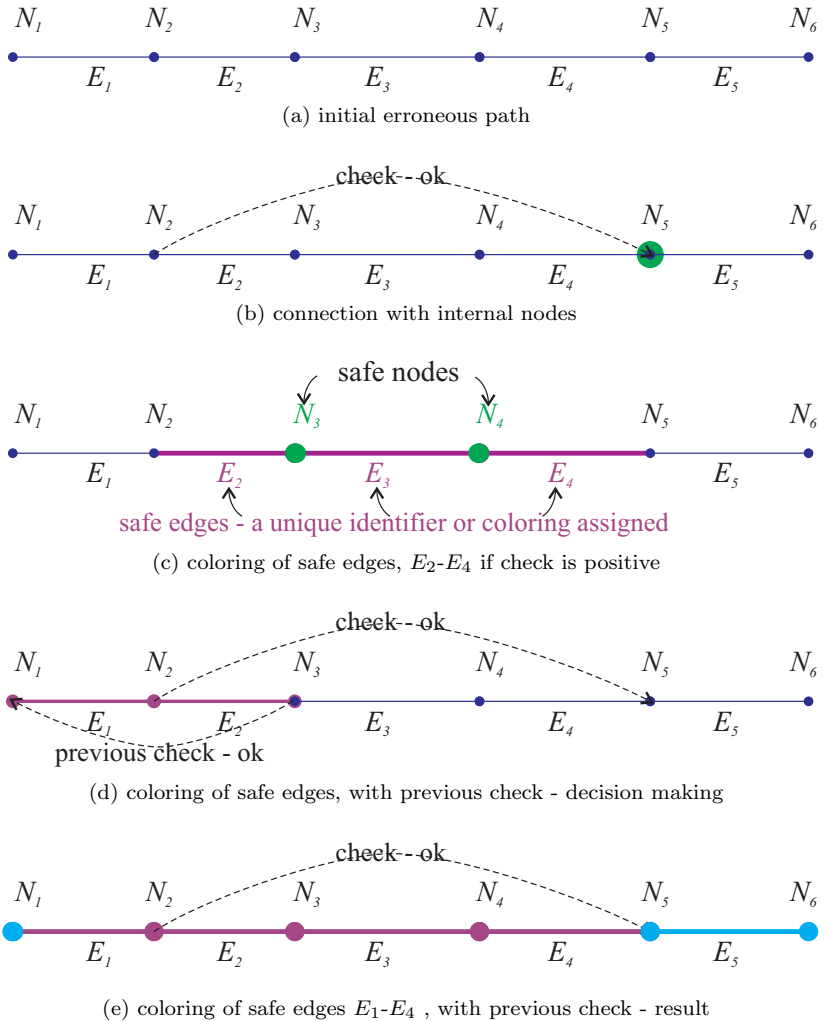
Figure 6.11: Successful verification of the segments by the internal alternative pathes and discrimination of the erroneous nodes.

(a) initial erroneous path.

(b) connection with internal nodes

(c) Narrowing erroneous path to N_2-N_5 after failed check

(d) Narrowing erroneous path with previous check - decision making

(e) Narrowing erroneous path to N_3-N_5 with previous check - result
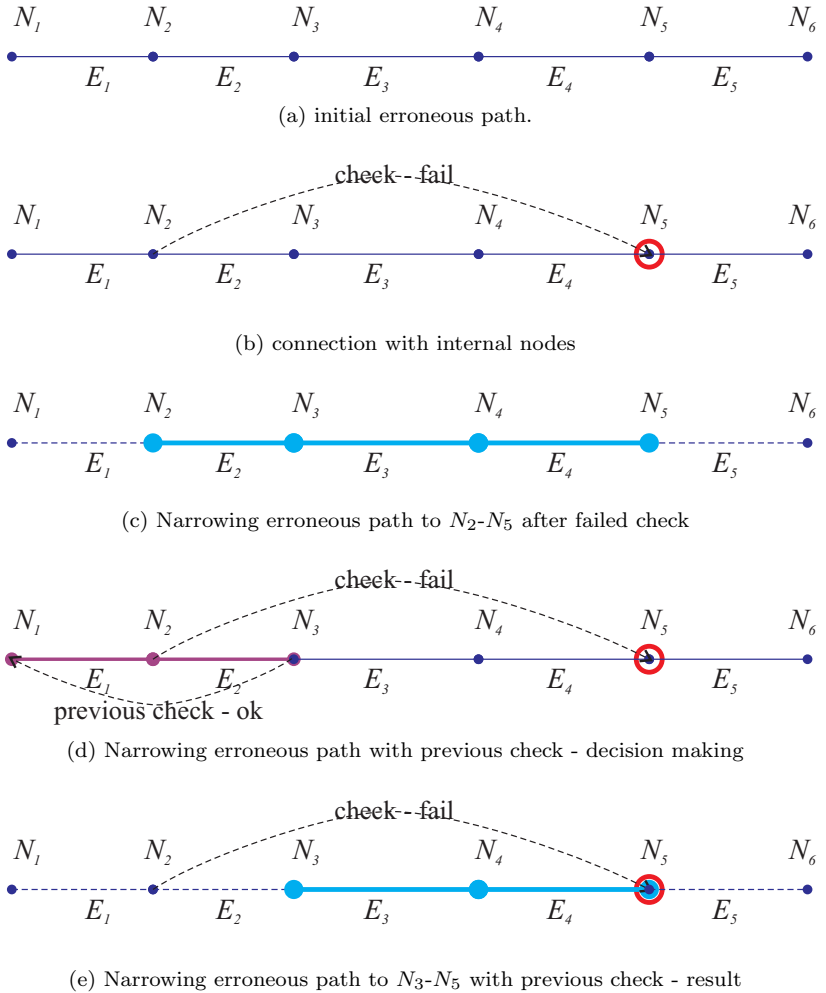
Figure 6.12: Failed verification of the segments by the internal alternative pathes and discrimination of the erroneous nodes.

pathes among erroneous nodes or between an erroneous and a verified node, as described in D.2.2.

It naturally follows that expected noise propagation ϵ is a very important criterion for the classification of erroneous or safe nodes. Therefore, the following section focuses on the evaluation of justified and the suitable for the particular conditions ϵ.

6.2.5   Criterion for the Error Detection

Measurement Noise Propagation

Previous sections discussed an approach to detection and localization of the topological error based on the comparison of the computed voltages. A discrepancy detected between two voltage evaluations is indicating an error. Let us focus now on this discrepancy or how large should it be to indicate an error - criterion for the error detection.

Measurements of electric parameters, as discussed in Section 5.2, are not exact - they contain noise, which can be described by the probability distributions, and measurement errors, which are disregarded here. Therefore, proposed sequential computation of the busbar voltages along the network will cause noise propagation in the computed values. We can, however quantify this noise and obtain voltage probability distributions, which gives us indication of the possible error margin.

Consider a Π-model of the transmission branch, single line diagram and detailed derivation is shown in Appendix B and in Fig. B.1. Given the voltage and the flows[2] in the beginning of the line, voltage in the end of the line can be computed as [2]:

$$\underline{U}_2 = -\underline{A}\underline{U}_1 - \underline{B}\frac{\underline{S}_1^*}{\underline{U}_1^*} \tag{6.9}$$

where $\underline{A}$, $\underline{B}$ are complex numbers depending on the parameters of the transmission branch.

Voltage and flows in (6.9) are random variables (rv). Since both the first and the second term in (6.9) contain voltage $\underline{U}_1$, resulting terms in (6.9) are not independent and the standard method of cross-variance [66], Appendix C.1.2 cannot be applied directly to subtract these. However,

---

[2]if measurements of current, including the angle between current and voltage are available in SCADA, the analysis can be simplified.

numerical characteristics of the pdf and, thus, tolerance range for the determined voltage values can be easily obtained applying a well-known Monte-Carlo method [66].

It is assumed that measurement errors of the angle and magnitude are independent normally distributed, although this assumption could be easily abandoned if more information is available. Let us notice that the second term in (6.9) follows Cauchy distribution Appendix C.1, [66], however, we assume that $\underline{U}_2$ is bivariate nrv, since in the parameter region compliant with the physical properties of power systems the obtained Cauchy distribution is close to normal. Neglecting dependency of the terms, we can also support the assumption on resulting $\underline{U}_2$ being nrv by the central limit theorem implications [66].

On the implementation side, Monte-Carlo method involves performing given number of trials and storing those results, thus, for the large networks its application can be restricted by computer memory size. In this case, once computed, set of random voltage values can be described by the numerical characteristics of multivariate normal pdf, i.e. expectation and covariance matrix. This would allow to significantly reduce demands on memory. A method for rv simulation from the distribution parameters is described in Appendix C.3, [66].

Perhaps, analytical expressions for the voltage pdf could also be derived when introducing feasible simplifications, this, however, is outside of the focus of the present thesis.

Comparison of the Voltage

In order to compare stochastic evaluations of two voltages, first we subtract them. Assuming that the voltage evaluations are independent, we can apply cross-correlation (also refereed as cross-variance) to pdfs $\underline{V}^{(1)}$, $\underline{V}^{(2)}$ to determine pdf of their difference:

$$f(\underline{V}_1 - \underline{V}_2)(\underline{z}) = (f_{V1} \star f_{V2})(\underline{z}) = \int_C f_{V1}^*(\underline{\tau}) f_{V2}(\underline{z} + \underline{\tau}) d\underline{\tau} \qquad (6.10)$$

where $\star$ is a cross-correlation function, f is a probability density function of a complex random variable, f^* is the complex conjugate of a pdf, $\underline{z}, \underline{\tau}$ are complex variables, C is the complex number space. An illustration on this method is provided in Appendix C.2. It is also applicable to independent non-gaussian distributions. If independence of voltages

$\underline{V}^{(1)}$, $\underline{V}^{(2)}$ cannot be assumed, analytical derivations lead to complicated expressions, instead one can apply numerical simulation to obtain pdf of the voltage difference.

Secondly, having pdf $f(\underline{V}_1 - \underline{V}_2)$ we can compute probability that voltage difference does not exceed some value value $\underline{\vartheta}$:

$$P(|\underline{v}_1 - \underline{v}_2| < \underline{\vartheta}) = \int\limits_{|\underline{z}|<\underline{\vartheta}} f(\underline{V}_1 - \underline{V}_2)d\underline{z} \qquad (6.11)$$

where $\underline{v}_1$, $\underline{v}_2$ are the values of random voltages, $\underline{\vartheta}$ is a user-defined tolerance for voltage difference, which can be derived from experience with the particular network, measurement infrastructure and variance of voltage.

Simplification of the integration intervals, leads to an approximate expression:

$$P(|\underline{v}_1 - \underline{v}_1| < \underline{\vartheta}) \approx \int_{-\vartheta_i}^{\vartheta_i} \int_{-\vartheta_r}^{\vartheta_r} f(\underline{V}_1 - \underline{V}_2)dz_r dz_i \qquad (6.12)$$

where z_r and z_i are the real and imaginary parts of $\underline{z}$ and ϑ_r and ϑ_i are the real and imaginary parts of $\underline{\vartheta}$, respectively.

This indicator $P(|\underline{v}_1 - \underline{v}_2| < \underline{\vartheta})$ can be used to define a criterion, whether two voltage evaluations indeed represent the same voltage. User can specify strictness of the criterion by choosing combination of $\underline{\vartheta}$ and the acceptable probability threshold.

This indicator describes well the behavior of random variables, however, it is computationally demanding. In the context of the proposed algorithm, it even becomes impractical at the presently available computing power as computations shall be performed for every branch. Therefore, we seek for simplifications of this criteria.

Simplified Approach

To reduce computational burden, the following simplified error detection criterion is proposed. The difference between obtained expectations of the voltage is compared with maximal standard deviation of the two obtained voltages:

$$|V_{1r} - V_{2r}|_1 < 3 * \sigma_r \qquad (6.13)$$

$$|V_{1i} - V_{2i}|_1 < 3 * \sigma_i, \qquad (6.14)$$

where σ_r, σ_i are maximal standard deviations of the real and imaginary parts of two compared voltages, respectively.

6.3 Topology Identification

6.3.1 Outline of the Algorithm

Once the substations that possibly have topological error have been localized, we can proceed with the identification of the substation topology, i.e. to find matching busbars for each branch - lines and transformers connected to the substation. This is done based on the analysis of the voltages in the end of each branch and the assumption that similar voltages occur on connected ends. Several variations of topology identification algorithm are possible, but the general approach can be summarized as follows:

1. Save initial network model;

2. For each node $N_{e,j}$ from the set of erroneous node $\mathcal{N}_e$, repeat:

   (a) Restore initial network model;

   (b) Select next node $N_{e,j}$ from $\mathcal{N}_E$, modify network topology to exclude influence of the current erroneous node;

   (c) Estimate the state of the network, unless the errors are detected in determined state to go the next step, otherwise considered node $N_{e,j}$ does not have a topological error, hence, go to step 2 - test next node;

   (d) Compute voltage probability density function at the end of all the branches connected to erroneous node $N_{e,j}$ (substation);

   (e) If all the nodes in $\mathcal{N}_e$ have been considered go to step 3, otherwise go to the step 2.

3. Determine branch-busbar connections;

4. Verify obtained topology with state estimation.

If the network contains one busbar configuration error, then the correct state can be obtained once the influence of the error is excluded. This
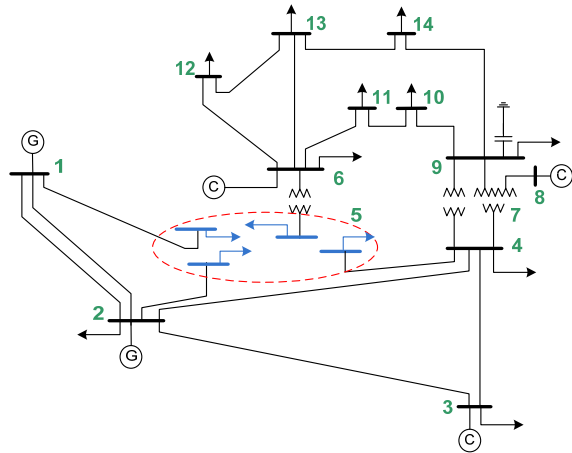
Figure 6.13: Modification of the network model to exclude influence of the topological error on the determined state.

can be done by "splitting" erroneous node into as many nodes as as there are connected branches to it, as shown in Fig. 6.13 with substation 5. Besides, all the injection measurements in substation 5 shall be removed from the measurement set or constraints, so that SE algorithm would be flexible to "push" flows caused by the topological error as injections. If there are multiple nonconforming errors, the analysis can be repeated for each of them. It is impossible to identify multiple conforming errors without additional information.

Such model modification ensures that the network state is not affected by the error, if the topology error was in the current erroneous node. The state can be computed with two approaches:

- State estimation;

- Network search.

State estimation should generally provide more accurate estimates than the network search. Due to the uncertainties such as measurement inaccuracy, the estimates of the voltage will not be exactly matching even for the branches connected to the same busbar. Therefore, we introduce a statistical criterion for identification of the connections based on

the voltage probability density. An approach using voltage probability density computation is discussed in details in the following subsection.

Both methods support error detection in the computed results. Therefore, if after the model modifications an error is still detected in the determined state (or SE does not converge), then the error is not in the currently considered substation and it can be disregarded in the further analysis. Other possibility is that there are multiple errors, which can be addressed with few modifications of the proposed approach, but a deeper discussion is out of the scope of this thesis.

Once the voltage pdf is obtained, the branch-busbar connections can be determined as described in the following subsections.

The topology should be verified with state estimation and full corrected system model. If verification fails, complete enumeration of the topologies is considered with local mini network state estimation, which implies a decreased computational burden. The best candidate topology or, possibly, several candidate topologies are used for the final verification with the full system model. It may turn out that still several candidate topologies are possible. In this case, a notification to the operator shall be provided and the topology shall be again verified in a more conclusive state of the power system - when it is possible to uniquely identify correct topology.

6.3.2 Computing Busbar Voltage pdfs

Voltage probability density computation is a necessary step in the proposed topology identification. Figure 6.14a shows the voltage probability density of a connection as a surface plot in 3D, while Fig. 6.14b shows the same data as a contour plot in 2D projection of the several chosen probability levels onto complex voltage plane.

Proposed computation algorithm slightly differs for two cases, when the branches connected to the erroneous substation are:

- Branches with known parameters;

- Branches with uncertain parameters, such as transformer tap position.

Let us first consider the case with known branch parameters. From the state estimation results we can obtain expected value of the voltage angle and magnitude as well as those variances as corresponding
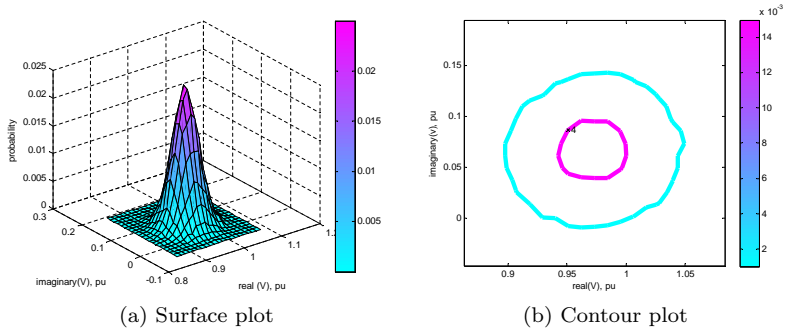
(a) Surface plot   (b) Contour plot

Figure 6.14: Graphical representation of voltage probability distribution

diagonal entries in the gain matrix G^{-1} at the convergence point [90], [93]. Covariances between the states of the different substation are also determined by the gain matrix, but we neglect those in the further analysis due to increased computational complexity. On the implementation side, multivariate normal pdf have analytical expressions and are either available in programming environment or can be easily programmed. The parameters of the probability density can also be obtained directly from the results of network search, which also gives correlation between voltage angle and voltage magnitude. However, if (in order to save memory) random values of voltage were described by numerical characteristics of pdf, the correlation of the the states at the different substations will be lost.

Figure 6.15a shows an example of voltage pdfs at the connections of erroneous substation, i.e. voltages in the connected transmission lines or transformers with known tap changer position. The black squares show true location of the busbar voltages computed with power flow.

A weak point of the suggested scheme is the dependency on the accuracy of the parameters of connected branches. If inaccuracies in branch parameters are suspected, it is necessary to introduce slight modifications of the algorithm.

By removing the erroneous substation and connected to it branches with possibly erroneous parameters from the network model, we can obtain correct state estimates for the remaining busses of the network (similarly to as described above, injection measurements from the first degree neighbors of the erroneous substation shall be excluded from the measurement set). From the distributions of voltages in neighboring

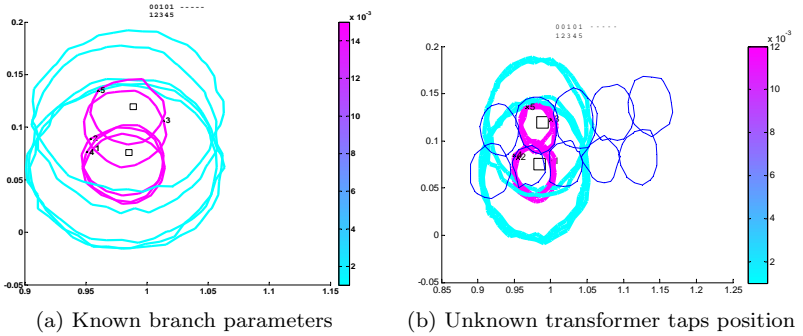(a) Known branch parameters   (b) Unknown transformer taps position

Figure 6.15: Voltage pdf for several substation connections.

substations, branch models and flow measurements, we can obtain pdfs of voltage in the erroneous node by applying Monte-Carlo method to simulate uncertainties (simulation method of a bivariate normal distribution is described in Appendix C.3).

Small uncertainties can easily be added by Monte-Carlo method to SE results, without influencing the topology identification algorithm. A large error in branch parameters could shift the location of the expected value and, possibly, influence the shape of the pdf. In this case the identification of the topology may become complicated. However, it should be possible to detect it by comparing obtained voltage pdfs graphically with each other. This is an additional valuable input for resolving the problems in SE.

Unknown tap position of the transformers imposes similar problems as large error presence in the branch parameters. Simultaneously, the information about possible tap positions is available from the transformer data sheet and, therefore, a set of possible transformer models is known. Assuming that a typical transformer is equipped with tap changers in the range of 10 % and the regulation step is 1.25 %, we can obtain voltage distributions as in Figure 6.15b. In this figure, the probability levels corresponding to several off-nominal tap positions are shown by the blue lines (same levels as magenta for the rest of the branches). In this case, the unknown taps position does not influence conclusion on the substation topology. It is clear that transformers are connected to different busbars, in addition most likely tap changers position can be identified. In other cases, the algorithm may detect several possible topologies depending on the tap position. If such a situation occurs,

perhaps, all the possibilities shall be evaluated by running the SE on full or local area network.

6.3.3   Determining Busbar Connections

Voltage pdf plots can be analyzed by the operator, however with the growing number of connected branches it might become complex, not obvious and not adequate for real time operation. Thus, a recognition algorithm is required.

The busbar voltages corresponding to several connections are random variables. Assuming that SE errors in the determined voltages are independent, we apply cross-variance as discussed in Section 6.2.5 to compare mutually these voltages. For the substation topology identification, the total number of voltage to be compared is much smaller than for the voltage error localizations and is feasible in the real time application. In the result of computations, we obtain a matrix of probabilities $\mathbf{P} \in \mathbb{R}^{n \times n}$ of the voltage differences not exceeding the threshold ϵ:

$$\mathbf{P} = \begin{bmatrix} P(|\underline{v}_1 - \underline{v}_1| < \underline{\vartheta}) & \dots & P(|\underline{v}_1 - \underline{v}_n| < \underline{\vartheta}) \\ P(|\underline{v}_2 - \underline{v}_1| < \underline{\vartheta}) & \dots & P(|\underline{v}_2 - \underline{v}_n| < \underline{\vartheta}) \\ \vdots & \ddots & \vdots \\ P(|\underline{v}_n - \underline{v}_1| < \underline{\vartheta}) & \dots & P(|\underline{v}_n - \underline{v}_n| < \underline{\vartheta}) \end{bmatrix} \quad (6.15)$$

This matrix is symmetric, thus $\frac{1}{2}n^2$ computations are needed.

The values of the probabilities depend on several empirically chosen parameters, yet we are not specifically interested in the probability level itself but rather in relative values of these probabilities. To reduce the subjective factor, we can "normalize" probabilities of cross-variances to average value of auto-variances and define the connection matrix $\mathbf{P_c}$:

$$\mathbf{P_c} = \begin{bmatrix} \frac{P_{11}}{P_{11}} & \cdots & \frac{P_{1n}}{0.5(P_{11}+P_{nn})} \\ \\ \frac{P_{21}}{0.5(P_{11}+P_{22})} & \cdots & \frac{P_{2n}}{0.5(P_{22}+P_{nn})} \\ \\ \vdots & \ddots & \vdots \\ \frac{P_{n1}}{0.5(P_{11}+P_{nn})} & \cdots & \frac{P_{nn}}{P_{nn}} \end{bmatrix}, \quad (6.16)$$

where $P_{c,ij} = \frac{P_{ij}}{0.5(P_{ii}+P_{jj})}$, P_{ij} are the probabilities - matrix entries in the previous Expression 6.15.

Entries in matrix $\mathbf{P_c}$ corresponding to connected elements are much higher than disconnected ones. Applying some discretization step, for example 0.8, the connection matrix transforms into a binary matrix, then subtracting identity matrix, we obtain the adjacency matrix of the substation:

$$\mathbf{A_s} = \mathbf{P_{c,bin}} - \mathbf{I}. \tag{6.17}$$

Finally, grouping of the connections can be done applying iteratively, for example, a breadth-first search algorithm as in Appendix D.1.

One should not exclude the possibility that the results of the connection identification might be not completely clear due to specific conditions in the network and associated uncertainty. In this case, the problematic bus together with the connected equipment are extracted to form a mini network and state estimation to a number of most likely topologies is applied, to determine best fit. For such small network, computation will be much faster than for the whole network. Alternatively, if the security of the system is not violated operator can wait for several snapshots, when identification results will be clear.

6.4 Illustrative Example

6.4.1 Test System

Performance of the proposed algorithms is studied on the example of IEEE 300 bus test system Fig. 6.16 [26]. Furthermore,

- The data for the electrical parameters is provided in Appendix A;

- Availability of the active and reactive power flow measurements on one end of each branch is assumed;

- Voltage magnitude measurements are installed at each substation;

- PMU measurements are installed at substation 4 and 216;

- The accuracy class of CT and VT is 0.6, as in Tables 5.1, 5.2. Resulting accuracy of the measurement chain for power flow measurement is assumed to be $\sigma_f = 1.5\%$ and for the voltage measurement $\sigma_V = 1.0\%$.
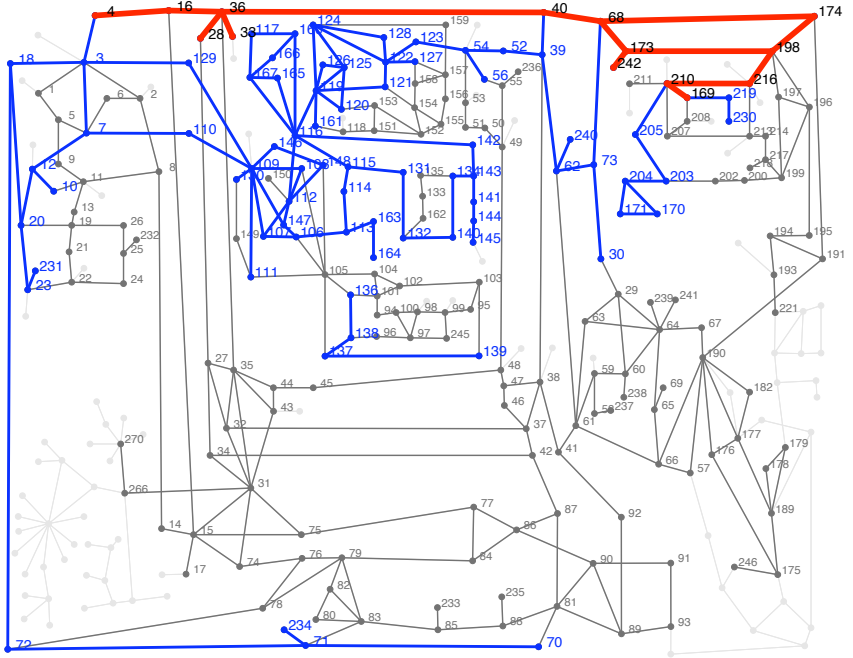
Figure 6.16: Single line diagram of IEEE 300 bus test system. Voltage levels are shown by the descending thickness of the lines for 345, 230, 138-115 kV and light gray color for the lower voltage network.

The system has 411 branches and 4 transmission and subtransmission voltage levels - 345, 230, 138, 115 kV and below. The analysis will be focused on the transmission level - 380 and 220 kV, since proposed algorithms were primarily designed for transmission network.

The results summarized below either capture algorithm performance statistics or, when particular conditions are simulated, represent typical case, which was confirmed in other simulations not included in the thesis.

6.4.2 Analysis of the Network

Flows and Network Connectivity

The proposed algorithm uses voltage difference in both magnitude and the angle to detect substation busbar connection error. It raises an immediate question, if the difference of the voltages on the disconnected busbars is sufficiently large not to be mistaken to a measurement noise. In real operation the number of the substations with regularly changing topology is limited and such analysis can be performed by power flow computations. Of course, power system experiences a large variety of operating conditions, in which the flows and voltage angles will change significantly. To keep confidence in the algorithm feasibility and awareness of the limitations, one can run combination of the off-line power flow analysis for the "typical" situations with an on-line power flow for the current operation point and set of potential topologies.

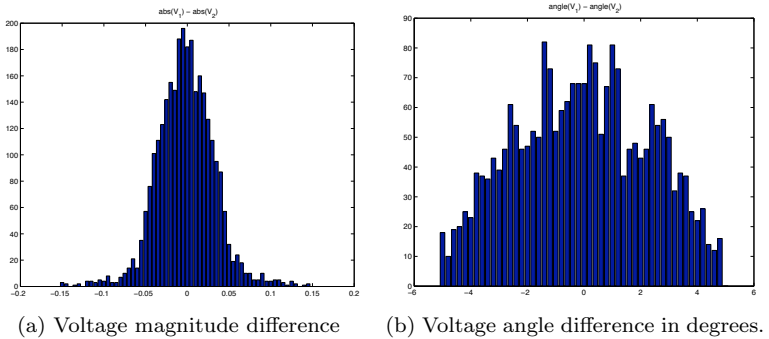(a) Voltage magnitude difference   (b) Voltage angle difference in degrees.

Figure 6.17: Distribution of the busbar voltage difference.

Power flow results for the studied network are summarized in Fig. 6.17 - 6.18. Here probability distributions are shown for the voltage magnitude and voltage angle differences at two disconnected substation busbars, applying brute-force analysis for all the substations, all possible topologies for which power flow has converged, splitting total substation load equally between two busbars and neglecting whether particular topology modification is meaningful for the system operation. It can be observed that voltage magnitude difference is smaller than 0.018 pu in approximately 42% of the cases, while voltage angle difference does not exceed 3.12 *deg* in about 61% of the cases. These limits correspond to 3σ of

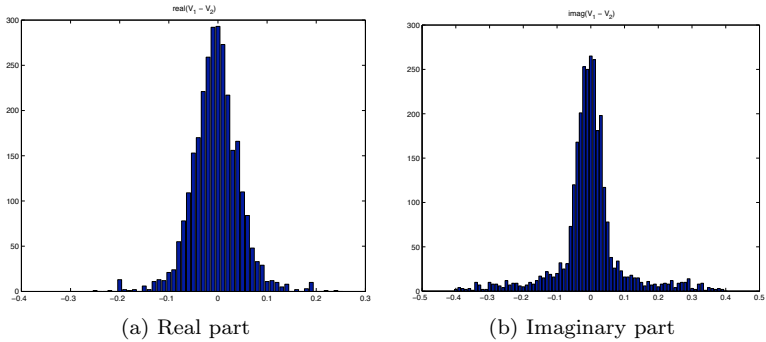(a) Real part   (b) Imaginary part

Figure 6.18: Distribution of the busbar voltage difference.

the voltage measurement transformer of accuracy class 0.6. Both limits simultaneously are not exceeded in 35% of cases.

Analyzing in the similar way results of the power flow computations for the real and imaginary parts of the voltage, we obtain that for the real part in 70% of cases the difference does not reach 0.045 pu. For the imaginary part in 31% of cases the difference is smaller than 0.018 pu. Combination of both limits is not restrictive in 30% of cases.

The sequential computations in the proposed algorithm raise concern, whether the noise propagation will endanger error detection capability. Let us determine what is the distance between the nodes or what is the number of necessary sequential voltage computations for the sample network. In case of the error presence on the PMU path, the maximal distance equals to the length of the path. In the addressed system, this distance is 8 nodes. If the topological error is not on the shortest PMU path, the number of sequential computations depends on the error location - distance till the PMU path.

Figure 6.19 shows characteristics of the network. If computations of the voltage start from an arbitrary node in the network and continue in accordance with breadth-first search, then depending on the initial node every k-neighborhood will contain different number of nodes. An average number of nodes depending on k-th degree of neighborhood is shown in Fig. 6.19a. It can be concluded that in average, 20-th degree neighborhood will contain almost entire network, while 25-th degree is enough to cover whole network. Fig. 6.19b shows distribution of the distance from the initial node, which allows to cover the entire network.

(a) Average number of nodes in k-th neighborhood

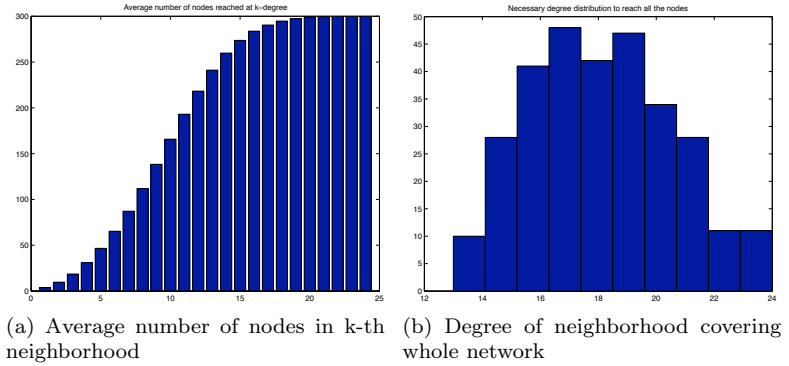(b) Degree of neighborhood covering whole network

Figure 6.19: Characteristics of the network graph.

For example, there are 10 nodes in the network that would lead to full coverage in 14 steps and 40 initial nodes that would cover entire network in 16 steps. It shows again that for the majority of the cases 20 steps will be sufficient to reach most distant node.

Naturally, these numerical characteristics will change for larger transmission networks. On the other hand, one can expect larger number of PMU installations and possibility to separate network in several regions. The distance from a path (PMU path) is shorter than from analyzed single node. Besides, it can be noticed that the analyzed network has relatively many radial connections, which is disadvantageous for the connectivity characteristics and for the proposed algorithm. Such structure of the networks is more typical for distribution networks, therefore the performance of the algorithm on realistic network will most probably be better.

Measurement Error Propagation

Theoretical measurement noise propagation is studied in Figures 6.20-6.25. First we analyze the shape of voltage distribution and possible changes with the distance. Then, we consider whether the chosen distribution modeling approximations are viable and simulations are accurate. Having the confidence in these results, we study noise influence and propagation with the distance from initial path.
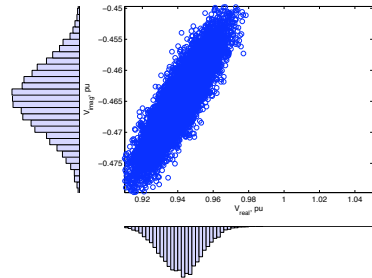
Figure 6.20 shows voltage distribution results of 10^4 Monte-Carlo trials, applying random measurements errors from the given distribution for
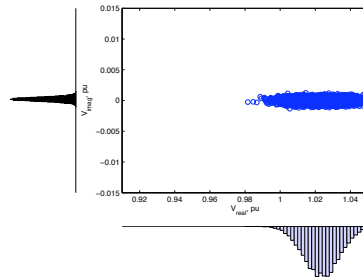
(a) First substation, st.4
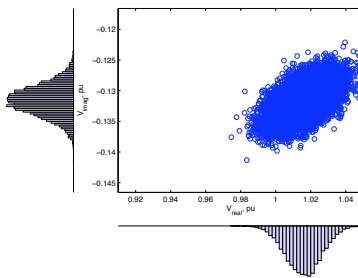
(b) Second substation, st.16   (c) Eighths substation, st.216

Figure 6.20: Voltage distribution at increasing distance from the initial node.
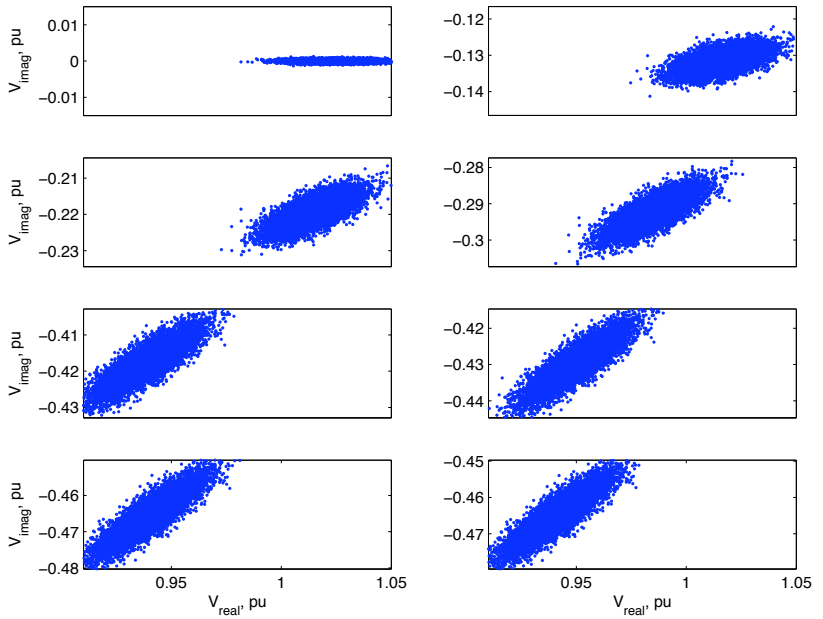
Figure 6.21: Voltage distributions along the path of substations 4, 16, 36, 40, 68, 173, 198, 216 respectively from left to right and top to down.
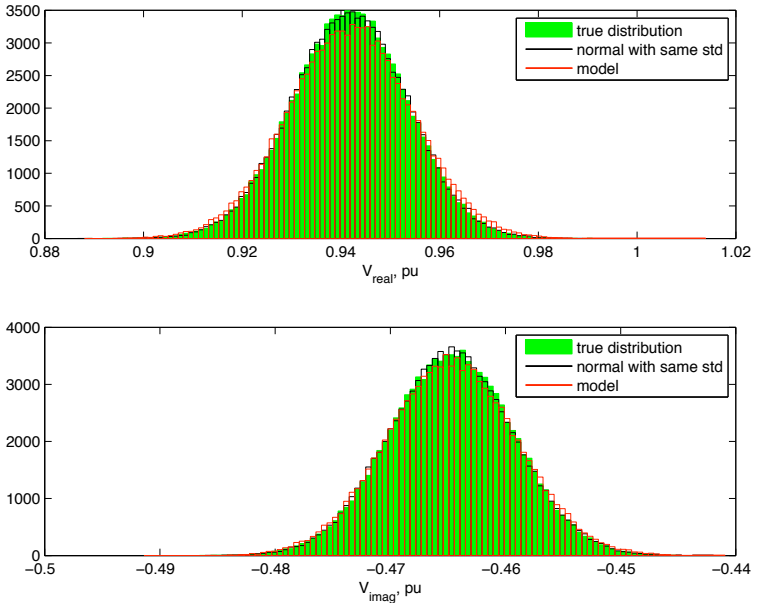
Figure 6.22: Comparison of the modeled and the real distribution.

each sensor along the path of substations 4, 16, 36, 40, 68, 173, 198, 216 respectively. The scaling of ordinates and abscissas is kept the same for all the plots for easier comparison of the results. The ordinate axis is shifted with the expectation of the distribution.

One can notice an increase of the correlation between the terms in the Expression (6.9) with the distance, whereas the increase of the standard deviation is not very significant. From the statistical point of view, the random variable computed in the chain with the input of independent normally distributed random variables shall sustain properties of normally distributed variable, i.e. it should be possible to determine voltage error margins with some level of confidence. Another visualization of the same study is provided in Figure 6.21. The scaling of axes is kept the same for all the plots.

Figure 6.22 shows real voltage distribution and the modeled normal distribution for the real and imaginary projections of the voltage at bus 216. A simplified analysis of the modeling can be performed visually comparing the histograms. The approximation is quite accurate.
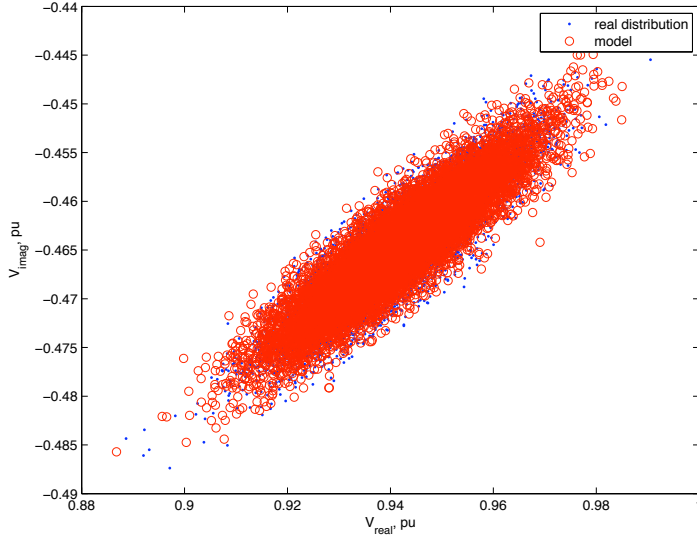
Figure 6.23: Comparison of the covariance of the modeling approxima-
tion and the real distribution.

Deviation from the shape of the normal distribution can be explained
by the non-gaussian (Cauchy) distribution of the second term in (6.9).
Figure 6.23 shows a good approximation of the covariances of the real
distribution and its model.

The analysis above demonstrated that chosen modeling and simulation
approach and assumptions are feasible. Thus, we can use numerical
characteristics of the distribution, i.e. standard deviation to study how
the error propagates from the initial node throughout the network and
indirectly to study the performance of the algorithm.

Figures 6.24 -6.25 show standard deviation of the voltage real and imag-
inary part depending on the distance from the PMU path by Box-and-
whiskers plots. Here median, lower quartile and upper quartile (0.25
and 0.75 quantiles, or simplistically, intervals containing 25% and 75%
of the values) are shown by the horizontal line and the box, correspond-
ingly. Whiskers extend from the end of the box to the most extreme
values within 1.5 interval of the interquartile range. Outliers are data
with values outside the ends of the whiskers.

Figure 6.24 addresses noise propagation in the network, when all the

Figure 6.24: Box-and-whiskers plot of standard deviations of voltage pdf (dots) - real (top) and imaginary (bottom) part vs degree of neighborhood from PMU path. Noise at PMU path is same as at the initial node.
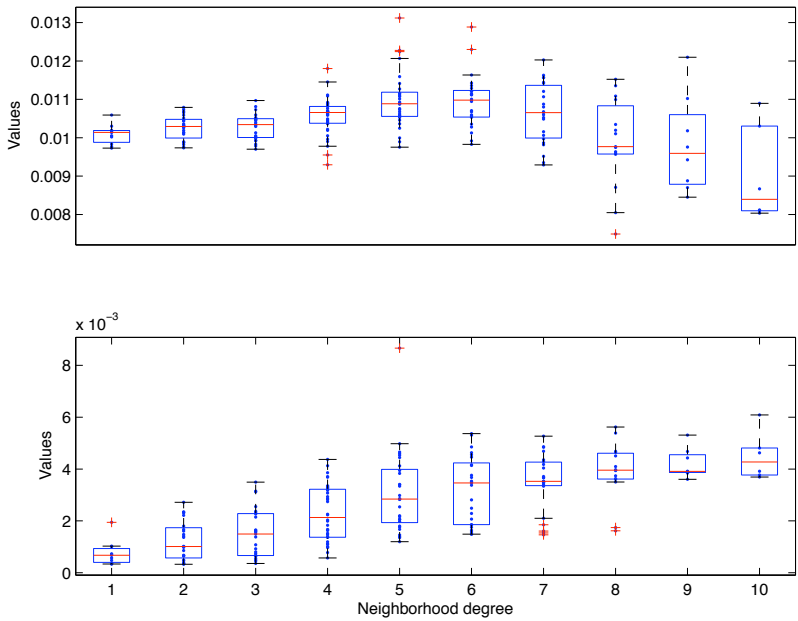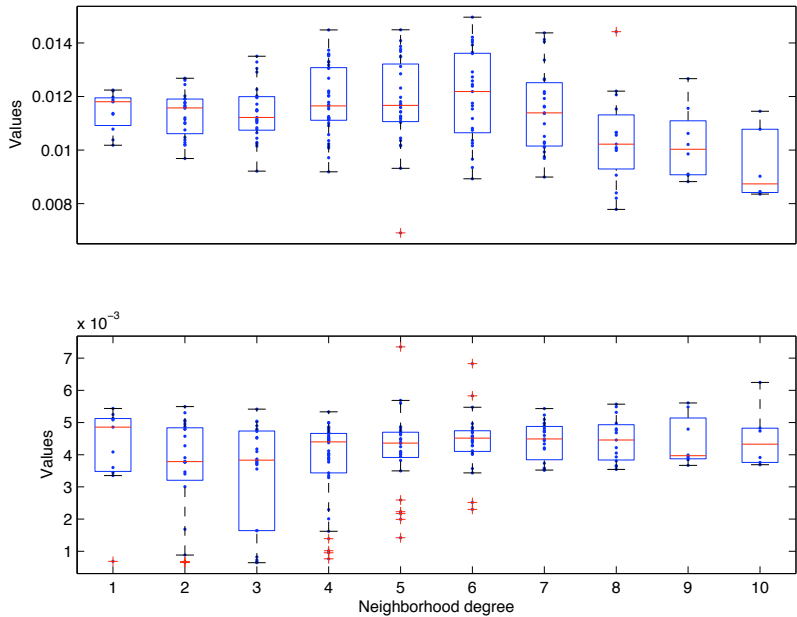
Figure 6.25: Box-and-whiskers plot of standard deviations of voltage pdf (dots) - real (top) and imaginary (bottom) part vs degree of neighborhood from PMU path. Noise at PMU path is computed from the initial node.

nodes at PMU path are treated as initial, i.e. standard deviation of the voltage magnitude is $\sigma_v = 0.01$ and standard deviation of the angle is close to zero $\sigma_\theta \approx 0$. This is to obtain "clean" result in terms of distance from the initial nodes. One can observe that for the real voltage part standard deviation does not increase very significantly and stays below 0.013, although the spread of the standard deviations increases. This can be explained by the contribution of several factors: the networks at higher distance have smaller flows with smaller absolute measurement errors and, possibly, increase of the voltage angle, turning the phasor with changing its' projections. For the imaginary part the steady trend of increasing standard deviation can be observed, although the increase is not dramatic - it does not exceed $\sigma < 0.006$.

Figure 6.25 shows the same type of study, when the standard deviations of the voltage at PMU path were not set as the same for the initial node, but instead the values are used, as obtained at the first walk along the PMU path. In the real part we observe an increase of the spread of the standard deviations with the distance, but hardly an increase of the median values. In the imaginary part the standard deviations are somewhat steady - they do not increase with the distance.

These results also suggest that noise propagation may vary and shall be studied for the particular network and operating conditions.

It should be noticed that the best accuracy and avoidance of the voltage expectation drift due to repetitive computations was improved by taking always the first computed value for the following computations.

6.4.3   Detection and Location of the Error

In the first simulation scenario, substation 3 has a topological error: busbars are split and branches connecting substation 1, 4 and 129 are at busbar A, while branches to 2, 7, 18, 249 are at busbar B. Then network model used for state estimation was not corrected and assumes substation 3 with merged busbars.

Figure 6.26 shows distance of the nodes from the initial PMU path. Considered substation 3 is a fist degree neighbor. Figure 6.27 shows voltage difference between two computed voltage values, real and imaginary part for each node visited twice before detection of the error. The error is detected at substation 5, when difference between two values in imaginary part reaches almost 0.25 p.u.
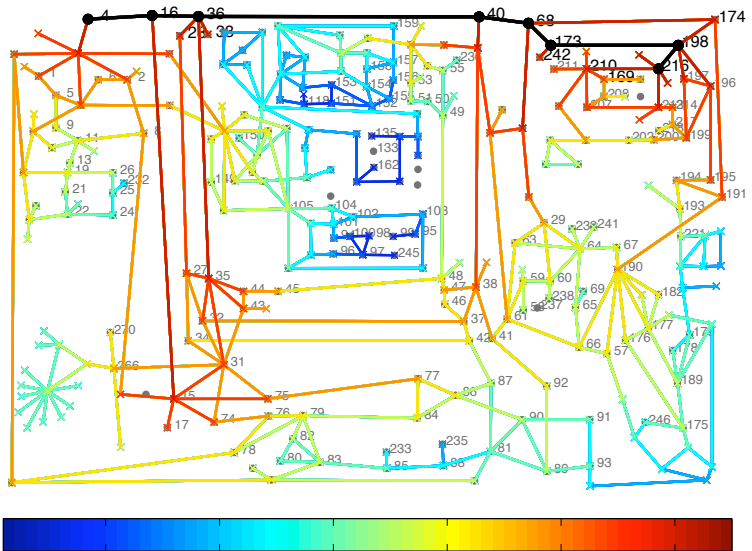
Figure 6.26: Coverage of the nodes at 1-10 step. Black line shows PMU path, dark blue corresponds to most distant lines.
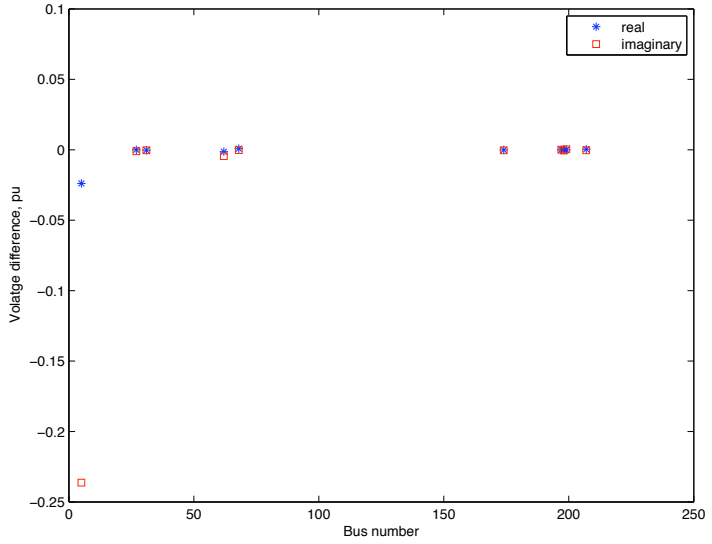
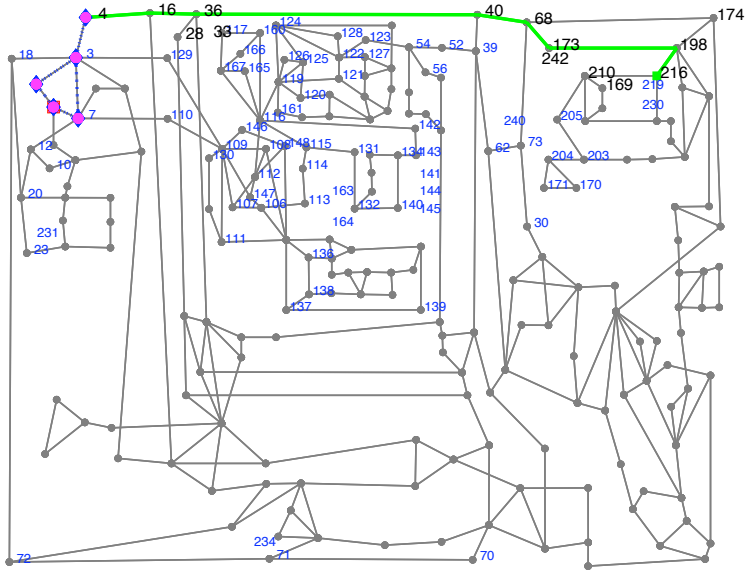Figure 6.27: Discrepancy in computed voltage.

Figure 6.28: Identified Bad path

Table 6.1: Values of the voltage standard deviation

Node	Angle	Magnitude
7	0.00114	0.000380
18	0.00137	0.000473
129	0.00133	0.000398
1	0.00139	0.000437
2	0.00113	0.000417
4	0.00011	0.000375

Established bad path is shown in Figure 6.28. It comprises nodes 4-3-7-5-1-3-4 and after pre-processing reduction limits to 3-7-5-1-3.

Next, the error location algorithm is applied. The first detected pair to be verified is 5-7 with the path 7-12-10-11-9-5, which checks. The next pair 5-16 fails with path 5-9-11-8-14-15-16. The erroneous path is reduced to nodes 3-7-5. The next check of 7-16 fails and the erroneous path becomes 3-7, in which the error cannot be localized further. Thus, these nodes are to be checked by the topology identification algorithm.

6.4.4 Topology Identification

Having two suspected substations, we remove first one of them and run state estimation, then restore initial model and repeat the procedure for the other substation. In both cases SE algorithm converges. When substation 3 is removed from the model, value of the SE objective function is 5451, while removing substation 7 gives much higher value 121908. It becomes clear that substation 3 has a problem.

The values of the standard deviation of the voltage estimates at the substation 3 busbars are provided in Table 6.1 obtained from the results of state estimation. These results can be transformed into rectangular coordinates as described in Appendix C.3. Thus, numerical characteristics of the voltage pdf are obtained. Figure 6.29 shows contour plots of the voltage pdf in rectangular coordinates. From this figure one could derive the preliminary conclusion that line connection groups 2, 7, 18 and 1, 4, 129 belong to different busbars. Connection of the line towards bus 249 to busbars cannot be determined at this stage, as 249 is isolated from the rest of the network.

We compute cross-variance for each combination of the voltage pdfs.
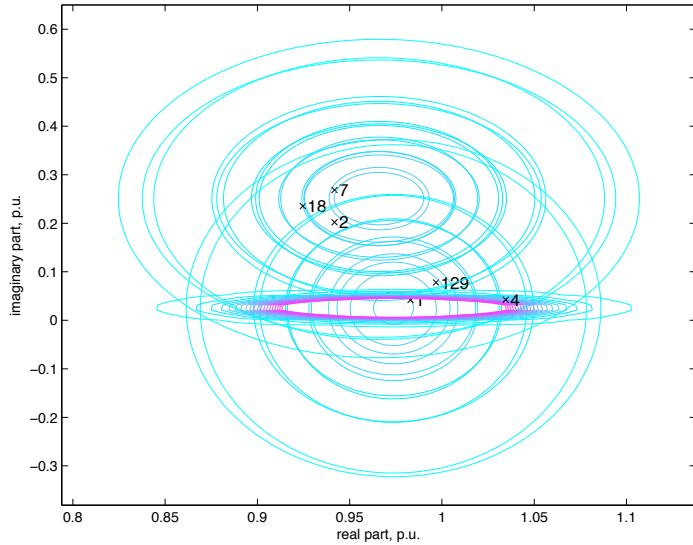
Figure 6.29: Voltage pdf at substation 3, contour plot

Two results are shown in 6.30a and 6.30b for the lines connected to the same busbar - 2-7 and different busbars 2-4.

We choose criterion $P(|\underline{v}_i - \underline{v}_j| < 0.01)$ and integrate cross-variance in the interval $[-0.01, 0.01]$ for both real and imaginary part, i.e. $\vartheta_i = \vartheta_r = 0.01$. The resulting probability matrix for the same sequence of the lines as in Table 6.1 is as follows:

$$\mathbf{P} = \begin{bmatrix} 0.3591 & 0.3141 & 0.2775 & 0.2666 & 0.3500 & 0.3219 \\ \dots & 0.2794 & 0.2413 & 0.2337 & 0.3076 & 0.2706 \\ \dots & \dots & 0.3942 & 0.3738 & 0.2559 & 0.4394 \\ \dots & \dots & \dots & 0.3560 & 0.2465 & 0.4171 \\ \dots & \dots & \dots & \dots & 0.3416 & 0.3128 \\ \dots & \dots & \dots & \dots & \dots & 0.4613 \end{bmatrix} \quad (6.18)$$

Applying normalization, i.e. dividing each entry by the average of the

(a) Lines to substation 2 and 7   (b) Lines to substation 2 and 4
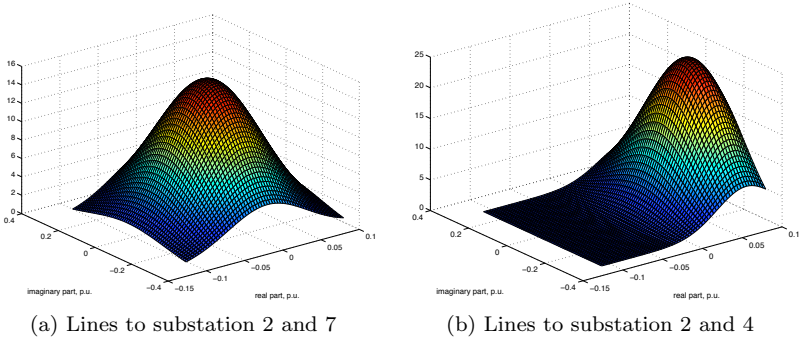
Figure 6.30: Cross-variance of the voltage pdfs.

corresponding diagonal values, we get normalized matrix:

$$
\mathbf{P}_c = \begin{bmatrix}
1.0000 & 0.9839 & 0.7368 & 0.7455 & 0.9991 & 0.7849 \\
\ldots & 1.0000 & 0.7163 & 0.7355 & 0.9908 & 0.7307 \\
\ldots & \ldots & 1.0000 & 0.9967 & 0.6955 & 1.0272 \\
\ldots & \ldots & \ldots & 1.0000 & 0.7069 & 1.0208 \\
\ldots & \ldots & \ldots & \ldots & 1.0000 & 0.7793 \\
\ldots & \ldots & \ldots & \ldots & \ldots & 1.0000
\end{bmatrix} \tag{6.19}
$$

Applying discretization criterion 0.8, we get substation adjacency matrix:

$$
\begin{bmatrix}
1 & 1 & & & 1 & \\
1 & 1 & & & 1 & \\
& & 1 & 1 & & 1 \\
& & 1 & 1 & & 1 \\
1 & 1 & & & 1 & \\
& & 1 & 1 & & 1
\end{bmatrix} \tag{6.20}
$$

Processing the connections we obtain connection encoding 001101 for lines to 7, 18, 129, 1, 2, 4, i.e. two groups 7, 18, 2 and 129, 1, 4. The identified substation topology is correct.

Similar analysis was applied to topological error at substation 190 and several others, randomly selected. The proposed algorithms succeeded in identifying the correct topology in all studied cases.

6.5   Concluding Remarks

The proposed algorithms for the identification of the node with a topological error and identification of the correct topology shows good performance.

The algorithms impose higher requirements on measurement infrastructure compared with classical state estimation, explicitly in measurement redundancy. However, it is realistic even in the present power systems. Bad data could be confused as a topology error at the first stage of the error localization. But once the identification is performed, it is rather easy to recognize bad data impact.

The difficulty for the topology identification may arise for the cases, when voltages on disconnected busbars are very similar, both in magnitude and angle. In this case, it is impossible to identify or detect topology error by the discussed algorithms or any other, without obtaining information. First, perhaps, that is not a very common system state in the real operation. Second, for such conditions state estimation should not be "confused" by the impact of topological error and the state provided by it shall be very close to the actual. Therefore, the impact of the topological error is diminished.

Two other limitations, which are less relevant for large meshed networks, are the radial connections and islands. If removal of the problematic substation breaks the system into two islands SE produces an arbitrary shift in the voltage angles between these networks and the application of the method is limited in its present form. Similarly, it is not straightforward how to identify an error in the radial connection, yet some heuristic methods can be applied.

The indicated limitations do not appear to be critical for the practical implementation. Besides, the algorithms are transparent and intuitive for the operator, are easily scalable and parallelized for distributed computations. Therefore, the proposed algorithms could contribute to the improvement of the topological models in practice.

Chapter 7

Slow Model Variations

If the accuracy of the state estimation is increased it means that a more reliable representation of the power system is obtained. Thus, the operation and control functions can make better decisions. This chapter studies the influence of changes of the transmission lines' resistance due to temperature variations on state estimation performance. The possibility to account for this effect in state estimation is shown by the use of Line Heat Balance equation and weather data.

7.1 Introduction

The performance and reliability of SE is strongly dependent on the accuracy of the defined power system model.

A number of methods has been developed for model parameter verification and estimation, as summarized in [141], [2]. State vector augmentation and the residual analysis methods are addressing estimation of rather limited number of selected parameters, while processing of several sequential snapshots either by the enlarged conventional SE or Kalman filter is more suitable for the multiple erroneous parameter identification. The usefulness and importance of these methods are indisputable. Particularly, efficient application of these methods should be expected in case of relatively large parameter errors and its impact on SE in systems with high measurement redundancy. However, less

significant deviations may be difficult to distinguish from the impact of measurement errors.

Besides the initial errors in databases, some parameters may vary because of different operating conditions. Changes in line capacitance due to different line sags are small. The resistance of the transmission lines changes significantly with temperature, however it does not invalidate state estimation performance [141] and have not previously been considered in the models. We believe that further enhancements of SE accuracy, particularly important for the correct transmission losses allocation in nodal pricing markets, can be achieved nowadays when powerful computational capabilities and communication links are available.

This chapter addresses the impact of transmission lines' resistance changes due to line currents and ambient weather conditions on the state estimation accuracy, as well as the possibility to account for these changes.

7.2 Mathematical Model

7.2.1 Resistance Dependence on the Temperature

In practice, the conductor temperature varies in the range $0°$ to $60°C$ or even larger, resulting in changes of the line resistance.

Since the stranding of the conductor has a negligible effect on the DC resistance [73] and the conductor operates in the temperature range far from the melting point, temperature dependence can be determined as:

$$R_{T1} = R_{T0}[1 + \alpha_a(T_1 - T_0)] \tag{7.1}$$

where $\alpha_a = 0.0039 \ [C^{-1}]$ is the temperature coefficient for aluminium, R_{T0} and R_{T1} are the resistances at temperatures T_0 and T_1, respectively.

The AC resistance increases due to the skin effect. For even number layered ACSR conductors it can be determined with a good accuracy either by the analytical expressions or through precomputed R_{ac}/R_{dc} curves [73]. For the conductors with odd number of layers, the additional influence of the eddy currents and hysteresis losses in the steel core cannot be neglected and the AC resistance depends on both temperature and the current.

In the following computations, we assume even number layered conductors and linear dependence of AC resistance only on the conductor temperature, although nonlinear dependence could be accounted for in the similar manner.

7.2.2 Current-Temperature Relationship of a Conductor

The current-temperature relationship of a bare overhead conductor is addressed by IEEE standard [51], which is essentially based on the House and Tuttle method [48]. The overhead line temperature depends on the following conditions:

- Conductor material properties

- Conductor electrical current

- Conductor diameter and surface conditions

- Ambient weather conditions: wind, solar radiation, air conditions.

Assuming that changes of the power system state are relatively slow, we employ the steady-state models suggested in [51] for the transmission line resistance correction. The contribution of the mentioned above factors in steady state can be summarized by the Heat Balance equation [48], as follows:

$$I^2 R_{Tc} + q_s = q_c + q_r \tag{7.2}$$

where I is the conductor current, R_{Tc} is resistance at the conductor temperature T_c, q_c and q_r are the heat losses due to convection and radiation, respectively, q_s is the solar heat gain.

The expressions below determine heat losses and gain, while the input parameters are summarized in table 7.1. The units of measurements indicated in the table correspond to the coefficients in (7.3) - (7.5) and adopted from [51].

- The *solar heat* gain can be computed in W/ft, as:

$$q_s = \alpha Q_s A' \sin\theta \tag{7.3}$$

where $\theta = \cos^{-1}[\cos(H_c)\cos(Z_c - Z_l)]$. Solar absorptivity α increases with the conductor age depending on the atmospheric pollution and line operating voltage. A value $\alpha = 0.7$ can typically be used, if the exact value is unknown.

Table 7.1: Input parameters

Parameter	Source
Weather	
V_w	velocity of the air stream, ft/h
ϕ	angle between conductor axis and the air stream, deg
T_a	ambient temperature, $°C$
$Q_s(H_c, H_e)$	total solar and sky radiated heat flux, W/ft^2
Atmosphere - weather dependent	
$\rho_f(H_e, T_{film})$	air density, lb/ft^3
$\mu_f(T_{film})$	absolute viscosity of air, $lb/(ft \cdot h)$
$k_f(T_{film})$	air thermal conductivity coefficient, W/ft
Line-Sun layout - location and time dependent	
Z_c	azimuth[1]of sun, deg
Z_l	azimuth of line , deg
H_c	altitude of the sun, deg
H_e	elevation of conductor above the sea level, ft
Conductor	
D	conductor diameter, in
A'	projected area of conductor, ft^2 per lineal ft
ϵ	emissivity
α	solar absorptivity
R_{T_c}	resistance per lineal foot of conductor at T_c, Ω/ft
SCADA/EMS output	
I	line currents, A

[1] Azimuth is a the horizontal component of a direction - the angle along the horizon, with zero degrees corresponding to North, and increasing in a clockwise fashion [99].

- The *radiated heat* loss is in W/ft:

$$q_r = 0.138 D\epsilon \frac{(T_c + 273)^4 - (T_a + 273)^4}{100^4}, \qquad (7.4)$$

where T_c is conductor temperature. Similarly to solar absorptivity, emissivity ϵ also increases over the years: $\epsilon = 0.5$ is the approximate value to be used.

- Forced *convection heat loss* at low wind speed is in W/ft:

$$q_c = K_\phi k_f (T_c - T_a) \left[1.01 + 0.371 \left(\frac{D\rho_f V_w}{\mu_f} \right)^{0.52} \right] \qquad (7.5)$$

where $K_\phi = 1.194 - \cos(\phi) + 0.194\cos(2\phi) + 0.368\sin(2\phi)$ is a term that accounts for the angle ϕ between the wind direction and conductor axis, k_f, ρ_f, μ_f depend on air film temperature $T_{film} = (T_a + T_c)/2$.

After a more careful consideration of the required parameters one can conclude that input of just four direct measurements is necessary for the application of the method: *wind, air temperature, heat flux and the conductor current.*

Let us consider possible variations of the conductor temperature by changing a single parameter in the base scenario determined by the following conditions:

- wind: north-east, $V_w = 2$ ft/s;

- ambient temperature: $T_a = 10°C$;

- sun: $H_c = 49.0°$, $Z_c = 172.5°$, $Q_s = 91.93 \ W/ft^2$;

- current: 300 A;

- conductor: 397.500 ACSR 30/7, $D = 0.806$ in,
  $R_{25°C} = 0.235$ ohm/mile, $\epsilon = 0.5$, $\alpha = 0.7$,
  $H_e = 850$ ft, $Z_l = 90°$ west-east direction.

Atmospheric parameters, such as air density are calculated by the approximation formulas provided in [51].
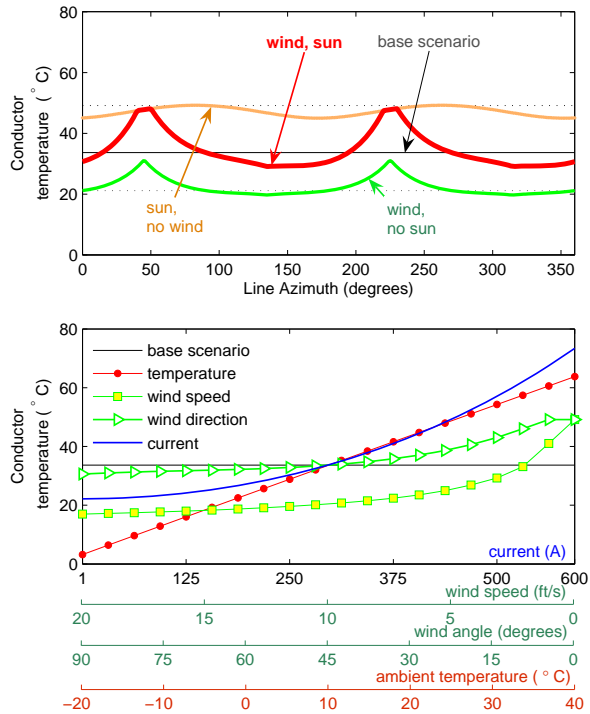
Figure 7.1: Influence of the single parameter variation on the conductor temperature

Fig. 7.1 shows the resulting conductor temperature variations. The upper plot addresses conductor temperature dependence on line azimuth Z_l, which indirectly impacts both the convected heat loss q_c and the solar heat gain q_s. Green and orange curves provided for a comparison evaluate these impacts separately: only angle ϕ changes at no sun conditions and only angle θ changes at no wind conditions. While the wind direction has slightly stronger influence than the sun, the combined impact of both parameters may result in approximately $20°C$ variations of the conductor temperature.

The bottom plots in Fig. 7.1 demonstrate the influence of the conducted current, ambient temperature, wind speed and direction on the wire temperature. One of the parameters is varied, while the others are kept constant as in the base scenario. The ambient temperature and the conducted current have a significant impact on the conductor temperature: for realistic ambient temperature variations in the range $[-20, 40]°C$ the conductor temperature varies in the chosen conditions from 0 to $60°C$. The conductor current was simulated from 0 to maximal conductor current carrying capacity limit of $600A$ causing $50°C$ increase. Wind blowing in perpendicular to the transmission line would produce $10°C$ cooling in comparison to wind blowing in parallel with the conductor. Realistic variation of conductor emissivity and absorptivity have little impact on the final evaluation of the conductor temperature.

The analysis of the temperature variations depending on the operating conditions shows that the variation range can easily exceed $50°C$ resulting in more than 20% changes of the conductor resistance, according to (7.1).

The measurements of the weather conditions may contain some error. Fig. 7.2 considers the influence of these uncertainties by Monte-Carlo simulations for the base scenario above and the increased wind speed $V_w = 5 \ ft/s$. In addition, it was assumed that the errors are normally distributed $N(\mu, \sigma^2)$, specifically:

- wind speed: $V_w \sim (5, 1)$, ft/s;

- ambient temperature: $T_a \sim N(10, 1)$, $°C$;

- sun flux: $Q_s \sim N(92, 5^2)$, W/ft^2;

- current: $I \sim N(300, 3^2)$, A;

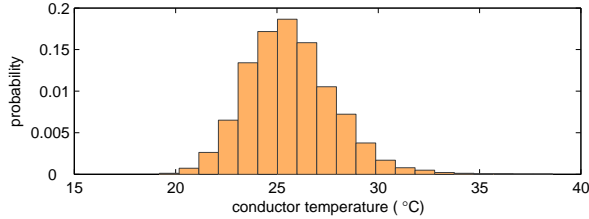- line: $Z_l \sim N(90, 5^2)$, deg, $H_e \sim N(850, 50^2)$, ft;

Figure 7.2: Probability distribution of the conductor temperature in presence of the parameters uncertainty.

Such combinations of uncertainties produce a standard error of $2°C$ (68.2% confidence interval). Thus, the described method of the conductor temperature calculation results in satisfactory accuracy in presence of realistic parameter uncertainty.

7.3   Proposed Modifications of SE Algorithm

The classical SE procedure can be modified to account for the discussed effect of the conductor heating in particular loading and weather conditions.

Fig. 7.3 shows the flow chart of the suggested algorithm. Analog measurements obtained by SCADA are processed by the 1st stage SE, followed by the resistance correction in accordance with estimated current and the weather conditions. The updated power system model is used then at the second stage SE. The system state is not expected to change drastically and the states obtained at the 1st stage seem to be a logical choice for the initial values of the 2nd stage SE. The following step is the decision about necessity to repeat resistance correction for all, or part of the lines. A small number of iterations is sufficient. The resistance correction may also be performed based on the measured current recomputed from the flow measurements values. However, one SE run may be suggested - at least due to possible lack of the necessary measurements in the system.

As an alternative to the algorithm in Fig. 7.3 that uses inputs for implicit conductor temperature calculations, the conductor temperature

measurement can be applied. For example, as discussed in [91] line thermal monitoring method based on PMU can be used.

The method described in subsection 7.2.2 was preferred for the discussion, as it is suitable for the simulation of thermal processes and is standardized. An additional advantage of this method is that it does not require installation of additional hardware: the weather conditions data can easily be obtained from the meteorological institutions usually having measurement stations at different locations around the country.
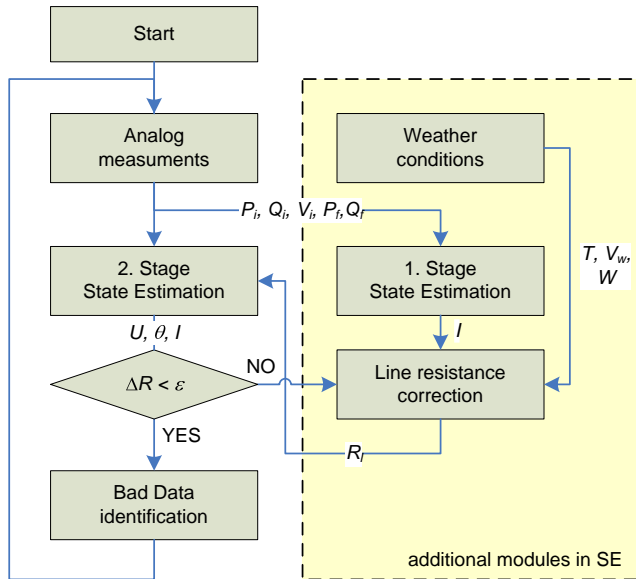

Figure 7.3: Proposed state estimation algorithm.

7.4 Illustrative Example

7.4.1 Test System

The study of the model inaccuracies impact on the SE results was conducted for the IEEE 14-bus test system [26]. The single line diagram of the system is shown in Fig. A.2.

The system consists of two voltage levels: busses 1-5 are operated at 132 kV and busses 6-14 at 33 kV. For the higher voltage lines 397.500 ACSR 30/7 conductor is assumed, as for the example in subsection 7.2.2, with $26 ft$ conductor spacing. For the lower voltage level 266.80 ACSR 26/7 conductor at $10 ft$ spacing is assumed having $R_{25°C} = 0.350 \ ohm/mile$ and $D = 0.642 \ in$. Line azimuths are:

$$Z_l = [90, 170, 160, 70, 160, 10, 60, ...$$
$$140, 10, 20, 30, 40, 100, 50, 80].$$

Since the selected test system represents a portion of the real power system in the Midwestern US (in February, 1962), the assumed location is Ohio and the geographical parameters are chosen accordingly: latitude $39°08'N$, longitude $84°31'W$, $H_e = 850$ ft, and the sun position can, thus, be calculated [99].

State estimation includes measurements of all the voltage magnitudes, all active and reactive power injections, as well as all active and reactive power flows. Assumed standard deviation of the measurements errors is $\sigma_U = 1\%$ for the voltage measurements and $\sigma_{pq} = 1.5\%$ for the power flow and injection measurements.

7.4.2   Temperature Impact on SE Accuracy

The impact of a resistance increase by 20% was studied. It corresponds to realistic conductor temperature increase from the regular $20°C$ design temperature to allowable $70°C$.

In Fig. 7.4 the actual values of the voltage magnitudes (computed by power flow) are compared with the output of two state estimators: using power system model for standard design conditions and model adjusted to the actual operating conditions. It can be concluded that in case when the conductor temperatures increase, the use of the uncorrected model would result in higher voltage profile than in reality. In case of state estimator based on the model adjusted to the corrected conductor temperature, the errors appear due to noise in measurements of electrical parameters.

Fig. 7.5 shows the residuals of active power flows on the transmission lines. The residuals are the difference between power measurements and the estimated values. In the case of uncorrected system model, the
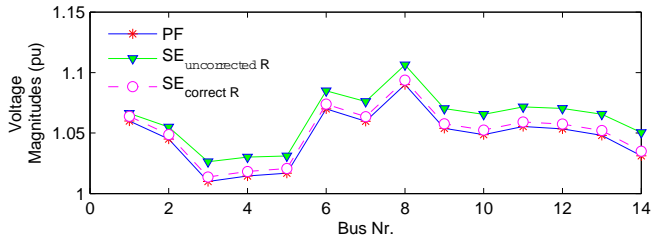
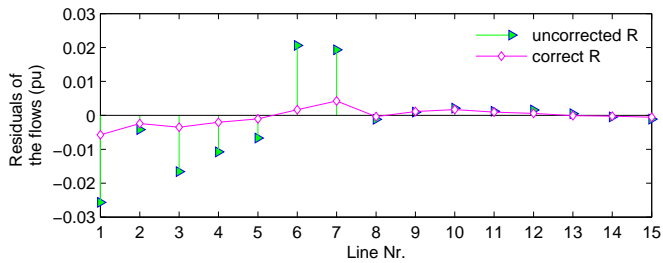Figure 7.4: Voltage magnitudes computed by power flow and estimated.

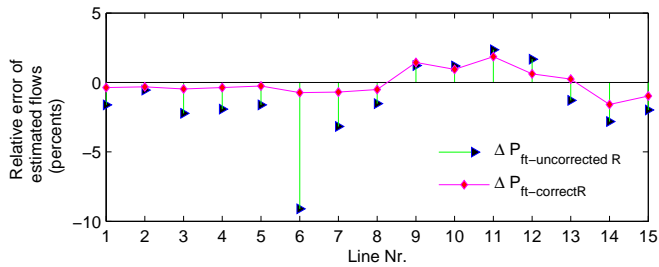Figure 7.5: Residuals of the determined flows.

Figure 7.6: Relative errors of the determined flows in percents to actual values.
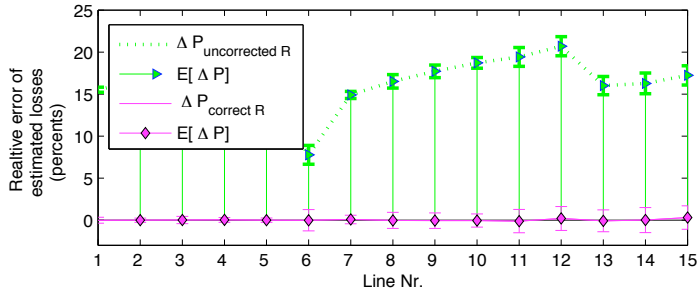
Figure 7.7: Expected errors and standard deviations of computed losses.

residuals are higher due to combined effect of both electrical measurement errors and the additional inaccuracy introduced by the uncorrected values of the line resistances. The latter is at least comparable to the measurement noise impact. Although in some cases, the resistance error "corrects" the measurement noise impact, in the overall the residuals are considerably smaller for corrected transmission model providing higher confidence in the obtained results.

Relative errors of the estimated active power flows compared to the true values (determined by power flow) are shown in Fig. 7.6:

$$error = \frac{true - estimate}{true} \cdot 100\%.$$

The overestimation of the conducted flows may reach almost 10 % due to neglected temperature impact. In power market conditions, this might represent financial implications, particularly in presence of congestion.

Moreover, the active power losses are estimated inaccurately in case of the uncorrected line resistance, as shown in Fig. 7.7. Here, Monte-Carlo simulations were applied to determine the distribution of the error in estimated losses: 100 trials of random electrical measurement errors followed by state estimation were conducted and the results were summarized. The expected value of the error and the standard deviation interval are shown. In case of the corrected model, the expected error in determined losses is zero. In case of use of uncorrected resistances, the underestimated losses may reach 20% for some transmission lines. The total value for the whole system approaches 15%, resulting in incorrect budgeting of the losses to ancillary services instead of being charged to producing companies.

7.4.3 SE Accuracy Variation during 24-hour Period

The impact of the conductor heating on SE accuracy may vary for different systems, topologies and states. As an example, we observe the SE accuracy during a 24 hour period, for an arbitrarily chosen day - October, 1st.

Two accuracy metrics were adopted from [59] to evaluate the performance of SE for both uncorrected and corrected power system models:

- Metric for complex power flow estimation accuracy, as follows:

$$M_{Sflow} = \sqrt{\sum_j \frac{\left|\vec{S}_{j,from}^{true} - \vec{S}_{j,from}^{est}\right|^2 + \left|\vec{S}_{j,to}^{true} - \vec{S}_{j,to}^{est}\right|^2}{MVA_j^2}},$$

  where $\vec{S}$ is complex power in the line j, MVA is the maximum capacity of the line;

- and the voltage accuracy metric:

$$M_V = \left\|\vec{V}^{error}\right\|_2 = \sqrt{\sum_j \left|\vec{V}_j^{true} - \vec{V}_j^{est}\right|^2},$$

  where $\vec{V}$ is complex voltage in the bus j.

Constant northern wind $V_w = 2\ ft/s$ and following temperature conditions are assumed:

$$hour = [0, 2, 4, 6, 8, 10, 12, 14, 16, 18, 20, 22]$$
$$T_a = [20, 20, 20, 22, 25, 26, 28, 30, 30, 28, 26, 22].$$

Loads changes are balanced by the slack generator at bus 1. Ratio of bus load to the total the system loading is normally distributed around the value obtained from the initial state [26] with 5 % standard deviation. The total system load is shown in Fig. 7.8, as well as sun flux and temperature variations normalized to peak values.

The results of the simulations in Fig. 7.8 show the expected values of the metric during the day at the simulated voltage and power measurement errors. For the comparison, the metric values for more detailed study

of 20 % resistance increase (as in subsection 7.4.2) are shown in Table 7.2.

It can be noted that values of these accuracy indices are close to ones at the loading peak in Fig. 7.8 and the observations from the previous subsection are applicable to both cases.

Table 7.2: Comparison of the SE metrics

Metric	Correct Resistance	Uncorrected Resistance
M_{Sflow}	0.0099	0.0538
M_V	0.0053	0.0459

For the chosen day the highest deterioration of the estimation accuracy M_{Sflow} due to temperature impact on the conductor resistances approximately coincide with the loading peak. Metrics of the SE with corrected line resistances are almost constant in the studied conditions. Thus, significant gain in SE accuracy can be achieved by correcting the transmission system model to actual conductor temperature.
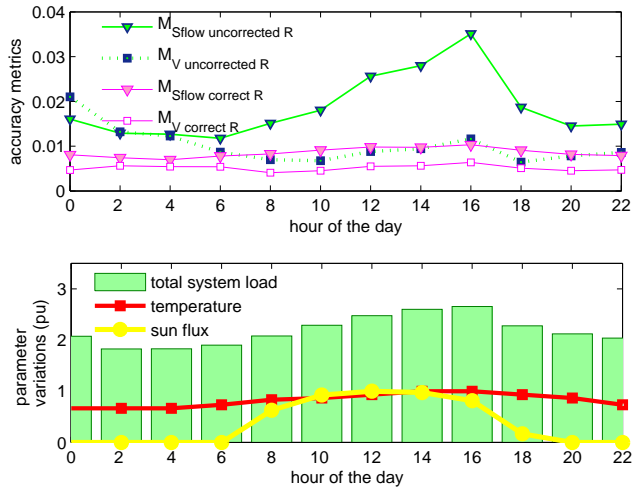
Figure 7.8: SE metric variations during 24 hour time period

7.5 Concluding Remarks

Changes of transmission line resistances due to temperature variations have non negligible impact on state estimation accuracy;

The accuracy of the state estimation results can be improved if resistance of power transmission grid model is corrected to particular weather and loading conditions by the methods discussed in the thesis;

Practical implementation of the proposed approach is possible and justifiable as it allows more accurate allocation of the transmission losses, determines more accurately power flows and the network voltage profile.

Chapter 8

Performance during Transient Conditions

This chapter proposes an approach to the state estimator performance monitoring and evaluation during transient conditions. Trajectory sensitivities are employed to determine efficiently the influence of the measurement chain components on the proposed performance index. Based on that we propose a method, which can be used to guide upgrading of a state estimation infrastructure to improve the state estimator performance during dynamic conditions. Using these results an approach to SCADA infrastructure enhancement is formulated.

8.1   Introduction

An accurate and reliable performance of a state estimation under all network conditions is crucial for the monitoring of power systems and thus their secure operation.

Standard state estimators nowadays employ algorithms using static system modeling, first proposed by Schweppe et al [118], [119], [115]. These methods based on static models assume that the system is in quasi steady state, which is necessary mostly due to the technological limitations of the measurement collection chain. However, underlying power system is in a permanent dynamic evolution of various time scales. The

most critical operation conditions occur when power system is in dynamic transition from one state to another. In this context, static state estimators shall determine instantaneous algebraic states of the power system. Yet, the discrepancy between the results of state estimation and the underlying actual system state is strongly influenced by the quality/accuracy of the measurement chain (discussed in Section 5.2), perhaps mostly by the so called time skew of measurements.

The term time skew refers to the state estimator processing in a single snapshot measurements taken at different time instants. This phenomenon has two major sources:

- differing communication delays,
- the deadbands - thresholds of the signal changes being reported by the Remote Terminal Units (RTUs).

The measurement infrastructure can vary within the same power system. The secondary technology used for the data collection differs from substation to substation as a consequence of many factors, equipment from different manufacturers, various equipment generations etc. Besides, the communication infrastructure between substations and the network control centre usually also vary. If the time skew and measurement inaccuracy are very significant, it may lead to the inability of the state estimation to converge and thus the inability to estimate the system state at all. This could leave system operators "blind", without appropriate system information exactly at the moment when this information is critical e.g. when the system undergoes dynamic changes, either these are caused by disturbances or just due to rapid changes implied by new schedule settings [124].

The problem of time skews could be solved with technology available today, explicitly with the total replacement of the RTUs by the Phasor Measurement Units (PMUs) [96], [18], [97], which were discussed in Chapter 5. These devices provide synchronous sampling with clock based on GPS signals. This would imply very high accuracy measurements, whose time stamp information would eliminate the problem with a different transmission time delay to the processing location (presumably state estimator in a control center). However, only few PMUs are installed in the systems. Despite obvious advantages, this technology is still far from massive deployment due to natural inertia for the replacement of the assets as well as measurement and control infrastructure.

It is also associated with high manpower and financial investments, requires high bandwidth communications and very powerful computers capable to process such large amount of data.

Therefore, necessity for the evaluation of the dynamic performance of SE and the effect of the time skews is actual. The different use of terminology with respect to dynamic SE was discussed in Section 5.4.2. In this thesis, the dynamic performance of the traditional state estimator is referred to as the performance during *electromechanical transient* conditions, i.e. during power swings. Furthermore, the measurement chain model proposed in this chapter can also be applied in steady or quasi steady-state conditions.

There has been a lot of innovative work reported in the literature, dealing with state estimation e.g. [89], [2]. In context of the present chapter, we would like especially to mention two publications, i.e. [87] and [23]. The ideas expressed in these papers, are in our view an additional confirmation of the necessity of the presented work. In [87] sensitivity of the estimation error and voltage estimates with respect to voltage, injection and flow measurements, line parameters and measurement weights, in addition the statistics of the sensitivities are determined for a number of static snapshots. The necessity to address dynamic response, both in the measurement and in the communication chain, is emphasized in [23]. The authors of [23] use constant time sampling of 20/200 ms and assume stochastic time delays with mean values of 0.0019 s in the 10-Mb/s Ethernet communication network. The system dynamics and the measurement chain noise are modelled by stochastic differential equations.

However, the performance of a traditional state estimator based on a static model during system dynamics has not been studied in depth and a systematic analysis approach has not been proposed in the literature to our knowledge.

This chapter targets two contributions to this topic by:

1. A concept for analysis of dynamic performance of state estimation;

2. An approach to improve state estimation performance during dynamic conditions by upgrading the SCADA infrastructure.

We believe that assessment of dynamic performance of a state estimator should be considered and even become a standard procedure in the

engineering and parameterization of the state estimator. The methods for the suggested steps of the analysis are proposed in this thesis, i.e. modeling of the SCADA for the state estimation purpose, evaluation of the dynamic performance and how to practically use these results in SCADA upgrades.

8.2 Proposed Dynamic Analysis

8.2.1 Dynamic Power System Model

An efficient framework for modeling of nonlinear systems featuring discrete states has been presented in [45]. Its application on power systems modeling has been further shown in [46] and [44], where a natural flexible modular structure following power systems components classification has been introduced.

Applying the original formulation from [45], we can write a model of the power system dynamics in a compact form:

$$\dot{x} = f(x, y, z, \lambda) \tag{8.1}$$

$$0 = g^0(x, y, z, \lambda) \tag{8.2}$$

with the changes in g^0 due to the structural change of the power system, defined by:

$$0 = \begin{cases} g^{i-}(x, y, z, \lambda) & y_{d,i} < 0 \\ g^{i+}(x, y, z, \lambda) & y_{d,i} > 0 \end{cases} \quad i = 1, \cdots, d \tag{8.3}$$

and the discrete variable switchings:

$$z^+ = h_j(x^-, y^-, z^-, \lambda) \quad y_{e,j} = 0 \quad j \in \{1, \cdots, e\} \tag{8.4}$$

$$\dot{z} = 0 \quad y_{e,j} \neq 0 \quad j \in \{1, \cdots, e\} \tag{8.5}$$

where

$$\begin{array}{llll} y_d = Dy & x \in X \subseteq \mathbf{R}^n & y \in Y \subseteq \mathbf{R}^m \\ y_e = Ey & z \in Z \subseteq \mathbf{R}^k & \lambda \in L \subseteq \mathbf{R}^l \end{array} . \tag{8.6}$$

Dynamic states are denoted x, algebraic states y and discrete state variables z. Switching of the status of discrete variables is governed by the equation (8.4) when the corresponding auxiliary variables of y_e are equal to zero. Auxiliary variables y_d determine the region of validity

of the equations (8.3). In power systems this may be explained by the example of a line, which changes its status. When the line is in service, equations linking the current through the line and voltages at both ends of the line as well as line parameters, namely line impedance and shunt admittance, are valid. When the line is out of service, i.e. disconnected, current flowing through it is zero. The auxiliary variable is in that case the difference between the time and the instant when the line was tripped. Matrices D and E are normally very sparse and their non-zero elements are equal to one on the positions corresponding to the auxiliary variables.

The above equations are solved numerically by employing e.g. trapezoidal integration.

8.2.2 Proposed Measurement Chain Models

In this chapter SCADA chain from the measurement up to the state estimation is addressed consisting of the following components:

- instrument transformer(s)

- transducer (active and reactive power computation)

- RTU

Adopting a convenient modular structure [46] for the framework of (8.1) - (8.6), each of the above listed components can be modeled as a module with internal variables and set of equations linked to other modules via external variables and coupling algebraic equations.

This flexible structure allows an individual choice of the model complexity for various components. For example, different types of RTUs with different sampling principles can be studied. Thus also communication delays can be included in the modeling if desired. Our objective is to present an analysis method, therefore the focus is put on other properties of the SCADA infrastructure, such as deadbands of RTUs etc. and the topic of time delay is neglected in the present work.

The above modular modeling approach is demonstrated on an example of a current measurement transformer - CT. Accuracy classes of current measurement transformers are derived from their multiplicative error at the nominal value of the measured current. Their measurement error is higher for lower values of the measured current. However, in a simplified

form it can be assumed that the error of the measured current is constant for the entire measurement range. Further, if per-unit system is applied for the computations, the measured current on the secondary side equals the measured current on the primary side of the transformer in the absence of an error. If the measurement is biased by an error, the current on the secondary side of the CT is distorted proportionally to the error. Similar to [46] in our modeling we adopted convention of expressing currents and voltages in complex plane by their rectangular real and imaginary part coordinates. In accordance with (8.1) - (8.6) CT quantities are defined as algebraic variables and the parameter:

$$
\begin{aligned}
\lambda : & \quad \epsilon \\
y_1 : & \quad I'_{Re} \\
y_2 : & \quad I'_{Im} \\
y_3 : & \quad I' \\
y_4 : & \quad I''_{Re} \\
y_5 : & \quad I''_{Im} \\
y_6 : & \quad I''
\end{aligned}
\tag{8.7}
$$

where superscript $'$ refers to the primary and $''$ to the secondary transformer's side quantities, i.e. sampled measurement. The parameter λ corresponds to the multiplicative error ϵ. Then it can be written:

$$
\begin{aligned}
\lambda : & \quad \epsilon \\
g_1 : & \quad 0 = y_1^2 + y_2^2 - y_3^2 \\
g_2 : & \quad 0 = y_1 \cdot (1 + \lambda) - y_4 \\
g_3 : & \quad 0 = y_2 \cdot (1 + \lambda) - y_5 \\
g_4 : & \quad 0 = y_3 \cdot (1 + \lambda) - y_6
\end{aligned}
\tag{8.8}
$$

The expressions $g_2 \ldots g_4$ in (8.8) describe in terms of algebraic variables how the measured current on the primary side of the CT is biased by the measurement error and the expression g_1 how the RMS value of the primary side current is linked to its real and imaginary coordinates.

Two additional equations are necessary to link the above module or description to the corresponding primary equipment component, whose current is measured, in other words how y_1 and y_2 are equal to the respective real and imaginary part of the current of a component (e.g. a line) whose current this CT measures.

Any dynamic simulator of power systems can be augmented by introducing new models reproducing the measurement and data collection chains, i.e the components directly giving input to the state estimation. Thus, the measurements o can be extracted from power system states available in the simulation model.

8.2.3 Evaluation of State Estimator Performance

The objective of a traditional state estimation [118], [119], [115] is to find the vector of states $\hat{v}$ minimizing the value of the function J_{SE}, i.e. minimizing the deviation between observations and the estimated values:

$$J_{SE} = \sum_{s=1}^{S} J_{SE,s} = \sum_{s=1}^{S} W_s \{o_s - h_s(\hat{v})\}^2, \qquad (8.9)$$

where o is a measurement vector and $\hat{v}$ is an estimated state vector.

The underlying assumption is, that the system model (i.e. the structure of the functions $h_s(\cdot)$) as well as measurements o are known. In power system state estimation o and v are commonly denoted as z and x, respectively. The new notations are introduced for consistency with the dynamic model (8.1) - (8.6). Note that the algebraic states v used in the state estimator (8.9) are a subset of Y.

The value of the J_{SE} indirectly expresses how good the solution of the state estimation is, i.e. the fit between the measurements and linking of system states. This widely accepted index does not fully serve our purpose. Indeed it shows how well the determined state fits to the observations but it does not reflect how far from the reality the estimate is.

Contrary to that, we propose to quantify the performance of a state estimator during dynamic conditions with the index expressing a weighted deviation of the *measurements* from the actual conditions:

$$J_p = \sum_{s=1}^{S} W_s(h_s(v) - o_s)^2. \qquad (8.10)$$

By actual conditions we mean the values which can not be obtained in reality, i.e. known to the actual state estimator running on-line. But they are available in the simulation environment, therefore they can

be utilized for the analysis of the performance of a state estimator in dynamic conditions.

In other words, this index expresses how the system states, if they would be perfectly known or estimated, would map into measurements' equivalents via measurement functions.

The example in the next subsection demonstrates that J_{SE} is not a reliable indicator for the evaluation of the accuracy of a state estimator when a power system is subjected to dynamically changing conditions. However the proposed index J_p gives a better indication of this accuracy.

The above introduced index J_p can be obtained in the simulation environment by expanding the model introduced in the subsection 8.2.2 by two other types of modules:

- module for the computation of an individual residual

- final module collecting all residuals

The overall setup is shown in the Fig. 8.1.

8.2.4   Illustrative Example

The nine bus test system is described in Appendix A.1. As a benchmark scenario the trip of the line (C) is chosen 5.3 seconds after the beginning of the simulation, due to a fault or switching. It is assumed that the topology change is instantaneously corrected in the model. It is crucial that state estimation would provide a correct result as soon as possible, since especially in the case of such an event the risk of an subsequent component outage due to an overload is higher.

The active and reactive power measurement errors induced by measurement chain are shown in Fig. 8.2, both the true value of the measured signal and the RTU output are shown for the line flow as well as squared residuals in the bottom plot, i.e. squared difference between the actual signal and the output of the RTU.

Along with the system dynamic simulation, the simulated measurements o_s are collected. Then, the proposed index J_p is computed. The simulated measurements o_s are also used as an input to a traditional static WLS state estimation involving orthogonal factorization [2] yielding $\hat{v}$. The evolution of the objective function value of the state estimator and
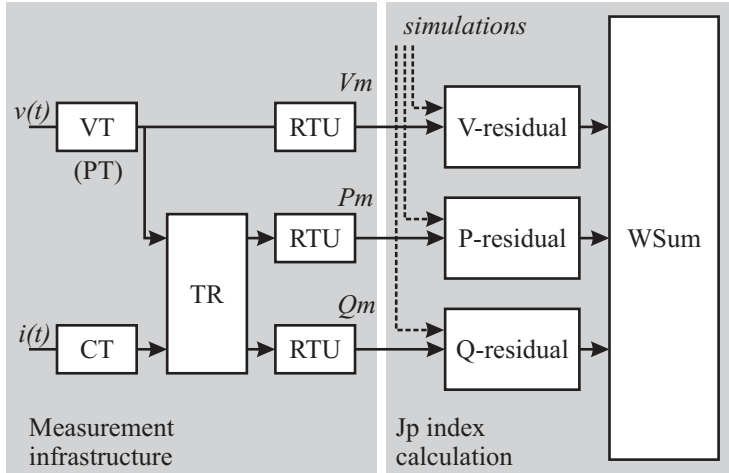
Figure 8.1: The measurement infrastructure and performance index calculation proposed for the state estimation performance evaluation in dynamic conditions. TR denotes transducer, Vm, Pm, Qm are the measurements. Residual calculation module uses simulated ideal measurements. The weighted sum (WSum) is a module collecting all residuals.

the proposed measure is shown in Fig. 8.3. Number of iterations needed for SE to converge has increased from 25 prior to the disturbance to 55 at the peak of the transients and about 35 in the end of the simulation. A strict convergence criterion was applied: a first norm of the states updates $|\Delta v| < 10^{-6}$.

To demonstrate the applicability of the proposed index J_p, in this example an additional measure J_r is shown accounting for the weighted deviation of the *estimates* from the actual conditions:

$$J_r = \sum_{s=1}^{S} W_s(h_s(v) - h_s(\hat{v}))^2. \tag{8.11}$$

For comparison, several further indicators are shown. The expectation of (8.9) for the normally distributed measurements $N(0, 1\%)$ with the standard deviation of the error $\sigma = 1\%$ is shown by $J_{SEnormal}$. The presence of the bad data in the sample shall be detected by the χ^2 tests. Since there are 17 states and 29 measurements, 12 degrees of

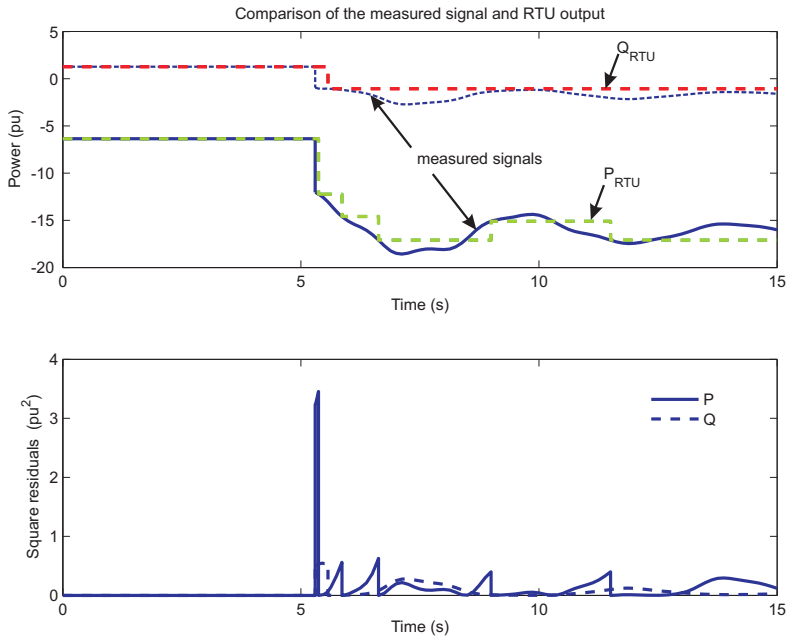Figure 8.2: The top part of the figure shows how the active and reactive power flows are reproduced by the part of the measurement chain consisting of the CT, VT, transducer and RTU. The residuals are shown in the bottom plot.
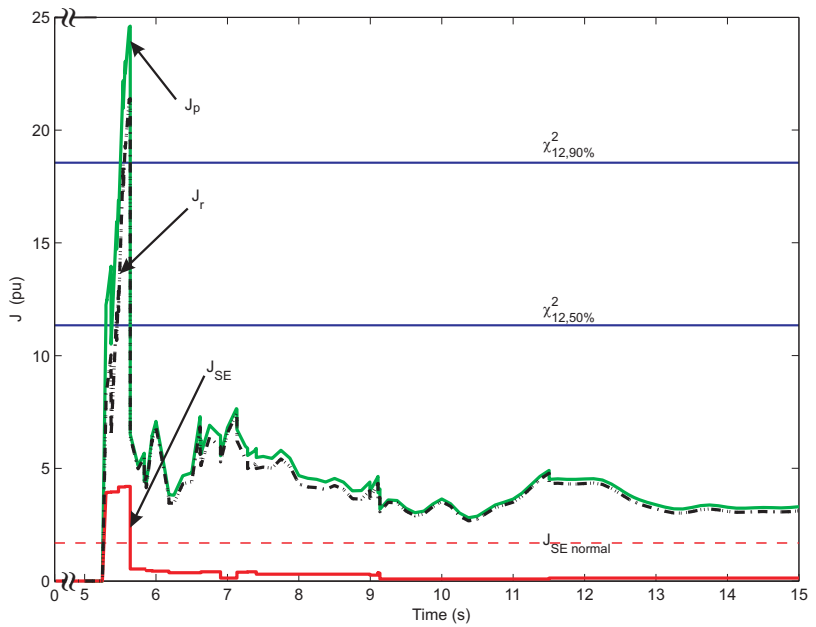
Figure 8.3: Behaviour of the state estimation during transient conditions: comparison of the objective functions of the state estimation and the proposed measure.

freedom are allowed. The interpretation of, for example, 90% confidence interval is following: objective function $J > \chi^2_{90\%}$ suggests that with 90% probability test sample contains bad data.

Even under assumption that the topology change is instantaneously corrected in the model, all the indices show higher values due to the transients and errors introduced by the measurement chain. It can be concluded that there is a small difference between J_r showing bad estimates and the computationally less intensive J_p. However, J_{SE} does not reflect fully the decrease of the estimator quality. In contrast to the proposed measure for the performance evaluation in dynamic conditions, J_{SE} does not exhibit very high values, since it "misses" to capture transients and operates with step-wise increasing values. In fact, J_{SE} would pass even such low as 50% confidence test for the bad data detection, while χ^2 test on J_p indicates that the measurement sample contains bad data with 90% confidence in the seconds following the disturbance. That may lead to the situation when SE fails to show that the obtained estimates are not reliable. In the addressed example, SE converged, yet in a large system convergence might be an issue.

Thus, the necessity to simulate SE performance in dynamic conditions and suitability of the proposed evaluation index is demonstrated.

8.3   Trajectory Sensitivities Analysis

Employing the modeling framework described in the previous section, the performance of state estimation can be investigated including the impact of the supervisory and monitoring infrastructure. To assess more efficiently the impact of various parameter changes, the trajectory sensitivities approach is used [45], [46], [44]. These sensitivities will suggest, which parameters shall be changed to achieve better performance of the state estimator.

Flow (i.e., time evolution) of the system from its initial point can be characterized by the time evolution of its variables [45], e.g. for algebraic variables we can write:

$$\phi_y(y_0, t) = y(t). \tag{8.12}$$

Trajectory sensitivities, i.e. Taylor expansion of (8.12), determine the impact of small changes in initial conditions and system parameters on

the system flow. When neglecting higher order terms the time evolution of the algebraic states can be written as:

$$\Delta y(t) = \frac{\partial y(t)}{\partial \lambda_0} \Delta \lambda_0. \tag{8.13}$$

The trajectory sensitivities, $\frac{\partial y(t)}{\partial \lambda}$ are generally time varying quantities. A numerical approximation of trajectory sensitivities can be computed by solving (8.1) - (8.6) for an incremental change of each parameter. However, that would represent a significant computational effort if many parameters are considered. The methodology for computation of trajectory sensitivities described for example in [45] involves only a minimal amount of additional computations, since it uses parts of the Jacobian evaluated when solving (8.1) - (8.6). Thus, the impact of the parameter changes on the state estimator performance can be computed efficiently.
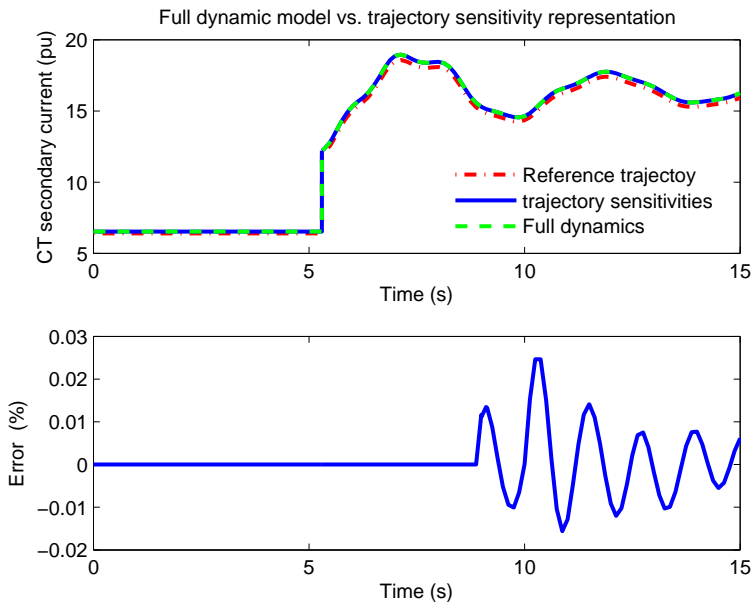

Figure 8.4: Accuracy of the reproduction of the system dynamics by means of trajectory sensitivities.

In Fig. 8.4 feasibility of a very accurate approximation using trajec-

tory sensitivities is demonstrated. Let us emphasize once again that an influence of a parameter change on the dynamic processes can be studied by running another full dynamic simulation, while trajectory sensitivity approach will provide an approximation yet requires negligible computational effort in addition to simulation of the nominal dynamic conditions.

The upper plot shows nominal trajectory with red dash-dot line, it was obtained with full dynamic time domain simulations for the reference system. Then, we study how the dynamic evolution of the current at the secondary side of CT would change if CT error is changed from 0 to a high value 0.02, what would correspond to a CT error class 2. The result obtained with trajectory sensitivity is compared to the exact computation of the dynamics with the new parameter. The upper plot shows both almost coinciding curves, while the bottom plot shows the difference between those. During the first 9 seconds of the simulation the error of approximation is close to zero. It slightly increases afterwards.

It should be noticed that as it is a numerical simulation, the result is a set of discrete point not a continuous curve. In this case two dynamic simulations produced vector of values at slightly differing time references. That is due to slightly different instances of the discrete events, such as reaching the limits of the generators excitation system. The trajectory sensitivity vector is produced at the time instance of the nominal case. To compare the results interpolation of the obtained values is necessary. In this case linear interpolation was applied, which could introduce an additional error. Therefore, in the bottom plot rather the magnitude of the error is importance than the particular shape of the error.

The results of computation of the sensitivities to the different components' influences are shown in Fig. 8.5-8.6. Here the sensitivity is studied on the example of line (A) flows from node 5 to node 7. Several measurement chain stages are analyzed.

Figure 8.5 shows from top to bottom: trajectory sensitivities of the transducer, of the RTU outputs and of measurements residuals with respect to the CT accuracy. The sensitivities of the transducer towards CT accuracy are continuous and somewhat constant at pre- and post-disturbance intervals.

The step-wise increase of the sensitivities in the middle plot can be explained by the deadband impact, which was shown in Fig. 8.2. If there was an error in the CT, RTU does not "notice" a change that
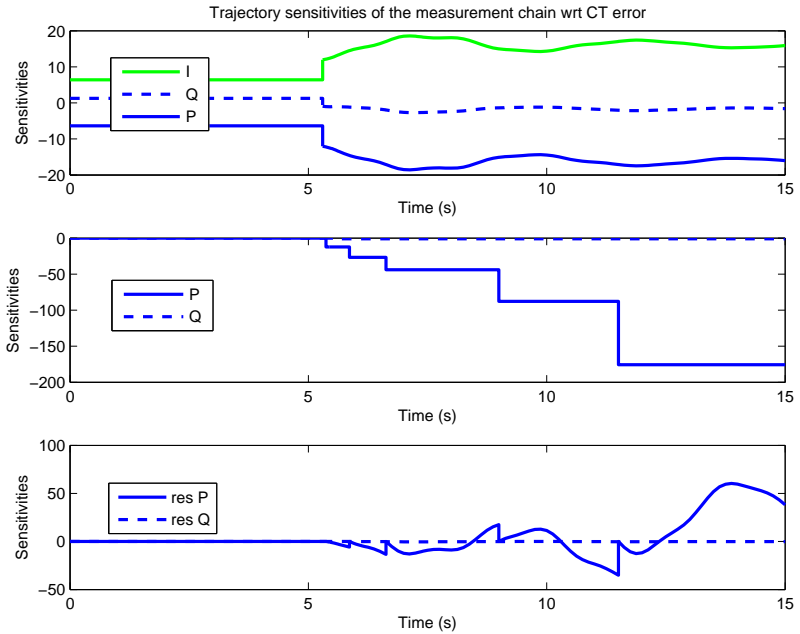
Figure 8.5: The effect of the measurement error of the CT. The top picture shows the impact on the transducer, the middle picture on the RTU and the bottom picture on the residuals of the corresponding active and reactive power flows.

should be reported and "delays" transmission of the new value. This effect accumulates in time and the sensitivity increases step-wise, as the new update is "missed".

The sensitivity of the residual of the active and reactive power flow measurements is shown in the bottom plot. Recalling the residuals presented in Fig. 8.2, we observe again some step-wise changes of sensitivities due to the deadbands. Sensitivity is varying as the true signal oscillates, but the value is not yet transmitted by the RTU. In addition, sensitivity increases significantly as the true signal deviates from the last transferred value.

The sensitivity of the objective function J_p to the CT error, deadband and the weight of the current measurement is shown in Fig. 8.6.
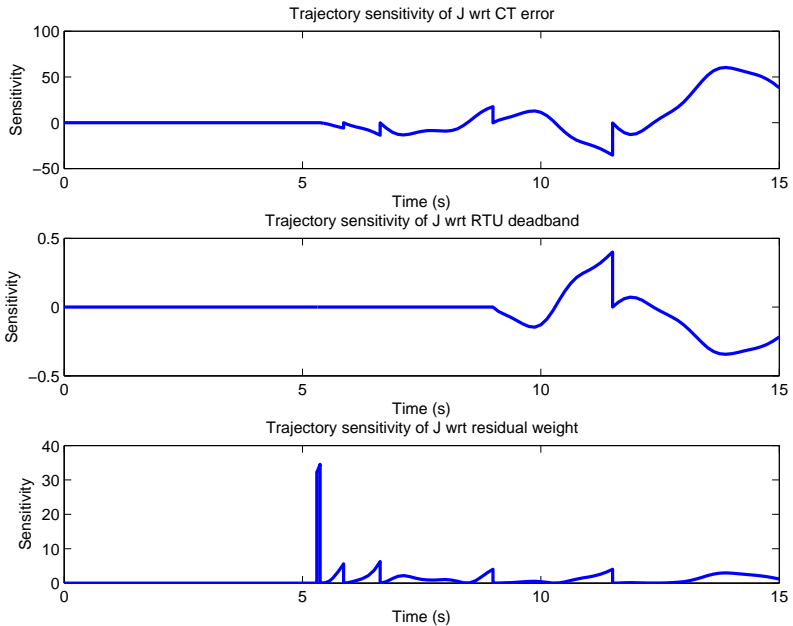
Figure 8.6: The impact of various parameters of the measurement chain on the cost function J_p. Top plot - sensitivity of the J_p to the accuracy of CT, middle - sensitivity to the RTU deadband, bottom - sensitivity to the residual weight.

The CT error seems to have the largest influence along the major part of the trajectory, while the measurement weight is playing a large role at the disturbance instant with the step change of the variables. Note that the feasible change of the parameters might be different for the different components, therefore both the sensitivity and span of the feasible improvement of the parameter must be taken into account.

For example for this current measurement, if replacing a CT of the class 2, with a CT of the class 0.1, the maximum parameter change, which can be considered, equals to the difference of maximal error in these accuracy classes, thus, $\Delta\epsilon$ of 0.019.

8.4   Guiding the Upgrade of the SCADA Infrastructure

Assume there is a given limited budget, which a TSO may dedicate to upgrade of the SCADA infrastructure. The objective may be to minimize the error of the state estimator during dynamic conditions by investing the upgrade budget into new RTUs. Below the procedure is outlined, how the locations and the types of upgrades can be efficiently determined.

1. A set of representative system conditions together with dynamic scenarios or contingencies with corresponding weighting factors is chosen. The number of scenarios may be denoted A_{sc} and the weighting factors W_{sc}.

2. Scenario a is simulated for a chosen time horizon. The nominal (i.e. pre-upgrade) evolution of the corresponding index $J_{p,na}(t)$ is stored as well as the vector of trajectory sensitivities $\frac{\partial J_{p,na}(t)}{\partial \lambda}$. Simulations are repeated for each scenario $a \in \{1, \cdots, A_{sc}\}$.

3. A candidate $b \in B$ from the set of possible SCADA upgrades can be expressed as an adjustment $\Delta\lambda_b$ of the corresponding parameter $\lambda_b \in L$, thus $\Delta\lambda_b \in \Delta L$. For example, if a RTU with a smaller deadband is considered for installation, then the corresponding change of the deadband parameter is negative $\Delta\lambda_b < 0$.

   Costs of individual upgrades ΔL are summarized in the vector C, whereas the budget for the overall upgrade would be C_{budget}.

4. The objective can be then expressed as:

$$\min \sum_{a=1}^{A_{sc}} W_{sc,a} \int_0^T J_{p,a}(t) \, \mathrm{d}t, \tag{8.14}$$

   subject to constraints:

$$J_{p,a}(t) = J_{p,na}(t) + \frac{\partial J_{p,na}(t)}{\partial \lambda} \cdot \Delta L \cdot U \tag{8.15}$$
$$\forall a \in \{1, \cdots, A_{sc}\}$$
$$C \cdot U \leq C_{budget}, \tag{8.16}$$

where the solution vector U contains binary variables with entries equal to 1 for the determined upgrades and entries equal to 0 for upgrades not to be implemented, i.e. $u_b \in \{0, 1\}$, $\forall b \in B$.

Thus, proceeding in accordance with the described algorithm TSO can determine optimal set of the RTUs to be upgraded to improve the performance of the state estimator during the transient conditions.

8.5   Concluding Remarks

The chapter discusses how the performance of a traditional static state estimation observing the system undergoing dynamic changes can be measured and how this information can be utilized for the improvement of the state estimation.

The necessity of such an analysis was demonstrated in the thesis. For this purpose utilization of common dynamic simulation solvers are proposed with an extension by models of the SCADA components and incorporation of additional computations of trajectory sensitivities. The discussed approach is shown to be feasible.

The performance of static estimation during the slower system transients is crucial, even critical, for a secure operation of stressed power systems. Thus, we suggest that the proposed approaches, or similar ones, shall become an integral part of engineering processes related to the commissioning and regular maintenance of the state estimation.

Part II

Offline Analysis: Fair Allocation of Profit and Losses

Chapter 9

Fair Allocation in Game Theory

This chapter briefly reviews profit or cost allocation according to Shapley value - a well known concept in Game Theory, which will be applied in the following two chapters.

In many economic tasks the question of fair division of the profits or costs arises as soon as there are more than one entity or player involved. In the context of liberalized power systems, the cost allocation for using common resources directly impacts competitiveness and profits of the market participants.

A simple way of sharing the costs or revenues c would be an *incremental method*, when each next player l joining the coalition C is allocated an additional profit [92]:

$$\Delta c(C, l) = c(C \cup \{l\}) - c(C). \tag{9.1}$$

The problem with such an approach is that it is not anonymous, i.e. the shares depend on the existing coalition and order in which the players join the coalition.

The Shapley value addresses and expresses a fairness of the cost allocation problem by taking a random ordering and charging the *expected incremental cost* to each player. Employing this idea one can proceed as follows:

- For the set $\mathcal{A}$ of $n_\mathcal{A}$ players, there is $n_\mathcal{A}!$ possible orderings.

- Define $C \subseteq \mathcal{A} \setminus \{l\}$ as any subset of $\mathcal{A}$ excluding player l and with the cardinality $|C| = n_C$.

- The probability that precisely set C comes before l in a random ordering is:
$$\frac{n_C!(n_\mathcal{A} - 1 - n_C)!}{n_\mathcal{A}!}. \tag{9.2}$$

- The Shapley value determining the profit share of the entity $l \in \mathcal{A}$ can then be defined as follows [92]:

$$\phi_l(c) = \sum_{n_C=0}^{n_\mathcal{A}-1} \left[\frac{n_C!(n_\mathcal{A} - 1 - n_C)!}{n_\mathcal{A}!} \sum_{\substack{C \subseteq \mathcal{A} \setminus \{l\} \\ |C|=n_C}} \Delta c(C, l) \right], \tag{9.3}$$

where $\phi_l(c)$ is a profit share, c is the profit in the coalition.

Naturally, the profit shares of all the entities add up to the total profit of the coalition:
$$\sum_{l \in \mathcal{A}} \phi_l(c) = c. \tag{9.4}$$

Let us consider a simple yet illustrative example of cost sharing according to Shapley value. Three players Anna, Bill and Cecil can get involved in some activity and need to cover the start-up costs. They can act independently or form a coalition. All three have different skills and considerations for the activity to get involved to. Anna would start α, Bill prefers β, Cecil considers γ.

However, there is an option to form coalition of two or three players. All activities have different utility or costs, but with the increase of coalition the relative cost decreases. It appears an attractive option for them to collaborate and share the costs. Players may find the compromise activity for each of them. For example, Anna and Bill would collaborate in ι, Bill and Cecil would choose κ, Anna and Cecil prefer λ, while all the players together would collaborate in μ. The results of their discussions are summarized in Table 9.1.

Assuming that nobody extra benefits or looses from switching to another type of activity and thus, equal sharing of the costs would not be fair,

Table 9.1: Shapley method example: Coalitions

	player		
	Anna	Bill	Cecil
	α	β	γ
	9 k€	6 k€	8 k€
Decision	ι		-
	14 k€		
	-	κ	
		12 k€	
	λ / 2	-	λ / 2
	$\sum$ 15 k€		$\sum$ 15 k€
	μ		
	20 k€		

we can apply the Shapley value to this problem. The cost shares can be computed as follows:

$$
\phi_A(20) = \sum_{n_C=0}^{2} \left[\frac{n_C!(2-n_C)!}{3!} \sum_{\substack{C \subseteq \mathcal{A} \setminus \{l\} \\ |C|=n_C}} \Delta c(C, l) \right] =
$$

$$
= \left[\frac{0!(2-0)!}{3!} \sum_{\substack{C=\{\}, \\ |C|=0}} (9-0) \right] + \left[\frac{1!(2-1)!}{3!} \sum_{\substack{C=\{Bill\}, \\ C=\{Cecil\}, \\ |C|=1}} \Delta c(C, l) \right] +
$$

$$
+ \left[\frac{2!(2-2)!}{3!} \sum_{\substack{C=\{Bill, Cecil\}, \\ |C|=2}} (20-12) \right] =
$$

$$
= \frac{2}{6} \times 9 + \frac{1}{6} \times [(14-6)+(15-8)] + \frac{2}{6} \times (20-12) = 8\frac{1}{6}.
$$

Similarly, for other players:

$$\phi_A = \frac{1}{3} \times 9 + \frac{1}{3} \times \left(\frac{14-6}{2} + \frac{15-8}{2} \right) + \frac{1}{3} \times (20-12) = 8\frac{1}{6} \approx 8.17$$

$$\phi_B = \frac{1}{3} \times 6 + \frac{1}{3} \times \left(\frac{14-9}{2} + \frac{12-8}{2} \right) + \frac{1}{3} \times (20-15) = 5\frac{1}{6} \approx 5.17$$

$$\phi_C = \frac{1}{3} \times 8 + \frac{1}{3} \times \left(\frac{15-9}{2} + \frac{12-6}{2} \right) + \frac{1}{3} \times (20-14) = 6\frac{2}{3} \approx 6.67,$$

the shares sum up to 20.0 k€, where the surplus of 10 € is due to the numerical rounding error.

Several papers suggest application of the Shapley value and the similar Aumann-Shapley value to cost and/or profit allocation problems in power systems, including firm-energy rights allocation among hydro power plants [34], expansion planning [111], congestion management [10], inter-TSO compensations [58], ancillary services [75], fixed asset costs [56] and loss allocation [16], [130].

The following chapters propose two applications of Shapley value to power systems: a new method to transmission loss allocation and an new scheme for profit sharing from the coordinated bidding and operation planning of wind and hydro producers.

Chapter 10

Allocation of Transmission Network Losses

This chapter describes the problem of loss allocation together with an overview of existing loss allocation methods. Some properties of loss allocation mechanism are studied and a new method based on game theory is proposed. The chapter closes with conclusions and outlines the future perspectives.

10.1   Introduction

One of the key elements of liberalized markets being faced by consumers and producers is a transparent cost structure of electricity supply. In most systems TSO covers the costs associated with the acquisition of ancillary services by allocating these costs on consumers in form of ancillary services charges. Naturally, it brings up many disputes on what a fair cost allocation among the market participants is, since it directly affects their profits and competitiveness.

Criteria judging the suitability of an allocation mechanism for these costs shall primarily target the objectives common to all free markets, namely:

- fairness or nondiscrimination

- transparency.

These objectives may be translated and extended into the following criteria [28]:

1. simple implementation

2. easy understanding

3. relation to the consumed energy and/or power

4. relation to the underlying physical properties of the ancillary service

5. providing appropriate economical signals

6. avoidance of volatility.

One of the costs associated with power system operation are resistive losses in the transmission network. This chapter proposes a feasible and fair method allocating costs for the loss coverage to consumers.

It should be noted that throughout the chapter we talk about allocation of power losses rather than the costs.

10.2   Loss Allocation Methods

The term losses refers to the difference between the produced and consumed energy. In practice the amount of losses is determined for a billing period, i.e. as energy. However, it is common in the literature to adopt the notion of losses per unit of time, i.e. in terms of power.

The difference between the total power injected into and withdrawn from the network is:

$$P_{loss} = \sum_{g=1}^{N_G} P_{Gg} - \sum_{d=1}^{N_D} P_{Dd}, \qquad (10.1)$$

where P_{Gg} is power injection in the generation bus g out of the total number of generation busses N_G and P_{Dd} is power injection in the demand bus d out of the total number of demand busses N_D.

Physical origin of losses is resistance of the conductor and flowing through it current RI^2, which causes heating of the conductors and corona.

Ex-ante, TSO tries to predict amount of losses and acquire power to cover them, either by tender or on a spot market. However, as the actual system state deviates from the predicted one, so do losses. The difference between the prediction and actual losses is covered similarly to load deviations by balancing power, i.e. secondary and tertiary frequency control reserves.

Ex-post, TSO determines an actual amount of losses and computes associated costs, i.e. the predicted/scheduled power and the corresponding portion of balancing power. To determine the contribution to be paid by each consumer TSO uses loss allocation methods.

We chose three out of several allocation methods used in practice and proposed by research community, which we briefly review in the next subsections using the criteria mentioned in the section 10.1.

10.2.1 Pro Rata: Proportionally to the Consumed Power

This allocation method is most common in practice, for example in England, Spain, Brazil etc. and the loss allocated to a consumer l is:

$$\phi_l(c) = P_{loss} \cdot P_{Di} / \sum_{d=1}^{N_D} P_{Dd}. \tag{10.2}$$

Advantages of this method are its simplicity both in implementation as well as principle, and avoidance of volatility. Only measurements and minimal computations are involved, not requiring any system model. Therefore, this method does not depend on the selection of a slack bus. On the other hand, this method fails to provide any indication how the particular load and its location in the system affects total amount of losses, thus it does not give a price signal for the more efficient network use.

10.2.2 Incremental Transmission Loss

This method considers that load or generator contributes to the losses in accordance with the sensitivities of system losses to active power

injection in that node. This method shall provide price signals for more efficient load or generation location. Norway, PJM are examples of the systems, where it was applied.

The sensitivities or incremental transmission loss coefficients (ITL) can be determined numerically, analytically or as a by-result of optimal power flow [80]. Obtained coefficients are used as weighting factors, defining the share of the total transmission system losses to be allocated to the particular load or, depending on the rules in the system, also generator. Here considering only loads:

$$\phi_l(c) = P_{loss} \cdot P_{Dl} \frac{\partial P_{loss}}{\partial P_{Dl}} / \sum_{d=1}^{N_D} \left(P_{Dd} \frac{\partial P_{loss}}{\partial P_{Dd}} \right) \tag{10.3}$$

Besides, some TSOs, for example PJM, use loss penalty factors rather than ITL to include the loss consideration already in the market clearing process, e.g. for the load at bus l:

$$Pf_l = 1 / \left(1 - \frac{\partial P_{loss}}{\partial P_l} \right). \tag{10.4}$$

The penalty factors are used to adjust the incremental cost of each generator so as to include effect of losses in the dispatch and are applied to each and every location of generation, load or virtual transaction. The loads are then paying locational marginal price that includes loss component.

The further differences in ITL interpretation are, as follows:

- If the normalization [28] to match the total system losses is not used in (10.3), the participants charges result in "overpayment" for the losses, since the sum of sensitivity factors is larger, in fact almost twice as large as the losses. Alternatively, overpayment is shared among the participant proportionally [80] to consumed power and stored as the credit for the next hour loss distribution.

- The calculation of values of the ITL coefficients appear to be sensitive to the chosen slack bus. Several approaches has been proposed in the literature that shall decrease or avoid such an influence. The concept of center of electrical losses or distributed slack bus is used in [80], [30], [39], [76].

- Since in some conditions ITL may obtain negative values, which could be interpreted as a cross subsidy, an unsubsidized ITL allocation method has been implemented. Ref. [28] provides more detailed discussion on this subject.

As the above discussion suggests, the advantage of this method is its direct consideration of the cause of the losses and provision of the economical signals. On the other hand, certain volatility may be experienced and the necessity of the system modeling makes it less simple to follow.

Should losses be paid by the loads or the generation or rather shared? The implementation differs from system to system, as mentioned earlier, in this thesis we adopt the philosophy that these costs shall be charged to loads as it is usually implemented in Europe.

10.2.3   Proposed Allocation of Losses

Several authors have approached the loss allocation problem by the means of methods using the Shapley value. Tracing electricity principle [12] based loss allocation was rationalized by Shapley value in [58] and proposed for the inter-area pricing. In these works, the contribution from each power source or load to the line flow is determined and the losses allocated correspondingly. Ref. [49] and [50] investigate the contribution of loads and generation represented by equivalent current injection to every line loss and applies Shapley to fair allocation. Ref. [95] derives expressions for the allocation of currents in branches to loads and generation avoiding the use of Shapley value, but preserving the fairness. In [139] allocation proportionally to the injected currents and uses loss sensitivity to generation current injections for Aumann-Shapley application is suggested. Loss allocation method for bilateral markets is described in [130].

These methods, except [56] address loss allocation problem by approximations at the system operational point, such as it is defined by all the consumers demands at the particular time instant.

We propose to consider the total load connected to a particular system node, as a selfish player that could use the network for its own purposes, but is forced to cope with the other players using the common network, while these players having the same rights. Thus, the loads connected to the network are forming a coalition. The loads prefer to join the

coalition and to bear some operational costs, since it allows them to get access to power supply. A load that does not participate in a coalition has no costs, but also no power supply. The allocation of fixed costs for network use is not considered in this approach.

In this way, one could study the incremental amount of losses produced by the nodal loads, when participating in different coalitions. What would be the additional impact, as an example, on the losses of the load # 2, if initially only load # 3 is using the network, and what if only load # 3 and # 7? Thus, we take into account the lost opportunity costs or what could have been, if there would not be a forced operation point determined together with the other loads. The generation is varied proportionally to base case at all the power plants to match the demand. Fig. 10.1 shows the algorithm for the Shapley value computation for such conditions. According to the algorithm, we compute incremental impact on the system losses of each load, if it joins the system in various sequences with the other loads. Then, we apply the Shapley value to compute loss share of this load.

Computational Complexity

Noteworthy, the depicted algorithm has a transparent, easy to understand structure, but it is not optimal from the computational point of view. A large number of load coalitions C is common for all the loads l and there is no need for recomputing the power flow each time. Instead, in real implementation, the results of power flow computations should be stored in a convenient form and properly indexed to be later accessed for the Shapley value computation.

For the general case, containing $n_{\mathcal{A}}$ loads the number of computed power flows shall be the sum of all the combinations of loads n_C selected from loads $n_{\mathcal{A}}$, which can be computed with the corresponding formula from the combinatorics:

$$\#PFs = \sum_{n_C=1}^{n_{\mathcal{A}}-1} \mathbb{C}_{n_C}^{n_{\mathcal{A}}} = \sum_{n_C=1}^{n_{\mathcal{A}}-1} \frac{n_{\mathcal{A}}!}{n_C!(n_{\mathcal{A}} - n_C!)}. \tag{10.5}$$

It should be noted that evaluation of the Shapley value is computationally hard [92], in general. However, random sampling may be used to approximate the Shapley value with the desired accuracy [92]. Then, instead of running a large number of computations of the power flows

Figure 10.1: Algorithm for the proposed loss allocation.

for all possible combinations of the loads as in Fig. 10.1, one could compute an incremental impact Δc_l of the considered load for a limited number of randomly chosen combinations for each n_C, then compute the expectation of incremental costs $E[\Delta c_l]$ for each n_C and, finally, determine the Shapley value as $\sum_{n_C=0}^{n_\mathcal{A}-1} E[\Delta c_l]/n_\mathcal{A}$.

10.3   Illustrative Example

10.3.1   Test System

The comparison of the loss allocation methods was conducted for the IEEE 14-bus test system [26]. The system contains eleven consumers, which are supplied by two generators at two voltage levels: busses 1-5 are operated at 132 kV and busses 6-14 at 33 kV. The single line diagram of the system is shown in Fig. A.2.

The production of both generators is adjusted proportionally to match the varying demand for the proposed method simulations. The slack bus of the system is bus number one that covers the system losses. Three scenarios were simulated:

- Base case - IEEE 14 bus system;

- Different generation pattern: an additional 1 pu generation is introduced at the Bus # 8. The generation in Bus # 1 is decreased correspondingly;

- Total loading is increased by arbitrarily chosen 50% : proportional increase at all the system busses.

Both active and reactive power are considered to be inseparable parts of consumption, therefore, for the Shapley value computations the status of the full load is changed. The total number of the simulated power flows for the proposed method is 2048 per scenario. The computational time per scenario is about 30 sec on the PIV, 3.8 GHz, 2 Gb RAM system using Matlab environment. Loss allocation in accordance with pro rata method was computed using (10.2) and the ITL were computed numerically, using one slack bus system, normalization and potentially subsidized formulation (10.3).
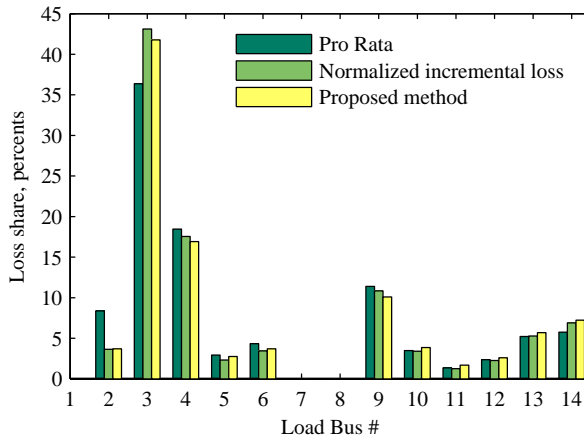
Figure 10.2: Comparison of the loss share among the consumers: Base Case

10.3.2 Results

Loss allocation according to three discussed methods is presented in Fig. 10.2 - 10.4. There, the amount of the losses that each of the loads is responsible for or the loss share is shown in percentage of the total system losses. In overall, the proposed method gives similar although not the same allocation with the incremental transmission loss method. This is not a very surprising result since both methods represent an incremental influence of the load on the system losses. While ITL considers the influences around given system operation point, the proposed method evaluates all the possible combinations and, thus, the span of possible operation points. However, the major influence is still given by the last steps, when the considered load is one of the last ones in the ordering, thus, approaching the operation point as considered by the ITL.

Comparing the performance of the ITL and the proposed method to pro rata, the major differences can be noticed for Bus # 2 and # 3, indeed, since Bus # 2 has a large consumption and local generation, incremental methods shall result in a lower loss allocation than pro rata that neglects generation presence. The inverse situation can be
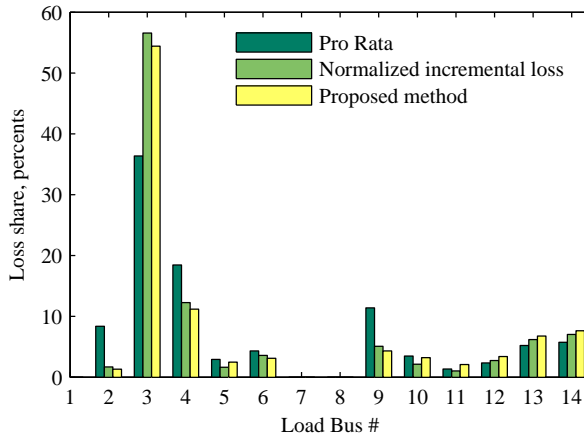
Figure 10.3: Comparison of the loss share among the consumers: adjusted generation pattern
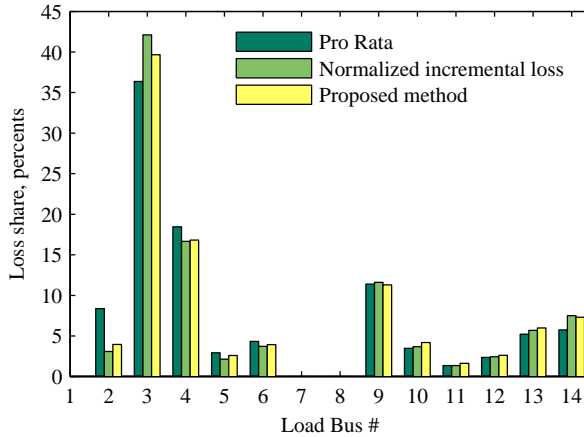

Figure 10.4: Comparison of the loss share among the consumers: increased system loading
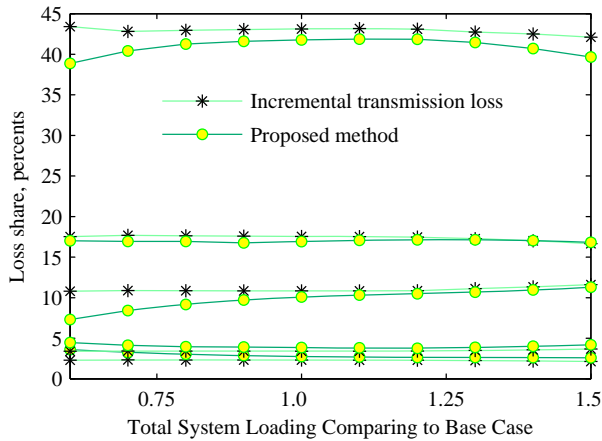
Figure 10.5: Comparison of the loss share changes among the selected consumers: different total system loadings - 50-150 %.

observed for Bus # 3 while it has a large consumption, in addition, it is electrically distant from the two generators, thus, the loss share shall be further increased. Another intuitive observation can be made for the Busses #13-14. These are distant busses and the incremental methods give higher loss allocation than pro rata, while for the Bus # 10-12 the shares are almost the same and for the closer Busses # 4-9 pro rata gives higher values.

Adding a generation in Bus # 8 shall decrease the shares of the neighboring loads in total system losses as it can be seen in Fig. 10.3. The loss share of Bus # 3 reaches 55%. It should be noted that the total system losses are almost half as compared with the base case.

The increase of the total system loading by 50% emphasizes conclusions made for the base case, ITL and the proposed method show slight differences in sensitivity to load increase.

Fig. 10.5 shows loss share for several representative busses, when the total system load is proportionally varied in the range $0.5 - 1.5$ of the base case. It can be concluded that ITL has, generally, more constant values in this study, while the proposed method shows changing contribution of the loads.
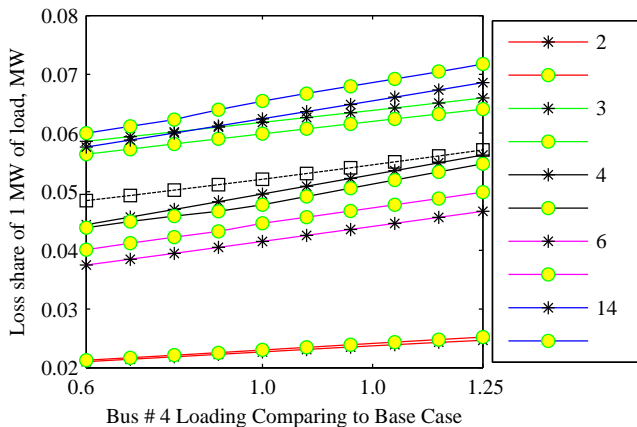
Figure 10.6: Comparison of the loss share among the consumers: Bus # 4 loading variations. The results for the same bus are shown by the same line color, (*) for the ITL and as (o) for the proposed method. Pro rata method is shown by dashed line with squares.

Fig. 10.6 shows changes in the loss share of the bus loads, if one of the loads is varying. The loss share is shown in the absolute values per MW of load. In the depicted case, Bus # 4 has a varying load, which however, affects the shares of the other loads. Pro rata is drawn by the single line, since for this method the loss share is same for any MW of load, irrespectively of the location in the network.

10.4   Concluding Remarks

The chapter discusses aspects of the loss allocation in power system transmission network and presents a new method for the loss allocation to consumers in electricity market. The fairness of the method is justified by the implications from the game theory.

The results of the loss allocation according to the proposed method exhibit similarities with the incremental transmission loss method. Although, the proposal introduces computational complexity, it however can be overcome by the approximations and modern computers. Pre-

liminary studies in this area show promising results that might decrease the number of necessary computations by several orders of magnitude. On the other hand, the reported results might be seen as a support of the incremental transmission loss allocation by the game theory. However, further insights and verifications of the general validity of this statement are needed.

It should be pointed out that this method can also be considered for fair cost allocation of other types of the ancillary services.

Chapter 11

Operation Planning and Bidding

Depending on market rules, particularly congestion management and balancing management rules, coordination between wind and hydro producers may be mutually beneficial. In this chapter we propose a new collaboration scheme and a fair and transparent method for splitting the extra profit caused by a coordinated bidding and operation strategy based on the Shapley value. Uncertainties in wind forecast and energy price evolution are accounted for.

11.1 Introduction

The most significant challenge of wind production compared with traditional resources is its variable nature, making accurate planning or scheduling of its **energy** production difficult and the significant volatility of its **power** production. From the perspective of a TSO, these disadvantages result in a higher demand for control reserves to balance deviations between production and consumption in the power system.

The amount of balancing energy required from a wind power plant can be minimized by creating a coordination scheme in conjunction with an easily dispatchable type of power plant, for example a hydro power plant (HPP). If power plants are geographically (and electrically) close,

sharing a connection to a bulk transmission system, coordination becomes even more of interest, particularly when connection to the power system is congested.

The coordination of wind power and hydro power has been studied earlier in connection with several different problems. Ref. [82] provides a comprehensive literature review on wind-hydro coordination. In [70] the coordination of wind farms with hydro power plants is considered in generation expansion planning. Two investment possibilities are compared in [70]: a new hydro power plant versus a new wind farm. In [134] and [135] the effect of wind power on market prices is analyzed. The research in [134] and [135] is directed towards assisting utilities with existing hydro power plants when considering investments in wind power. In [67] the coordinated operation of several geographically distributed wind farms (WFs) and HPP sharing the same transmission capacity is simulated over a period of several years, considering wind and water inflow uncertainty.

In [68] a dynamic programming algorithm is presented for daily planning of coordinated operation of wind farms and a generic energy storage in areas with limited export capability. In [24] the optimization problem is formulated for daily production planning of wind farms and pumped storage hydro power plants, but transmission bottlenecks are not considered.

One of the most recent publications on coordinated planning of wind and hydro power plants is [7], where the coordination is applied in order to minimize imbalance costs of the WF.

In [81] a daily planning algorithm is developed for the coordinated bidding on the spot market and operation of the a multi-reservoir hydro power plant with a wind farm in a network with limited transmission capacity pre-allocated to the hydro producer. A similar system is shown in Fig. 11.1. The algorithm employs a coordination strategy proposed in [55] and stochastic optimization [57].

According to [81], the HPP shall determine its optimal production for the given price scenarios. Simultaneously, assuming uncongested transmission, the WF determines its production in the planning day for each of the wind scenarios. Since the HPP has priority on transmission, the WF would need to cut its production if the total scheduled production of both producers implies congestion. Instead, they coordinate before submitting the bids to the spot market, i.e. the HPP agrees to adjust, to some extent, its production to that of the WF. For this service, the
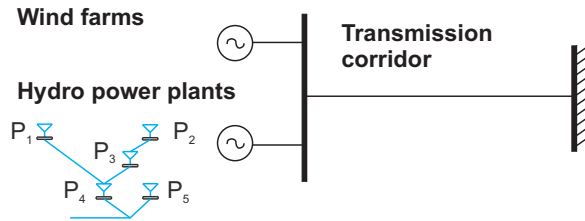
Figure 11.1: The wind and hydro power producers injecting power into the same node connected to the rest of the system by one line. The depicted structure of the hydro power plant cascade corresponds to the example treated in this chapter.

WF pays the HPP a pre-agreed price per MW of the obtained transmission capacity in the hours of potential congestion. In the simulations it was assumed that this price was equal to the average spot market price determined from the data of the previous year. Thereafter, the HPP determines its optimal production to bid on the spot market and the remaining transmission capacity is allocated to the WF.

In [83] this work is extended to account for the wind imbalance payments. Additionally, if transmission capacity is available, the HPP can bid on the intra-day regulating market. These papers contained neither a discussion how the price shall be determined, nor the maximization of the common profit of the coalition.

In none of the above mentioned publications or in any other ones to our knowledge, a fair systematic splitting scheme for the profit obtained by wind-hydro coordination has been proposed.

The following sections describe:

- A new coordination scheme employing stochastic optimization to maximize total profit, including the imbalance penalties, of the wind-hydro coalition.

- A new proposal for splitting the extra profit gained by a coordinated bidding and operation strategy with the fair and transparent method justified by coalitional game theory. The method is based on the Shapley value that considers incremental impact of the individual members of the coalition on the total profit [92], see Chapter 9.

11.2   Proposed Scheme Outline

11.2.1   Problem Formulation

The problem we address is inspired by an actual case occurring in Sweden. The main electricity consumption centers are located in the southern part of Sweden, while on the other hand, convenient and economically attractive conditions for hydro and wind power production are available in the northern part of Sweden. Rivers flowing through long valleys have given rise to many hydro power plants with several hydraulically coupled reservoirs. However, the transmission system bringing power from the northern part to the south is frequently congested. The local lines of the river cascades could be congested as well. This restricts the otherwise promising potential for installation of wind power plants in the north.

To assure applicability of our approach in a wider scope in various power systems and market conditions, we consider the problem on a higher level of abstraction. Thus, a more general formulation could be described as follows:

- There are two independent generation companies. One possesses a hydro power plant consisting of several reservoirs. The second company operates a wind power plant. Both power plants are located in geographical proximity to each other and are feeding power into the same substation, which is connected via a line or a group of lines to the rest of the power system as shown in Fig. 11.1.

- In the assumed market, electricity is traded only via a day-ahead market. Imbalances are penalized.

- We assume that the new power plant has the right (an additional options to reinforcement or installed capacity reduction, as discussed in Section 1.1) to use the existing infrastructure provided that it reduces its production in the congestion hours upon a day-ahead request of the existing power plant. In some circumstances/markets, such coordination may need an additional regulatory support. We demonstrate that it can be advantageous for all the involved sides, without harming free competition. Therefore, this is a justified option.

  In the example, the existing transmission capacity is allocated to the HPP. The WF is allowed to connect to the network, if it

accepts HPP's priority in nominating and allocating the transmission capacity.

Individual uncoordinated planning of production and bidding yield a suboptimal situation for all involved parties. Producers may suffer from a lower economic efficiency (e.g. wind power production can be curtailed) and frequent TSO interference in the congestion management may be necessary. This drawback could be overcome by a planning and operation coordination scheme. A necessary characteristic of such a scheme is that it provides an incentive for all involved parties to cooperate. In a market environment this can be achieved only by a fair sharing of the profit resulting from the coordination.

11.2.2 Coordinated Operation

Our proposal is to coordinate (as far as legislation allows) planning and bidding strategy of the wind and hydro power producers. In many systems, a shared bidding strategy by two or more market participants could be perceived to have cartel agreement elements, typically not allowed by law. On the other hand, legislation allows mergers of power production companies, unless the resulting market share exceeds a certain value. Therefore we make the assumption that there is a legal framework enabling coordinated planning and bidding by power producers. The details of such a framework are outside the scope of this thesis and would likely be country specific.

Coordinated planning and bidding would yield a benefit on the side of power producers, allowing them to optimize their profits by means of optimal utilization of their production facilities with respect to external conditions, in this case transmission restriction, and their technical properties, in this case storage capability of the hydro power plant and low operation costs of the wind power plant.

Besides power producers, TSOs may also benefit from the coordination of the producers, as this would create a self-regulating effect on producers, which should be a desired property of transmission system operation [136]. Benefits for TSOs would be twofold: a high utilization of transmission assets and a minimal need for TSO involvement in the congestion management. In other words, the TSO does not have to initiate any congestion relief actions, as the concerned market participants initiate them themselves.

11.2.3 Sharing of Profit Between Producers

To provide an incentive for producers to coordinate their planning and operation a scheme for sharing either production costs or resulting profit has to be introduced. This scheme has to be transparent and fair, in other words the additional benefit brought by the participation of each producer has to be evaluated and allocated. According to game theory, these properties are guaranteed by the Shapley value [92], [34].

In this case, we treat profit sharing from a coordinated use of the transmission capacity. This transmission capacity has been allocated to the hydro power plant since the newly built wind producer wanted to avoid the costs for the necessary grid expansion. Thus, we compute how the aggregated profit of these two entities changes when they form a coalition. To guarantee transparency we suggest that the following procedure would take place in the planning and operation horizon, i.e. in this case of short-term day-ahead planning. Thus, every day an ex-post calculation is done:

1. The data for the previous day is collected. This data includes input parameters, e.g. wind speeds, water inflows, spot prices, as well as profit data resulting from the coordinated planning and operation: revenues from the sale of the energy and the balancing energy costs.

2. Profits for the hypothetical individual (uncoordinated) operation of producers are computed.

3. The profit figures for coordinated and uncoordinated strategy are inserted into Shapley expression (9.3), determining the profit share of the entity $l \in \mathcal{A}$:

$$
\phi_l(c) = \sum_{n_C=0}^{n_{\mathcal{A}}-1} \left[\frac{n_C!(n_{\mathcal{A}}-1-n_C)!}{n_{\mathcal{A}}!} \sum_{\substack{C \subseteq \mathcal{A}\backslash\{l\} \\ |C|=n_C}} \Delta c(C,l) \right],
$$

where $\phi_l(c)$ is a profit share, c is the profit in the coalition. Thus, the profit share for the previous planning and operation day is determined.

Simulations demonstrating the advantage of the coordinated planning and operation versus uncoordinated strategy are described in the next sections.

11.3   Mathematical Formulation

Let us first consider the deterministic problem formulation, i.e. both the price and wind forecasts are perfect and available before the spot market closure. First, as the result of the optimization to be run prior to bidding on the spot market, we determine the (expected) profit of the producers and optimal decisions concerning:

1. Production to be submitted to the spot market for each hour of the next operation day;

2. Optimal actual water discharges, spillages and thus the reservoir content for each generating unit and each hour of the planning horizon;

3. Optimal actual wind production for each hour of the planning horizon.

These decisions are based on a given hydro cascade model, WF model, water inflows and forecasts of the wind and price. The hydro cascade model describes discharge production equivalents, couplings between reservoirs etc. The problem is constrained by the physics of the hydraulical system, discharge and reservoir limitations, targets of the hydro reservoirs' content, wind farm physics and transmission capacity constraints. Next, the spot market is cleared. During the operation day producers just have to follow their decisions concerning actual production and spillages.

Stochastic formulation allows one to consider uncertainties defined by scenarios with assigned probabilities, in our case price and wind scenarios, and to optimize expectation of some quantity, in our case profit. The water inflows are here considered as deterministic. The decision variables can be structured in a tree in accordance with the decision stages and time evolution, as in Fig. 11.2. Here, each branch of the tree corresponds to one scenario with a particular wind speed profile, a spot price profile and is given a probability of occurrence. A tree representing three price and three wind scenarios is shown. These scenarios should be available at least 13 hours prior to the operation day, i.e. at least one hour before the spot market clearing and should cover the entire operation day, thus 37 hours ahead. Then the variables for the entire tree are computed.
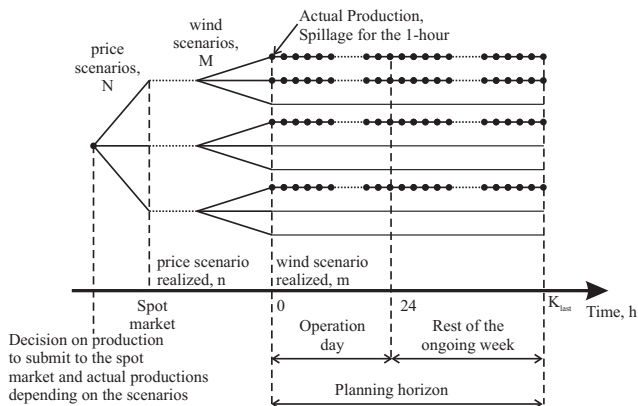
Figure 11.2: Scenario tree for day-ahead planning.

From the problem formulation side, for the hydro planning only price uncertainty is relevant and the tree contains N branches, corresponding to the number of price scenarios. For the coordinated decisions, the tree contains $N \times M$ branches, where M is a number of wind scenarios. As the first stage decisions optimization shall find, for each price level n, a single spot production which maximizes expected profit, i.e. a compromise between M wind profiles weighted by their probabilities. Simultaneously, optimization determines the decisions on actual production in the operation day, which are different for each price and wind scenario - second stage recourse decisions. Thus, decisions taken in uncertainty are adjusted in the operation stage to the actual conditions, i.e. the realized scenario.

In contrast to determining the bid, we determine optimal production to bid on the spot market at the defined clearing price level. We do not address structuring of the bids, but assume that it is possible to submit price dependent bids. This means that we determine that, at price A €/MWh, the accepted production on the spot shall be optimally B MWh. In the simple case the production amount corresponding to the lowest price scenario coincides with the bid, however bids corresponding to higher prices will contain only the increment from the next lower price bid. The probability of the price scenario affects only expected profit prior to the spot market, but not the decisions.
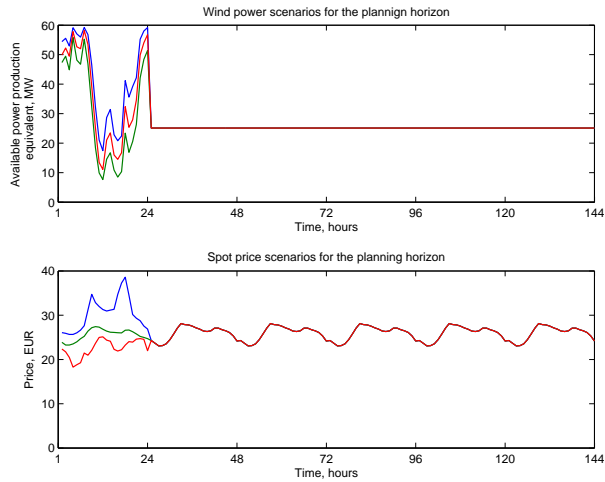
Figure 11.3: Wind (top) and price (bottom) scenarios considered for the planning of the first day in the week. Wind scenarios have the probability from top to bottom: $0.38, 0.223, 0.397$. The price scenarios have the probabilities from top to bottom: $0.037, 0.866, 0.097$.

Thus this is a two stage stochastic programming with recourse. The non-anticipativity constraints, which impose the requirement that solutions shall be based only on information known at the time of decisions, are satisfied.

Considering Fig. 11.2 from the user perspective we conclude that the expected profit is linked to the root node together with optimal spot productions at each price level. As soon as the market is cleared, the price is known. The expected value of the profit can be updated. Then, based on the observations of the actual wind conditions, the producer determines which wind profile scenario has been realized. At the beginning of the operation day, both realized price and wind scenarios are known. The producer shall then operate power plants in accordance with pre-computed decision variables at the branch of the tree corresponding to the actual conditions, following the same branch during the entire day. Planning is then repeated daily.

The decision variables for the hours k of the rest of the ongoing week, i.e. $K_{last}^{day} < k \leq K_{last}$ are not used, neither in the submission of the

production nor at the operation stage. These must, however, be included into the optimization problem to comply with the target values of the hydro reservoirs content in mid-term hydro planning [37]. For the rest of the current week, the same averaged price profile is assumed for all the price scenarios, for example as in Fig. 11.3. Wind power production is limited by average monthly wind power production based on the historical data, i.e. in all the scenarios $\overline{P}_w^{sc}(k, m) = P_{av}$.

To consider penalties for the deviations from the schedules, we employ the following balance settlement model, as seen from the producer or generally a balance group.

- The price for the overproduction is:

$$c_{pos}^{imb}(k, n) = k_o \cdot c^s(k, n). \tag{11.1}$$

- The penalty for the underproduction is defined, as follows:

$$c_{neg}^{imb}(k, n) = k_u \cdot c^s(k, n), \tag{11.2}$$

where expected overproduction penalty coefficient $k_o = 0.95$, expected underproduction penalty coefficient $k_u = 1.05$, $c^s(k, n)$ is the spot market price for hour k and price scenario n. The values of the coefficients k_o and k_u in the expressions above are obtained as expected values of the imbalance payments from the statistics of Nordel regulation market in January 2004.

This model does not aim at reproducing balancing energy payment rules of a particular market. This model rather represents a general concept of penalizing imbalances so the formulations we further propose could be applied also in other markets.

We introduce planning and bidding strategies in general terms with intuitive interpretations. These general expressions are expanded in Appendix E.

11.3.1   Individual Strategies

When power producers do not coordinate their strategies, they plan individually as explained below.

Hydro Power Plant

It is assumed that the hydro power plant does not cause any imbalance, i.e. it can follow its scheduled production perfectly and thus its objective can be expressed as a pure maximization of the profit from the energy accepted at the spot market z_h^s, subject to price uncertainty:

$$\max z_h^s \tag{11.3}$$

$$s.t. \quad g_h^{hb} = 0 \tag{11.4}$$
$$g_h^{rt} = 0 \tag{11.5}$$
$$h_h^{rl} \leq 0 \tag{11.6}$$
$$h_h^d \leq 0 \tag{11.7}$$

$$h_h^t \leq 0 \tag{11.8}$$

The set of constraints from (11.4) to (11.7) describe hydraulical properties of a hydro power plant, explicitly: g_h^{hb} are hydraulical balance constraints, g_h^{rt} are reservoir target values provided by medium-term planning, h_h^{rl} are reservoir limits and h_h^d are discharge limitations.

The hydro power producer has a higher priority for the allocation of the transmission capacity, therefore its planning and operation is completely decoupled from the wind farm producer and thus the constraint (11.8) takes into account only the own production. In other words, this constraint limits the overall production of the hydro power plant to the value given by the rating of the transmission line.

Wind Farm

Due to the stochastic nature of the wind, actual production of the wind farm may deviate from the scheduled production and thus induce an imbalance with respect to its bid on the spot market. This is included in the cost function as well as in the auxiliary constraints (11.10) and (11.11):

$$\max z_w^s + z_w^{imb} \tag{11.9}$$

$$s.t. \quad g_w^{imb} = 0 \qquad\qquad (11.10)$$

$$h_w^{imb} \leq 0 \qquad\qquad (11.11)$$

$$h_w^t \leq 0 \qquad\qquad (11.12)$$

Here z_w^s is the profit from wind production accepted at the spot market and z_w^{imb} is the profit from wind imbalance. The amount of energy which can be injected into the network by the wind farm, equation (11.12), is given as the transmission capacity remaining after the allocation of the hydro power production injection.

11.3.2   Coordinated Strategy

The objective of the coordinated strategy is to maximize the overall profit from the combined production of the hydro power plant and the wind farm:

$$\max \ z_h^s + z_w^s + z^{imb} \qquad\qquad (11.13)$$

$$s.t. \quad g_h^{hb} = 0 \qquad\qquad (11.14)$$

$$g_h^{rt} = 0 \qquad\qquad (11.15)$$

$$h_h^{rl} \leq 0 \qquad\qquad (11.16)$$

$$h_h^{d} \leq 0 \qquad\qquad (11.17)$$

$$g_w^{imb} = 0 \qquad\qquad (11.18)$$

$$h_w^{imb} \leq 0 \qquad\qquad (11.19)$$

$$h_{h+w}^t \leq 0 \qquad\qquad (11.20)$$

Both hydraulical and wind imbalance constraints have to be met. The transmission constraint in this case couples production from both power plants.
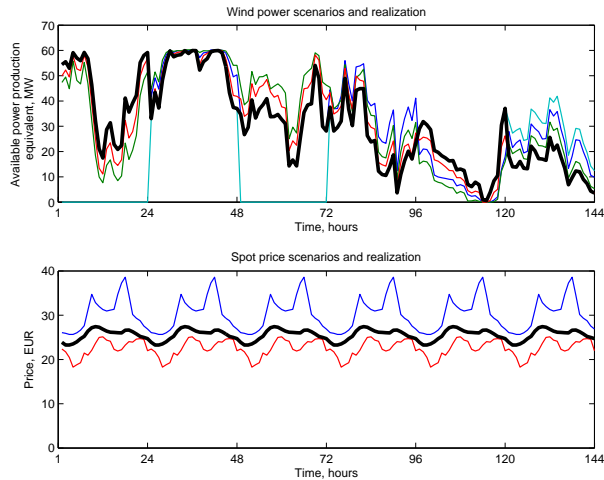
Figure 11.4: Wind (top) and price (bottom) scenarios and realizations. Realization of stochastic variables expressed by the thick solid line.

11.4 Illustrative Example

11.4.1 Test System

The example we consider has the following characteristics:

- The HPP consists of 5 interconnected reservoirs, as shown in Fig. 11.1. The overall rating of generators of the HPP is 250 MW. The WF has the power rating of 60 MW. There is no local load connected to the common bus.

- The power is injected into the rest of the transmission system via the line with the capacity of 250 MW.

- The inflow data correspond to recordings of Ume river from 2001.

- There are three wind scenarios for each day, derived from real recordings. There are three price scenarios for each day derived from the actual price statistics in Nordel in 2004.

Both for individual and coordinated strategies the same input data are used. An example for the first day of the week and averaged values representing the rest of the week is shown in Fig. 11.3.

For evaluation and comparison of strategies the realization of input scenarios shown in Fig. 11.4 is applied. After determining individual and coordinated strategies this realization is inserted into equations (E.1), (E.2) and (E.3) in the Appendix to obtain financial figures, i.e. z_h^s, z_w^s, z^{imd}, z_w^{imb} allowing comparison of the uncoordinated and coordinated strategy.

The stochastic optimization has been implemented in GAMS [106] to solve this non-linear continuous optimization problem. The total number of variables in 9 blocks is 47008. The number of equation blocks is 17, resulting in 20233 equations. Computation of the optimal production for the next day takes 735 sec on an Intel®Duo Core™2 Duo CPU, 4GB RAM with Windows rating 3.2, Windows Vista system, and the Matlab 2007 interface for the pre-/post- processing of the results.

Figure 11.5: Bids to the spot market and the actual production in the uncoordinated case. The black solid line is hydro power production and the solid gray line wind power production. The bids are expressed by the dashed gray and black lines. The solid thin black line corresponds to available wind power production.

11.4.2   Individual Strategies

Applying individual uncoordinated strategies yields results as shown in
Fig. 11.5. The hydro power producer plans its production first and as
it has a higher priority regarding transmission capacity, it fully utilizes
the transmission capacity during the expected price peak hours. The
wind power producer adjusts his bid to this and must go down to zero
production even though wind is expected to be available. Besides this,
there are several cases when the available wind evolved according to the
highest speed forecast and the actual wind production exceeds the bid.

11.4.3   Coordinated Strategy

Results of the coordinated strategy are shown in Fig. 11.6. As expected,
the coordinated strategy leads to a full utilization of the transmission
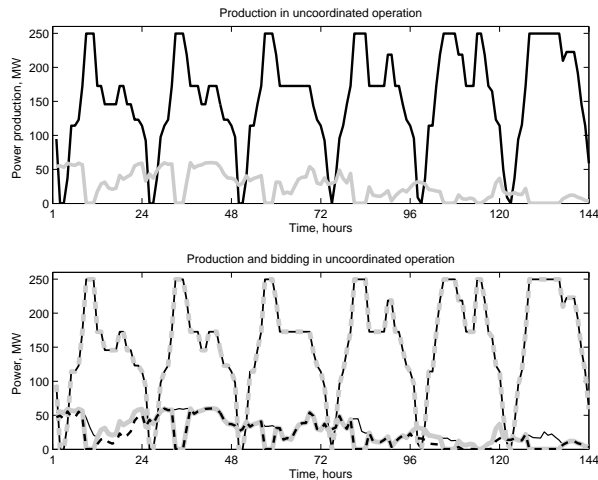capacity, i.e. 250 MW, without a need for spillage of the wind farm
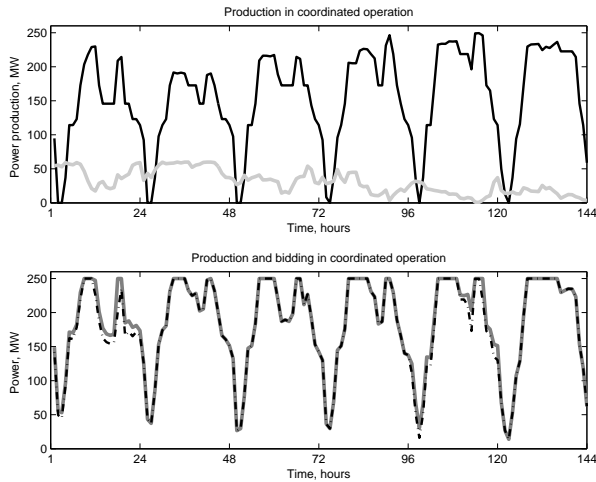

Figure 11.6: Bid to the spot market and the actual production in the
coordinated case. The black solid line is hydro power production and
the solid gray line wind power production. The common bid is expressed
by the dashed-dot black line. The solid dark gray line corresponds to
the overall production of the hydro and the wind power.

production due to the adjustment of the hydro power production.

The reservoirs' content is fixed at the end of the week in accordance with mid-term planning. The "extra" water saved due to the high wind shall be used for either overproduction in the operation day or for spot production in the coming days, whatever is optimal. A combination of factors determines that a partial overproduction is more profitable than full adjustment of hydro production. Explicitly: transmission limits the possibility to increase production in the coming days, particularly in the peak hours and, simultaneously, the balance price for overproduction in the high price hours is sometimes higher than the spot price in off-peak hours.

Fig. 11.7 confirms the intuitive expectation that the coordinated strategy leads to an increase of the sum of revenues of both producers, while no significant change in penalties for balancing energy is observed. The loss in the balancing energy in Fig. 11.7 is computed as imbalance energy times the difference between the spot price and the price to be either paid or received by the producer. Positive values correspond to the opportunity loss (penalty for the overproduction) and the negative values are a penalty for the underproduction.

11.4.4   Profit Sharing

The profit of a producer, or producers, is obtained by summing up revenues and balancing payments, which can be either negative or positive depending on the type of imbalance. The comparison of profits for the uncoordinated and coordinated cases is summarized in table 11.1.

Table 11.1: Comparison of the weekly profits of the individual and coordinated strategies.

Producer	Individual Strategy, €	Coordinated Strategy, €	Change in the Profit
Hydro Power Plant	579,956	590,108	+1.8%
Wind Farm	91,332	101,484	+11%
Overall profit	671,288	691,592	+ 2.9%

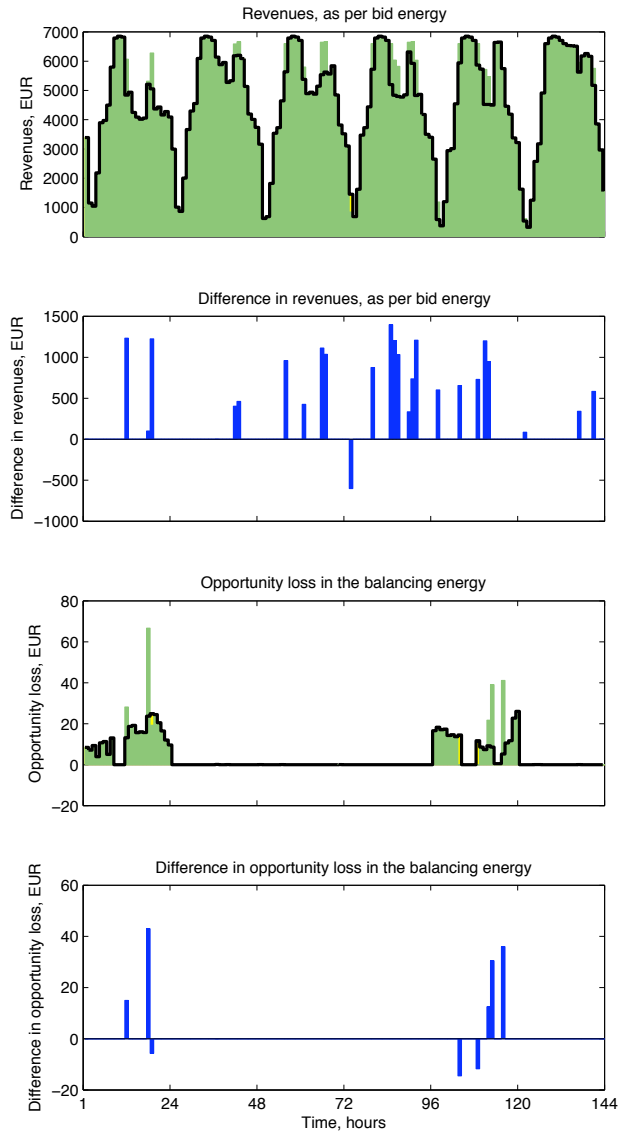While the allocation of profits among the producers is straightforward

Figure 11.7: Comparison of the uncoordinated and coordinated strategy. The shaded area represents coordinated strategy, whereas the solid black line expresses the sum of uncoordinated strategies.

in the case of the individual strategies, for the coalition we apply the Shapley value (9.3) to profit allocation.

Both cases hydro is the first member of the coalition and hydro joins the coalition as the second member - have 50% probability. Therefore, for the hydro producer we get:

$$\phi_h(c) = \frac{1}{2} \times 579,956 + \frac{1}{2} \times (691,592 - 91,332) =$$
$$= 590,108. \tag{11.21}$$

Similarly, profit share of the wind producer is:

$$\phi_w(c) = \frac{1}{2} \times 91,332 + \frac{1}{2} \times (691,592 - 579,956) =$$
$$= 101,484. \tag{11.22}$$

It should be noticed that in this example of just two players, the profit sharing is somewhat trivial - extra profit of the coalition in absolute values is distributed equally between the players. Each player shall receive extra $10,152 €$. However, in the case of three and more players, profit sharing is not obvious and Shapley value is very helpful.

For this particular example and the particular set of conditions an increase of profit of 11% is achieved for wind producer and 1.8% for the hydro producer if they coordinate their planning and bidding compared with their uncoordinated operation.

11.5   Concluding Remarks

This chapter addresses the problem of two producers injecting power into the transmission grid via a line with insufficient capacity to accommodate a peak production from both producers.

We present how these two producers can coordinate their planning and bidding strategies by means of stochastic optimization and by doing so, they may achieve a higher common profit than without coordination. We propose how this profit may be fairly shared by these producers applying the concept of Shapley value from game theory. We use a realistic example to demonstrate applicability of our proposals.

Although we considered a particular example consisting of a wind and hydro producer, the introduced concepts can be applied to various types

of power producers, which could benefit from a coordinated planning and bidding strategy.

It is assumed that coordination takes place only in the day-ahead planning and bidding stage. This has some advantages, as only a limited amount of information has to be exchanged between the producers in a noncritical time. Even stronger coordination and participation in the intra-day market may be implemented. In addition to the maximization of revenues in the planning stage, this would allow further minimization of costs for balancing energy.

Closure

Summary and Conclusions

Modern power system operation, planning and billing are utmost complex tasks involving many uncertainties on one side and subjected to high requirements on the other. Simultaneously, when addressing these tasks we can benefit from technological developments in many areas over the past decades - communications, sensors, primary equipment, computers. New technologies allow the reduction of the influence of uncertainties by providing better and more accurate information or by enabling the use of powerful statistical methods.

Many present works are exploring these possibilities. This thesis is contributing to these developments, particularly, to the development of methods with more extensive quantification of the impacts and uncertainties. This objective cannot be achieved completely in a single thesis and, perhaps, in general. Yet contributions discussed here shall help, according to the author, to make another step towards development, implementation and support of stochastic "thinking" as such. Several examples from different areas were used in the thesis to demonstrate that it has a natural fit applicable to almost every concept in power systems.

Major conclusions can be formulated, as follows:

- Power system efficiency can be improved in both technical as well as economic aspects with an extensive modeling and statistical approach;

- Proposed methods are feasible and advantageous, and are positioned in the context of current practices and systems;

- Implementation of the proposed methods requires development of software tools and shall be associated with minor to moderate investments.

Thus, the practicality of the contribution is demonstrated.

With more detailed consideration, it can be concluded that for the real time algorithms:

- Uncertainties in measurements, model parameters and model topology may endanger secure operation of the power system and influence the economy;

- Proposed modifications and enhancements of the algorithms facilitate identification of the topological errors, thus improving the security and basis for economic decisions;

- Disregarding the temperature dependency of the line conductor resistance may have a non-negligible effect on the performance of the state estimator. Proposed approach to account for the temperature changes is practical and justifiable.

- Simulation and analysis of the performance of steady state estimator during transient conditions will contribute to understanding of the SE results in real operation. Proposed approach shall assist in tuning measurement infrastructure and SE at the engineering, commissioning and maintenance stage.

These problems are examples of areas, where quantification of the uncertainty leads to improvements in the resulting decisions.

For the off-line analysis, it can be concluded that:

- Proposed loss allocation method is similar to incremental transmission loss method and can be seen as a support of the incremental method by game theory implications.

- Proposed application of Shapley value to profit sharing between hydro and wind producers encourages collaboration, efficiency and offers a fair profit splitting scheme.

These improvements in the analysis have a direct impact on the competitiveness of the players and, in overall, on the power system operation efficiency.

Future Research

Further improvements of the proposed algorithms can be done in many aspects, however, this author believes that the general concepts have been demonstrated and proven by the simulations in sufficient level of details.

Directions for the future developments can be split in two categories:

- Identification of further topics in power systems and study benefits of application of statistical methods ;

- Precision and further elaboration of the proposed concepts and topics.

The first category is very broad. To mention a few examples that are particularly appealing to me - stochastic power flow, stochastic network planning and cost splitting applications. Already a number of excellent works have addressed this topic. Yet, I believe there is a high potential and importance for further work.

To list some examples of the further work in the in the second category, I would like to mention:

- Investigation of the possibilities to combine the proposed method for topology error detection with SE and multiple PMUs;

- Derivation of analytical expressions and consideration of further statistical dependencies in topology error detection;

- Advanced models for the measurement chain in the analysis of dynamic performance of state estimation;

- Studies of approximate computational methods in loss allocation.

- Inclusion of further markets and conditions in operation planning by a power producer.

The work on these aspects could bring further benefits and support rational and justified decisions.

Appendix A

Test Systems Data

A.1 The 9-Bus Test System

A 9-bus test system is used in Chapter 8 of the thesis. The system data are available under [6] and the system is shown in Figure A.1. All the system parameters are modeled as in the base case, except that a simple AVR model is adopted for G2-G3 as for G1, no PSS. The line (C) parameters were modified as follows: $Z = 0.003226 + j0.00695$, $B = 1.449$ pu.

The locations and types of measurements are summarized in the Table A.1. Substation 5-9 are equipped with measurement devices and communication links, voltages are measured at all these substations and active and reactive power at several locations.

A.2 The IEEE 14-Bus Test System

The system is shown in Figure A.2. Data for electrical parameters are available in [26] and were not modified from the source.

A.3 The IEEE 300-Bus Test System

The system is shown in Figure A.3. The electrical parameters are described in [26] and were not modified in the simulations.
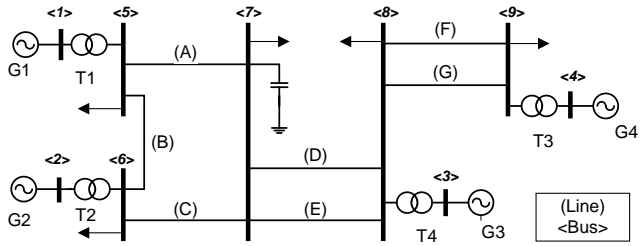
Figure A.1: Single line diagram of the 9 bus test system.
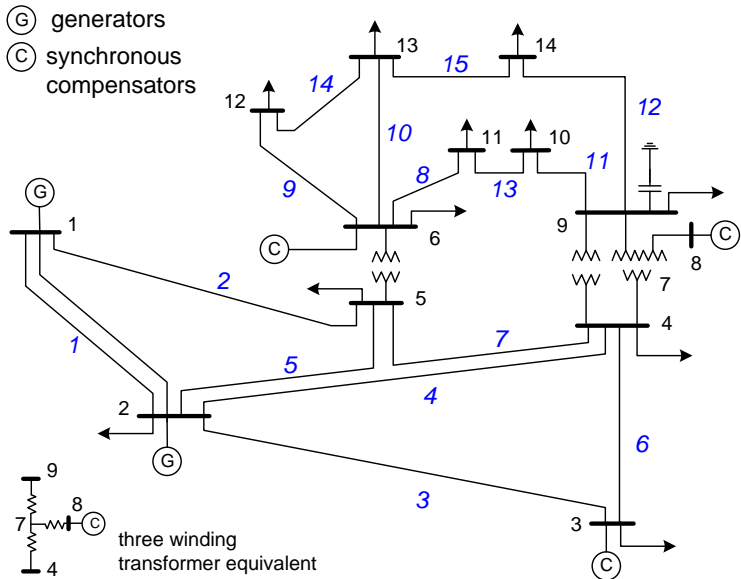
Figure A.2: Single line diagram of the IEEE14-bus.

Table A.1: Measurement Infrastructure

Bus	Location	Type
5	A, B, T1	PQ, V
6	T2, Load	PQ, V
7	D, E	PQ, V
8	F, G, T3	PQ, V
9	T4 , Load	PQ, V
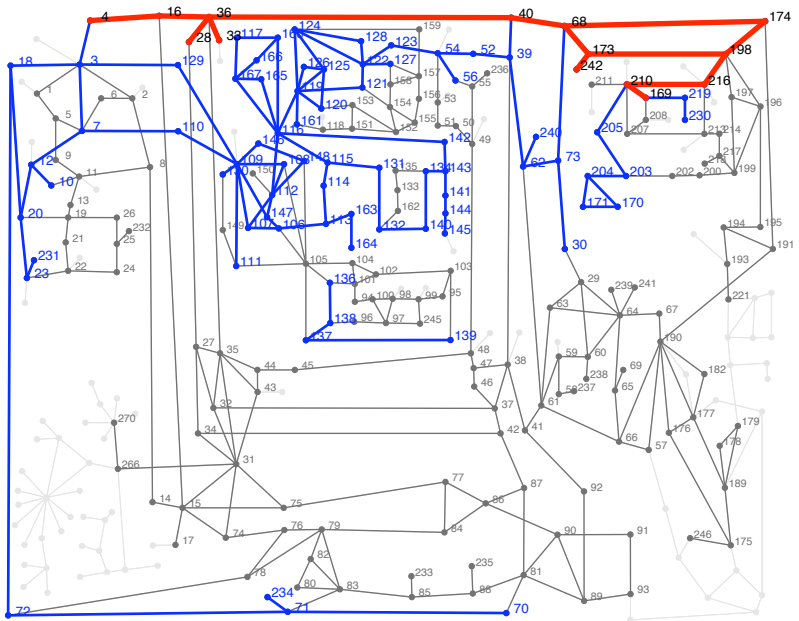
Figure A.3: Single line diagram of the IEEE300-bus.

Appendix B

Modeling of the Electric Parameters of the Transmission Branch

B.1 Transmission Line

Consider the model of the line as shown in Fig. B.1. Current flowing in the conductor creates thermal losses that are dependent on the resistance r of the line and the current. The parameter jx is a representation of the reactance that creates an electromagnetic field around the line.

In addition, as the line operates under certain voltage, there is a difference of the potentials between the different phases and the ground creating a capacitive element - susceptance jb. Moreover, small parts of current are being lost in the isolators of the line and due to ionization of the air around the conductor causing corona phenomenon. This is modeled by the conductance g, which also gives rise to losses.

The currents $\underline{I}_{ij}$ in the beginning and $\underline{I}_{ji}$ in the end of the line can be expressed through the voltages at the line ends (see Fig. B.1):

$$\underline{I}_{ij} = y_{ij}(\underline{V}_i - \underline{V}_j) + y_{ij}^{sh}\underline{V}_i \qquad (\text{B.1})$$

$$\underline{I}_{ji} = y_{ij}(\underline{V}_j - \underline{V}_i) + y_{ji}^{sh}\underline{V}_j \qquad (\text{B.2})$$
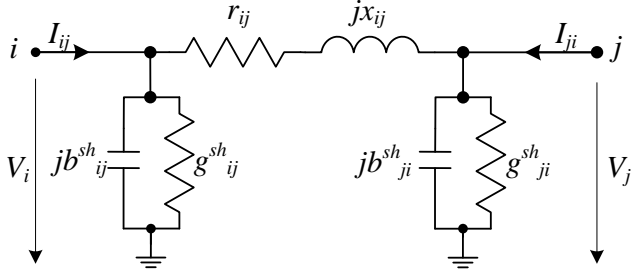
Figure B.1: Equivalent transmission line circuit

where
$y_{ij} = 1/(r_{ij} + jx_{ij})$ is the series admittance of the line.
$y_{ij}^{sh} = y_{ji}^{sh} = g_{ij} + jb_{ij} = g_{ji} + jb_{ji}$ is the shunt admittance of the line connected at the busses i, j;

B.2   Transformer

Due to the losses it is profitable to operate transmission lines at high voltage. However, generators and loads are designed for lower voltages. The transformation of the power to higher/lower voltage level is made by the transformers.

Voltage e_1 applied to primary winding of the transformer results in terminal current i_1 that creates magnetizing flux ϕ_m and leakage flux ϕ_1. The magnetizing flux ϕ_m induces current in the secondary winding, that creates leakage flux ϕ_2. To summarize:

$$\phi_1 = k_1 n_1 i_1 \tag{B.3}$$

$$\phi_2 = -k_2 n_2 i_2 \tag{B.4}$$

$$\phi_m = k_m(n_1 i_1 - n_2 i_2) \tag{B.5}$$

where k_1, k_2 and k_m are the permeance of the corresponding flux pathes.
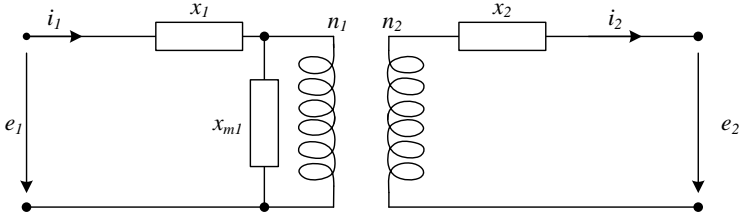
Figure B.2: Transformer equivalent circuit

Taking into account (B.3) and expressing e_1:

$$e_1 = \omega n_1(k_1 n_1 i_1 + k_m(n_1 i_1 - n_2 i_2)) =$$
$$\omega([k_1 + k_m]n_1^2 i_1 - k_m n_1 n_2 i_2) = ([x_1 + x_{m1}]i_1 - x_{m1}\frac{n_2}{n_1}i_2) \quad \text{(B.6)}$$

where $x_1 = k_1 n_1^2$ - is the leakage inductance of the winding 1 and $x_{m1} = k_m n_1^2$ is the magnetizing inductance;

Similarly e_2 can be expressed. This leads to transformer equivalent circuit, as depicted in Fig. B.2.

As the reactance x_{m1} is very large in contrast to x_1 and x_2 it is frequently ignored, resulting in open circuit.

Equivalent Impedance of the Transformer

Let us examine the ideal transformer in Fig. B.2. If the leakage fluxes are ignored, then it can be written:

$$\frac{v_1'}{v_2'} = \frac{n_1}{n_2} \quad \text{(B.7)}$$

Moreover taking into account power equality $v_1' i_1^* = v_2' i_2^*$:

$$\frac{i_1}{i_2} = \frac{n_2}{n_1} \quad \text{(B.8)}$$

If voltage drop across the leakage reactance of primary winding is $x_1 i_1$, transforming it to the secondary side (fig.B.3) we obtain:

$$x_1 i_1 \frac{n_1}{n_2} = x_1 i_2 \left(\frac{n_1}{n_2}\right)^2 \quad \text{(B.9)}$$
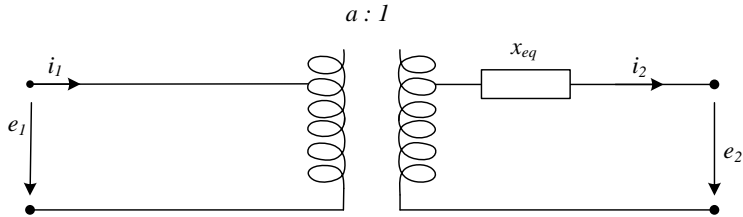
Figure B.3: Standard transformer equivalent circuit

Therefore equivalent transformer impedance can be obtained:

$$x_{eq} = x_1 \left(\frac{n_1}{n_2} \right)^2 + x_2. \tag{B.10}$$

Off-nominal Tap Ratio

The overall voltage profile in the transmission network may vary within certain limits. One of the means to keep the voltage in the distribution and sub-transmission network at permissible level and to provide reactive power support to transmission network is changing the turns ratio of the transformers. For this purpose frequently transformers supplying consumers are equipped with tap-changers.

To transform the equivalent representation of the transformer to off-nominal tap ratio, the similar approach can be applied as for the primary to secondary side transformation.

In case of the off-nominal tap ratio, the additional "ideal-transformer" is modeled and the reactance becomes:

$$x'_{eq} = a^2 x_{eq}. \tag{B.11}$$

In similar manner one could derive expressions for the transformer equivalent impedance, taking into account resistive losses in the windings.

B.3 Two Port Equivalent

Formula (B.1) gives the current values at the ends of the line depending on the connected bus voltages. Rearranging the terms, we get:

$$\underline{I}_{ij} = y_{ij}\underline{V}_i + y_{ij}^{sh}\underline{V}_i - y_{ij}\underline{V}_j \tag{B.12}$$

$$\underline{I}_{ji} = -y_{ij}\underline{V}_i + y_{ij}\underline{V}_j + y_{ji}^{sh}\underline{V}_j. \tag{B.13}$$

Similarly for the transformer, one can obtain [90]:

$$\underline{I}_{ij} = a^2 y_{ij}\underline{V}_i - y_{ij}\underline{V}_j \tag{B.14}$$

$$\underline{I}_{ji} = -y_{ij}\underline{V}_i + y_{ij}\underline{V}_j. \tag{B.15}$$

This derivation leads us to general branch model, as follows;

$$\left[\begin{array}{c} \underline{I}_{ij} \\ \underline{I}_{ji} \end{array} \right] = \left[\begin{array}{cc} A & B \\ C & D \end{array} \right] \left[\begin{array}{c} \underline{V}_i \\ \underline{V}_j \end{array} \right] \tag{B.16}$$

where A, B, C, D are complex parameters corresponding to transmission line or transformer.

The power flow thought the line can be obtained, as :

$$\underline{S}_{ij} = \underline{V}_i \underline{I}_{ij}^* = \underline{V}_i [y_{ij}(\underline{V}_i - \underline{V}_j) + y_{ij}^{sh}\underline{V}_i]^* = V_i^2(y_{ij}^* + y_{ij}^{sh*}) - y_{ij}^* \underline{V}_i \underline{V}_j^* =$$
$$= V_i^2[g_{ij} + g_{ij}^{sh} - j(b_{ij} + b_{ij}^{sh})] - (g_{ij} - jb_{ij})V_i V_j e^{j(\theta_i - \theta_j)} \tag{B.17}$$

Introducing notation $\theta_{ij} = \theta_i - \theta_j$ and separating the real and imaginary part, it can be obtained:

$$P_{ij} = V_i^2[g_{ij} + g_{ij}^{sh}] - V_i V_j(g_{ij}\cos\theta_{ij} + b_{ij}\sin\theta_{ij}) \tag{B.18}$$

$$Q_{ij} = -V_i^2[b_{ij} + b_{ij}^{sh}] - V_i V_j(g_{ij}\sin\theta_{ij} - b_{ij}\cos\theta_{ij}). \tag{B.19}$$

Continuing with the analysis in the similar way for the transformer we can obtain the following:

$$P_{ij} = a^2 V_i^2 g_{ij} - a V_i V_j(g_{ij}\cos\theta_{ij} + b_{ij}\sin\theta_{ij}) \tag{B.20}$$

$$Q_{ij} = -a^2 V_i^2 b_{ij} - a V_i V_j(g_{ij}\sin\theta_{ij} - b_{ij}\cos\theta_{ij}). \tag{B.21}$$

Appendix C

Statistical Properties of Random Variables

This appendix reviews some operations with random variables, which were used in Chapter 6.

C.1   Some Properties of Random Variables

C.1.1   Normal Random Variables

The numerical characteristics of the random variable obtained as the result of operations with independent normally distributed variable X and Y, can easily be obtained analytically recalling statistical properties of the normal distribution, as follows [66]:

- If $X \sim N(\mu_X, \sigma_X^2)$ and a and b are real numbers, then:

$$aX + b \sim N(a\mu_X + b, (a\sigma_X)^2); \qquad (\text{C.1})$$

- If $X \sim N(\mu_X, \sigma_X^2)$ and $Y \sim N(\mu_Y, \sigma_Y^2)$ are independent normal random variables, then their sum is normally distributed with:

$$U = X + Y \sim N(\mu_X + \mu_Y, (\sigma_X)^2 + (\sigma_Y)^2); \qquad (\text{C.2})$$

- If $X \sim N(0, \sigma_X^2)$ and $Y \sim N(0, \sigma_Y^2)$ are independent normal random variables, then:

  their product follows a distribution with density p

  $$p(z) = \frac{1}{\pi \sigma_X \sigma_Y} K_0 \left(\frac{|z|}{\sigma_X \sigma_Y} \right), \tag{C.3}$$

  where K_0 is a modified Bessel function of the second kind [66].

  their ratio follows Cauchy distribution

  $$X/Y \sim Cauchy(0, \sigma_X / \sigma_Y). \tag{C.4}$$

If the standard deviation of $Cauchy$ distribution is relatively small, it can be approximated by the normal distribution without significant loss in the accuracy. Fig. C.1 shows comparison of pdfs with average standards deviation values.
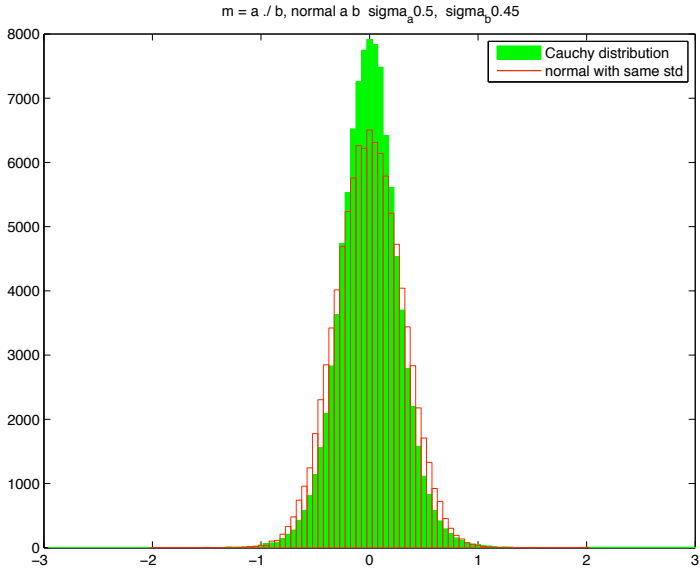
Figure C.1: Comparison of the true distribution of the i.n.r.v. ratio X/Y and the normal distribution with same standard deviation

C.1.2   Independent Random Variables

To obtain the sum or difference of the independent random variables X, Y with arbitrary probability distribution, one can apply convolution and cross-variance methods as shown for the two dimensional case in Fig. C.2 and in Fig. C.3 correspondingly.

Thus, probability density of $(X+Y)$ is a convolution of their probability densities f, g:

$$(f * g)(t) = \int_{-\infty}^{\infty} f(\tau)g(t - \tau)d\tau. \tag{C.5}$$

Probability density of $(X - Y)$ is a cross-variance of the probability densities:

$$(f \star g)(t) = \int_{-\infty}^{\infty} f^*(\tau)g(t + \tau)d\tau. \tag{C.6}$$
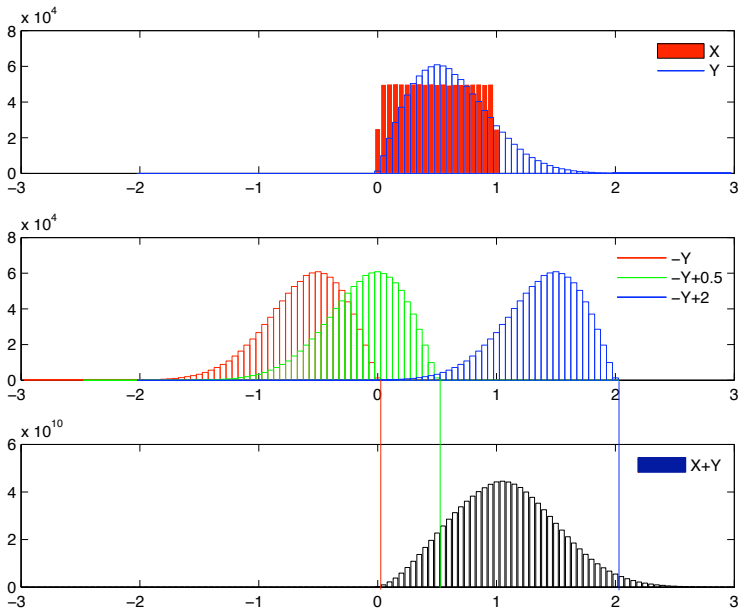
Figure C.2: Illustration of convolution to summation of irv

An analytical derivation and computation of the integral can be performed in simple cases. In a three dimensional cases, it would require
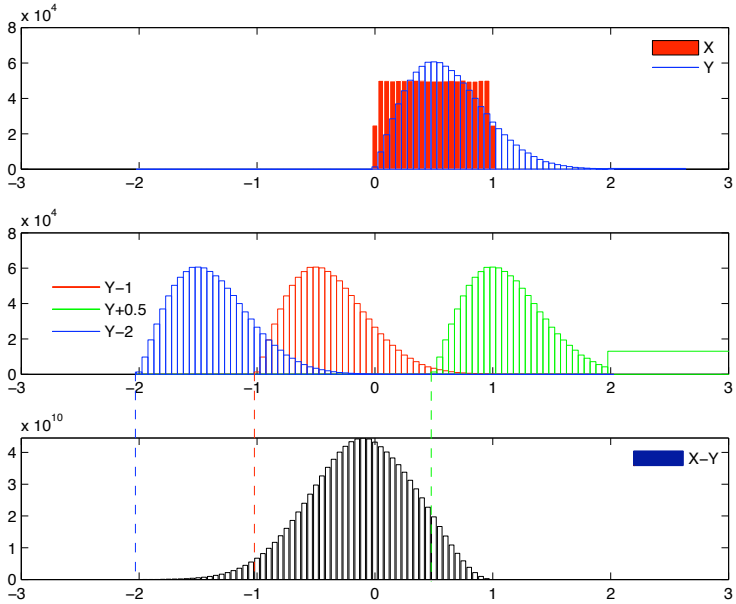
Figure C.3: Illustration of cross-variance to subtraction of irv.

computation of the joint probabilities and becomes complex. In the general case, we apply numerical methods and approximate each distribution with discrete representation and apply computation procedure for the discrete functions. For example, for the convolution we proceed:

$$(f * g)(n) = \sum_{m=-\infty}^{\infty} f(m)g(n - m). \tag{C.7}$$

Expression for the cross-variance can be obtained in a similar manner.

C.2   Transformation of the pdf Parameters

State Estimation computes not only an expectation of the states, but also an associated variance. In several cases in this thesis, for example, when comparing two voltages, the pdf parameters need to be transformed from the polar coordinates to rectangular ones as in [93] or similarly, as follows.

These transformations of the voltage random variable with normally distributed magnitude and angle into the real and imaginary axis is shown in Fig. C.4. In this figure, variation of the random angle and the magnitude are decoupled. The upper picture shows projections of the standard deviation of the random angle, using the linearization and the geometrical projections. We can apply linearization, since standard deviation of the voltage angle is small. The bottom picture derives results for the magnitude variations.

With these observations and using (C.2), we obtain:

$$\Re(\underline{X}) \sim N(E\{X\}\cos(E\{\chi\}),$$
$$(E\{X\}\tan(\sigma_\chi)\sin(E\{\chi\}))^2 + (\sigma_X\cos(E\{\chi\}))^2) \quad \text{(C.8)}$$
$$\Im(\underline{X}) \sim N(E\{X\}\sin(E\{\chi\}),$$
$$(E\{X\}\tan(\sigma_\chi)\cos(E\{\chi\}))^2 + (\sigma_X\sin(E\{\chi\}))^2), \quad \text{(C.9)}$$

where $E\{.\}$ is the expectation of random variable, $\underline{X}$ is a random complex variable, with magnitude $X \sim N(E\{X\}, \sigma_X^2)$ and angle $\chi \sim N(E\{\chi\}, \sigma_\chi^2)$.

C.3   Modeling and Simulation of the Bivariate Normal Distribution

Probability distributions in Chapter 6 were approximated by the normal bivariate distributions, without significant loss of accuracy. The models were described by the expectation and covariance matrix, i.e $X \sim N(\mu, \sum)$. The model parameters were determined with maximum likelihood estimator using standard tools available in Matlab.

Simulation approach to bivariate normal variable, with given model parameters, is well known and can be summarized, as follows:

- Compute Cholesky decomposition of the covariance matrix $\sum$, such that $\sum = AA^T$;

- Create matrix $Z \in \mathbb{R}^{2 \times n}$ of the instance of independent standard variables;

- Targeted variable is $X = \mu + A^T Z$

This simulation method was used in the thesis.
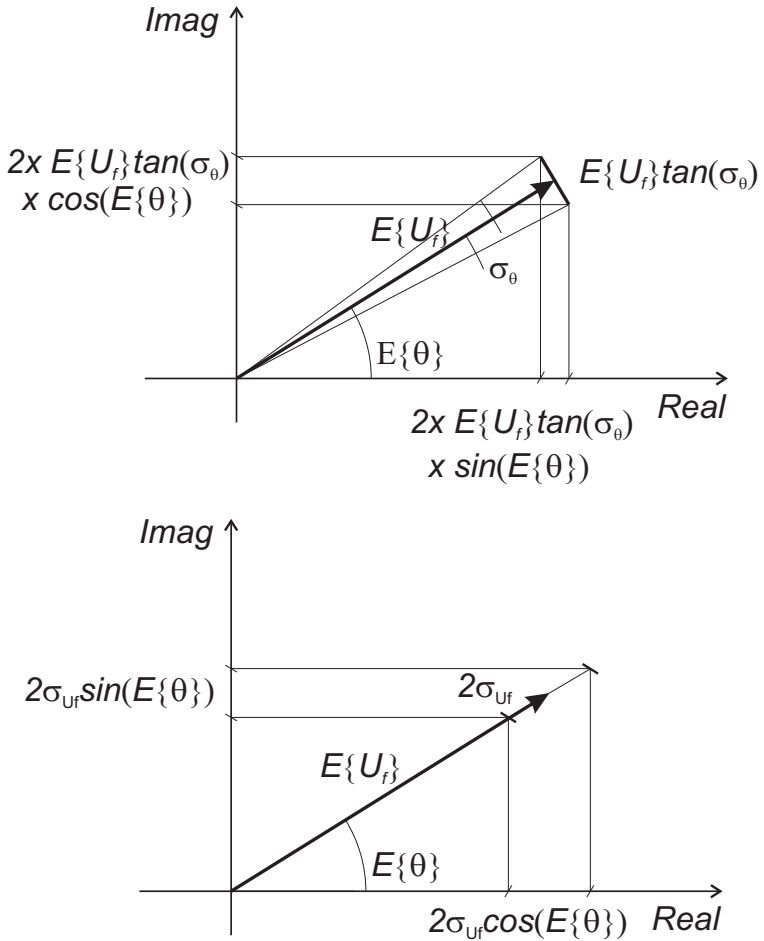
Figure C.4: Derivation of the distributions of the real and imaginary components.

Appendix D

Graph Algorithms

This appendix describes some of the auxiliary algorithms, which were used in Chapter 6.

D.1 Breadth-first search

Breadth first search algorithm [121] was employed to determine k-degree neighborhood of the reference node. In accordance to this algorithm, the adjacency matrix is multiplied by the vector of k-degree neighbors to obtain neighbor vertices of the next step as shown in Fig. D.1.
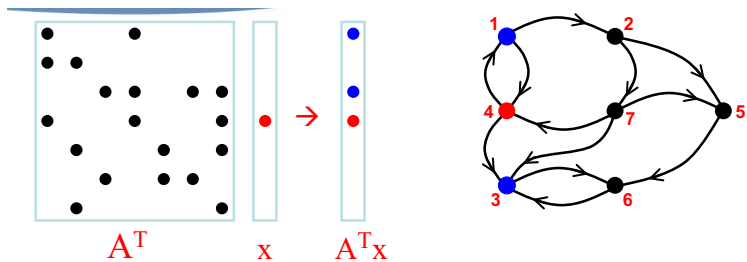
Figure D.1: Principle of the breadth first search algorithm [121]

D.2   Proposed Shortest Path Algorithms

In the scope of this work the distance is a number of edges between considered nodes. The algorithms below are implemented with bit-wise operations rather than set operation, since this is faster for the computer implementation.

D.2.1   Back-tracking algorithm

Once a discrepancy in the network is detected, a back-tracking algorithm shall be initiated from the erroneous path. The following algorithm was developed and applied to the test cases. The principle is shown in Fig. D.2.

In the first stage a breadth-first search is run starting from the last visitor of a conflict node till any node from the PMU path is detected:

1. Form a column vector neighbors $n^0 \in \mathbb{R}^{|\mathcal{N}|}$:

$$n_j^0 = \left\{ \begin{array}{ll} 1 & \text{if } j \text{ matches conflict node visitor } I(n_j^0, \mathcal{N}) = N_{Vc}, \\ 0 & \text{if otherwise.} \end{array} \right.$$
(D.1)

   where $I(n_j^0, \mathcal{N})$ is an operator that performs from a nonzero entry in n^0 a corresponding node $N_{Vc} \in \mathcal{N}$.

2. Set iteration number $k = k + 1$;

3. Set

$$n^k = n^{k-1} \oplus (A_N \otimes n^{k-1}),$$
(D.2)

   where A_N is a network adjacency matrix.
   Thus, $I(n^k, \mathcal{N}) = N_{Gk}[I(n^0, \mathcal{N})]$ contains all neighbors of $I(n^0, \mathcal{N})$ with degree not more than k.

4. If $I(n^k, \mathcal{N}) \cap \mathcal{N}_{PMU} \neq \varnothing$ - a PMU node was detected, assign $k_{last} = k$ and stop, otherwise go to step 2.

At the second stage, all vectors n are analyzed to distinguish only k^{th} degree neighbors for each k. Thus,

1. $k = k_{last}$

2. $n^k = n^k \ominus n^{k-1}$

3. Set iteration number $k = k - 1$;

4. If $k = 0$ stop, otherwise go to step 1.

Then, find $(k_{last} - k)$ neighbors of the detected PMU path node, which are an intersection with corresponding n^k, as follows:

1. $k = k_{last}$

2. Set $m^k \in \mathbb{R}^{|\mathcal{N}|}$ as:

$$
m_j^k = \begin{cases} 1 & \text{if } j \text{ matches PMU node, s.t.} \\ & I(n_j^k, \mathcal{N}) = I(m_j^k, \mathcal{N}) = N_{PMU}, \\ 0 & \text{if otherwise.} \end{cases} \tag{D.3}
$$

3. $m^{k-1} = n^k \otimes (A_N \otimes m^k)$, find $(k_{last} - k)$ neighbors of PMU node and k neighbors of the conflict N_c;

4. Keep just one non-zero entry in m^{k-1};

5. Set iteration number $k = k - 1$;

6. If $k = 0$ stop, otherwise go to step 3.

Vectors m^k contain entries corresponding to the shortest paths between conflict node and a PMU path node. Alternatively one could develop an algorithm based on the information $\mathcal{V}_j(\mathcal{V}(\mathcal{N}_V), \mathcal{N}_V)$ in $\mathcal{V}$ (structured variable NODE) about all the visitors of each node.

Note that there might be multiple options for the path, yet all the paths have the same length k_{last}. This is valid since every edge of the network graph has the same weight. In other words, accuracy of the equipment installed in the network was assumed to be the same for each branch, as well as the increase of the possible error that will be introduced by the computations. Therefore, just a single entry is preserved in m^k for each k.

A second "half" of the erroneous path shall be determined analogically, starting from the second last visitor of the conflict node. Thus, erroneous path nodes $\mathcal{N}_e$ are found.

$n^0 =$

$$\left[\begin{array}{ccccccccc} 0 & \ldots & \underbrace{1}_{\left\{n_j^0 \,\middle|\, I\left(n_j^0,\mathcal{N}\right)=N_{vc}\right\}} & & \ldots & 0 & \ldots & 0 & \ldots & \underbrace{0}_{n_{|\mathcal{N}|}^0} \end{array} \right]$$

Conflict node
visitor entry

$n^{k\_last} =$

$$\left[\begin{array}{ccccccccc} 0 & \ldots & \underbrace{1}_{\left\{n_j^k \,\middle|\, I\left(n_j^k,\mathcal{N}\right)=NGk(Nv)\right\}} & & \ldots & 0 & \ldots \; \underbrace{1}_{n_j^k \,\middle|\, I\left(n_j^k,\mathcal{N}\right)=NGk(Nv)} \; \ldots & 0 & \ldots & \underbrace{0}_{n_{|\mathcal{N}|}^k} \end{array} \right]$$

PMU node entry

$m^{k=k\_last} =$

$$\left[\begin{array}{ccccccccc} 0 & \ldots & \underbrace{0}_{\left\{m_j^k \,\middle|\, I\left(m_j^k,\mathcal{N}\right)\neq N_{PMU}\right\}} & & \ldots & 0 & \ldots \; \underbrace{1}_{\left\{m_j^k \,\middle|\, I\left(m_j^k,\mathcal{N}\right)=I\left(n_j^k,\mathcal{N}\right)=N_{PMU}\right\}} \; \ldots & 0 & \ldots & \underbrace{0}_{n_{|\mathcal{N}|}^k} \end{array} \right]$$

$m^k =$

$$\left[\begin{array}{ccccccc} & \text{Non-viable entry} & & \text{First viable entry} & & \text{Second viable entry} & \\ 0 & \ldots \; \underbrace{0}_{\left\{m_j^k \,\middle|\, NG1\left(m^{k+1},\mathcal{N}\right)\neq NGk\left(n^0,\mathcal{N}\right)\right\}} \; \ldots & \ldots & \underbrace{1}_{\left\{m_j^k \,\middle|\, \begin{array}{l} I\left(m_j^k,\mathcal{N}\right)=I\left(n_j^k,\mathcal{N}\right) \\ NG1\left(m_1^{k+1},\mathcal{N}\right)=NGk\left(n^0,\mathcal{N}\right)\end{array}\right\}} & \ldots & \underbrace{0}_{\left\{m_j^k \,\middle|\, \begin{array}{l} I\left(m_j^k,\mathcal{N}\right)\neq I\left(n_j^k,\mathcal{N}\right) \\ NG1\left(m_1^{k+1},\mathcal{N}\right)=NGk\left(n^0,\mathcal{N}\right)\end{array}\right\}} & \ldots \; \underbrace{0}_{m_{|\mathcal{N}|}^k} \end{array} \right]$$

$m^0 =$ Conflict node entry

$$\left[\begin{array}{ccccccccc} 0 & \ldots & \underbrace{1}_{\left\{m_j^0 \,\middle|\, I\left(n_j^0,\mathcal{N}\right)=I\left(m_j^0,\mathcal{N}\right)=Nv\right\}} & & \ldots & 0 & \ldots & 0 & \ldots & \underbrace{0}_{m_{|\mathcal{N}|}^0} \end{array} \right]$$

Figure D.2: Back-tracking algorithm, forward and back tracking vectors

D.2.2 Finding an alternative path

The following three algorithms shall find the shortest internal connections of the erroneous path and the external connections to the erroneous nodes $P_a(\mathcal{N}_a, \mathcal{E}_a)$:

- Finding terminals of new P_a ;

- Finding external pathes from erroneous path to PMU;

- Finding internal pathes between two erroneous nodes.

For the computer implementation two variables `Roots` and `Internal interconnections` are defined and contain the most important the information to determine P_a.

Finding new P_a terminals

1. Set iteration $k = 0$;

2. Form a column vector of neighbors $n^0 \in \mathbb{R}^{C_N}$ with $|\mathcal{N}_e|$ nonzero entires:

$$n_j^0 = \begin{cases} 1 & \text{if } j \text{ corresponds to erroneous node } I(n^0, \mathcal{N}) = \mathcal{N}_e, \\ 0 & \text{if otherwise.} \end{cases}$$

3. Initialize $R \in \mathbb{R}^{|\mathcal{N}_e| \times |\mathcal{N}|}$ sparse matrix `Roots` with dimensions of erroneous nodes times number of nodes in the network. $R(\cdot, 1) = \mathcal{N}_e$, as in Fig. D.3.

4. Set $n^{k+1} = A_N \otimes n^k$, where A_N is a network adjacency matrix.

5. Define $\mathcal{N}_{NGk} = N_{Gk}(\mathcal{N}_e) = I(n^k, \mathcal{N})\}$,
   then, sort newly discovered nodes $I(n^{k+1}, \mathcal{N})$ by the "originating" node.
   For each $\forall N_{NGk} \in \mathcal{N}_{NGk}$,

   - find indexes L of rows in matrix R containing node N_{NGk} ; for each $l \in L$:
     - find 1-st degree neighbors of N_{NGk}, such that:

$$\mathcal{M} = N_{G1}(N_{NGk}) \not\supseteq R(l, \cdot). \tag{D.4}$$

– add $\mathcal{M}$ as new entries to $R(l, \cdot)$.

6. Construct interconnection matrix $C \in \mathbb{R}^{|\mathcal{N}_e| \times |\mathcal{N}_e|}$, for that find set $\mathcal{N}_r$ of non-unique or repeating entries in matrix R. For each $N_r \in \mathcal{N}_r$:

a. Find M - indexes of rows in matrix R containing node N_r, then

If $N_r \in \mathcal{N}_e$ is one of the erroneous nodes, find m_r s.t. $R(m_r, 1) = N_r$, assign to an interconnection matrix C value N_r at the indexes corresponding to originating erroneous nodes $R(M \setminus m_r, 1)$ and a common erroneous node N_r, as in Fig. D.3:

$$C(M \setminus m_r, m_r) = N_r; \qquad\qquad \text{(D.5)}$$
$$C(m_r, M \setminus m_r) = N_r;$$

else $N_r \notin \mathcal{N}_e$ is not an erroneous node, find $M_P = {}^2P_M$ as all the permutations from 2 of originating node indices M. Set in the interconnection matrix C a repeating node N_R as an entry on the index of the row and column corresponding to the originating nodes:

$$C(M_P) = N_r;$$

b. Erase from matrix C the entries corresponding to known pairs of nodes:

- find entries $\mathcal{X} = \{X \in \mathbb{R}^2 \mid \exists j \quad R(X, 1) = N_T(\mathcal{N}_{a,j})\}$,

- erase known alternative pathes $C(\mathcal{X}) = 0$.

- reset $N_r = \{c \in C \mid c > 0\}$.

7. If $I(n^{(k+1)}) \cap \mathcal{N}_{PMU} \neq \varnothing$ contains any verified reference nodes $\mathcal{N}_{PMU}$, initiate algorithm **"External path"**, as described below. Then, if returned result is not empty, stop.

8. If $I(n^{(k+1)}) = \varnothing$ or there are non-zero entries $c > 0$ - stop, otherwise set iteration number $k = k + 1$ and go to the step 3.

Should any repeating entries be detected after the exit from this loop, an **"Internal Pathes"** algorithm will find internal pathes P_a as described below.

$$R = \begin{bmatrix} N_{e1} & \underbrace{N_{NG1,1} \quad N_{NG1,2} \quad N_{NG1,3}}_{\mathcal{M}=N\_G1(N\_e1)} & \underbrace{\cdots \quad \cdots}_{NG2(N\_e1)} & 1 \\ N_{e2} & \underbrace{N_{NG1,1} \quad N_{NG1,4}}_{N\_G1(N\_e2)} & \cdots & 2 \\ N_{ej} & \underbrace{N_{NG1,5} \quad N_{NG1,6} \quad N_{NG1,7}}_{N\_G1(N\_ej)} & \cdots & \\ \cdots & N_{NG1,8} & \cdots & \\ N_{e|\mathcal{N}e|} & N_{NG1,9} & \cdots & \end{bmatrix}$$

$\underbrace{\quad}_{\mathcal{N}\ e}$ $\underbrace{\mathcal{N}\_NG1= \\ N\_G1(\mathcal{N}\ e) = \\ I(n^{\wedge}(1), \mathcal{N})}$ $\underbrace{\mathcal{N}\_NG2= \\ N\_G2(\mathcal{N}\ e) = \\ I(n^{\wedge}(2), \mathcal{N})}$

$\mathcal{N}\ r$ (top)

1, 2 — M are the row indexes

(a) Root matrix R

$$C = \begin{bmatrix} 0 & N_{NG1,1} & cj=0 & \cdots & 0 \\ N_{NG1,1} & 0 & 0 & \cdots & 0 \\ 0 & 0 & 0 & \cdots & 0 \\ \cdots & \cdots & \cdots & \cdots & \cdots \\ 0 & 0 & 0 & \cdots & 0 \end{bmatrix}$$

$\mathcal{N}e$ (top) $\mathcal{N}e$ (right)

(b) Interconnection matrix C

Figure D.3: Structure of the Root R and Interconnection C matrices.

Finding External Paths

If $I(n^{(k+1)}) \cap \mathcal{N}_{PMU} \neq \varnothing$ contains any verified reference nodes $\mathcal{N}_{PMU}$, external pathes shall be found between $\mathcal{N}_e$ and $\mathcal{N}_{PMU}$, as described below. For clarification, these steps are shown in Fig. D.4. Thus,

1. If a found reference node N_{PMU} is a terminal of erroneous path - **stop**, otherwise continue.

2. Find indexes L of rows in matrix R containing node N_{PMU}; For each $l \in L$ build a tree structure that includes path from the reference node N_{PMU} to erroneous node $R(l, 1)$:

   (a) Set iteration $k = 0$, $\mathcal{N}^{(0)} = N_{PMU}$, $t \in \mathbb{R}^{|\mathcal{N}_e|}$;

   (b) For each $N^{(k)} \in \mathcal{N}^{(k)}$:

     - find neighbors $\mathcal{M}^{(k+1)} = N_{G1}(N^{(k)})$, such that:
       - $\mathcal{M}^{(k+1)} \subset R(l, \cdot)$ are in root matrix;
       - $\mathcal{M}^{(k+1)} \nsubseteq \mathcal{N}^{(m)} \quad \forall m < k$ were not assigned to the tree previously;
       - $\mathcal{M}^{(k+1)} \nsubseteq (\mathcal{N}_e \setminus N_r)$ are not erroneous nodes, except for the searched one;
     - Assign $t(\mathcal{M}^{(k+1)}) = N^{(k)}$ connection tree entries a parent node $N^{(k)}$;
     - Set $\mathcal{N}^{(k+1)} = \mathcal{N}^{(k+1)} \cup \mathcal{M}^{(k+1)}$;

   (c) If $\mathcal{N}^{(k+1)} \supseteq N_{PMU}$ erroneous node detected - **stop**, otherwise set iteration $k = k + 1$ and go to the step 2(b).

Upon the finalization of these steps, return to the main loop described in D.2.2, finding P_a terminals.

Finding Internal Paths

Should any repeating nodes have been detected after exit from **finding P_a terminals** in D.2.2 the following procedure is initiated to find corresponding internal pathes P_a.

For each repeating entry $N_r \in \mathcal{N}_r$:

1. Find indexes $\mathcal{M}_r$ in the interconnection matrix $C(\mathcal{M}_r) = N_r$;

2. Assign $\mathcal{M}_c = \quad ^2C_{\mathcal{M}r}$ - all combination of 2 from the unique row and column indexes to determine all connected with N_r pairs;

   Discriminate from $\mathcal{M}_c$ already known pairs to obtain $\mathcal{M}_n$.

3. If $\mathcal{M}_n = \varnothing$ - go to step 1, otherwise - continue;
   For each found pair $\{M_{n,1}, M_{n,2}\} \in \mathcal{M}_n$ build connection tree, as it was described in step 2(a)-(c) of the previous subsection **finding external pathes**.

   (a) Start from a node in $M_{n,1}^{(0)} \in \mathcal{M}_n$ and continue k iterations till a repeating entry N_r is found or a PMU node N_{PMU}:

   If $M_n^{(k)} \supseteq N_{PMU}$ and a pair $\{M_{n,1}^{(0)} N_{PMU}\}$ is known, set $M_{n,2}^{(0)}$ as a starting node and go to step 3(a).
   Otherwise, this pair has not been yet verified, thus assign $\mathcal{N}_a = \{M_{n,1}^{(0)} N_{PMU}\}$ and go to step 3.

   elseif $M_n^{(k)} \supseteq N_r$ and $N_r \in \mathcal{N}_e$ common node is erroneous node, set $\mathcal{N}_a = \{M_{n,1}^{(0)} N_r\}$ and go to the step 3.

   elseif $M_n^{(k)} \supseteq N_r$ and $N_r \notin \mathcal{N}_e$, go to step (b).

   (b) Assign $M_n^{(k)} = N_r$ a repeating node and build a tree for m iterations till the second node of $M_{n,2}^{(0)}$ is found or a PMU node N_{PMU}:

   If $M_n^{(k+m)} \supseteq N_{PMU}$:
   if $\{M_{n,1}^{(0)} N_{PMU}\}$ has not been previously verified, set $\mathcal{N}_a = \{M_{n,1}^{(0)} N_{PMU}\}$.
   Set replaced pair $\mathcal{N}_s = \mathcal{N}_s \cup \{M_{n,1}^{(0)}, M_{n,2}^{(0)}\}$.

   else $M_n^{(k+m)} \supseteq \mathcal{N}_e$, set $\mathcal{N}_a = \{M_{n,1}^{(0)}, M_{n,2}^{(0)}\}$.

4. Go to the step 3.

These steps are similar to the ones shown in Fig. D.4, in case of internal pathes, however, first a part of the tree till a repeating node shall be formed and then, proceeding similarly till the second terminal node of P_a.

All the replaced pairs $\mathcal{N}_s$ shall be used in the further iterations to prevent the alternative path searching algorithm from the preliminary exit, similarly as the information about verified pairs.
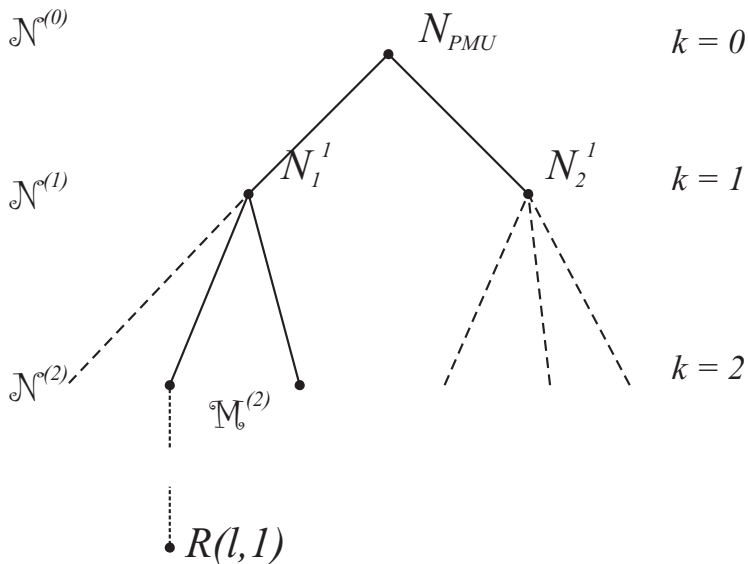
(a) Constructing the tree.

$$t = [0\ ...\ 0\ ...\ \underbrace{N_{PMU}}_{N_1^{\ 1}}\ ...\underbrace{N_1^{\ (1)}}_{\in \mathcal{M}^{(2)}}\ ...\ \underbrace{N_{PMU}}_{N_2^{\ 1}}\ ]$$

(b) Tree structure.

Figure D.4: Forming the tree P_a and the corresponding t vector

Appendix E

Hydro Wind system modeling

The equations provided below are used in modeling hydro and wind power production systems connected to a transmission network by several lines with limited capacity as described in Chapter 11.

Objective function term z_h^s

$$z_h^s = \sum_{k \in K} \sum_{n \in N} c^s(k,n) p(k,n) \sum_{i \in I} \sum_{s \in S_i} P_{is}^s(k,n) \tag{E.1}$$

Objective function term z_w^s

$$z_w^s = \sum_{k \in K} \sum_{n \in N} c^s(k,n) p(k,n) P_w^s(k,n) \tag{E.2}$$

Objective function terms z^{imb} and z_w^{imb}

$$z^{imb} = \sum_{k \in K^{day}} \sum_{n \in N} \sum_{m \in M} \tag{E.3}$$

$$\{c_{pos}^{imb}(k,n) \cdot p(k,n) \cdot q(k,m) \cdot (1 - b(k,n,m)) \cdot$$

$$(P_w^{sc}(k,n,m) - P_w^s(k,n) +$$

$$\sum_{i \in I} \sum_{s \in S_i} [P_{is}^{sc}(k,n,m) - P_{is}^s(k,n)])$$

$$-c_{neg}^{imb}(k,n) \cdot p(k,n) \cdot q(k,m) \cdot b(k,n,m) \cdot$$

$$(-P_w^{sc}(k,n,m) + P_w^s(k,n) -$$

$$\sum_{i \in I} \sum_{s \in S_i} [P_{is}^{sc}(k,n,m) - P_{is}^s(k,n)])\}$$

The objective function term (E.3) is valid for the coordinated study. For the uncoordinated case it naturally follows that z_w^{imb} does not contain any hydro related terms.

Complementarity constraints

The constraints below encode conditions for the charges for the imbalance of the producers and allow only either positive or negative imbalance.

The use of continuous variable for b - a switch of one or the other imbalance term, is allowed by introducing the complementarity constraint:

$$b(k,n,m)(1 - b(k,n,m)) = 0, \tag{E.4}$$

$$\forall k \in K, \forall n \in N, \forall m \in M.$$

The objective function (E.3) specifies that the overproduction of the coalition corresponds to the $b = 0$ condition, while the underproduction corresponds to the $b = 1$.

Thus if $b = 1$ the following constraint becomes active and enforces underproduction:

$$D(1 - b(k,n,m)) \geq P_w^{sc}(k,n,m) - P_w^s(k,n) + \tag{E.5}$$

$$\sum_{i \in I} \sum_{s \in S_i} [P_{is}^{sc}(k,n,m) - P_{is}^s(k,n)]$$

$$\forall k \in K^{day}, \forall n \in N, \forall m \in M,$$

while $b = 0$ activates the following constraint and ensures overproduction:

$$Db(k,n,m) \geq - P_w^{sc}(k,n,m) + P_w^s(k,n) - \tag{E.6}$$
$$\sum_{i \in I} \sum_{s \in S_i} [P_{is}^{sc}(k,n,m) - P_{is}^s(k,n)]$$
$$\forall k \in K^{day}, \forall n \in N, \forall m \in M,$$

here D is a large positive number that exceeds any maximum feasible value of the imbalance.

Imbalance equality constraints g_w^{imb}

Since all the variables after the next planning day and for the rest of the planning period are deterministic, the imbalance shall be zero:

$$P_w^{sc}(k,n,m) - P_w^s(k,n) = 0 \tag{E.7}$$
$$\forall k > K_{last}^{day}, \forall n \in N, \forall m \in M,$$

and

$$P_{is}^{sc}(k,n,m) - P_{is}^s(k,n) = 0, \tag{E.8}$$
$$\forall k > K_{last}^{day}, \forall i \in I, \forall s \in S_i, \forall n \in N, \forall m \in M.$$

Hydraulical balance constraints g_h^{hb}

The actual hydro unit production is defined by the production equivalent and the water discharge:

$$P_{is}^{sc}(k,n,m) = \mu_{is} u_{is}(k,n,m) \tag{E.9}$$
$$\forall i \in I, \ \forall s \in S_i, \forall k \in K, \ \forall n \in N, \forall m \in M.$$

Reservoir content results from the discharges of the power plant, the inflows of hydro systems and the delayed discharges of upstream HPPs:

$$x_i(k+1,n,m) = x_i(k,n,m) + \tag{E.10}$$
$$w_i(k) - y_i(k,n) - \sum_{s \in S_i} \frac{P_{is}^{sc}(k,n,m)}{\mu_{is}} +$$
$$\sum_{j \in \Omega_i} y_j(k - \tau_{ij}, n_{\tau_{ij}}) + \sum_{j \in \Omega_i} \sum_{s \in S_j} \frac{P_{js}^{sc}(k - \tau_{ij}, n_{\tau_{ij}}, m_{\tau_{ij}})}{\mu_{js}}$$
$$\forall i \in I, \ \forall k \in K, \ \forall n \in N, \forall m \in M.$$

Reservoir target constraints g_h^{rt}

Initial reservoir content is assumed known and reservoir content at the end of the planning period is fixed in accordance with mid-term production planning:

$$x_i(0, n, m) = x_i^o, \tag{E.11}$$
$$\forall i \in I, \forall n \in N, \forall m \in M.$$

$$x_i(K_{last}, n, m) = x_i^{last}, \tag{E.12}$$
$$\forall i \in I, \forall n \in N, \forall m \in M.$$

Reservoir limits constraints h_h^{rl}

There are also reservoir content limitations.

$$0 \leq x_i(k, n, m) \leq \bar{x}_i, \tag{E.13}$$
$$\forall i \in I, \ \forall k \in K, \ \forall n \in N, \ \forall m \in M$$

Hydro production inequality constraints h_h^d

The bid on the spot market shall not exceed the installed capacity.

$$0 \leq P_{is}^s(k, n) \leq \mu_{is} \bar{u}_{is} \tag{E.14}$$
$$\forall i \in I, \ \forall s \in S_i, \forall k \in K, \ \forall n \in N$$

Further the hydro production is limited by the technical water discharge constraints:

$$0 \leq P_{is}^{sc}(k, n, m) \leq \mu_{is} \bar{u}_{is}, \tag{E.15}$$
$$\forall i \in I, \ \forall s \in S_i, \forall k \in K, \ \forall n \in N, \ \forall m \in M$$

Wind production inequality constraints h_w^{imb}

The wind power bid to the spot market is defined in the following interval:

$$0 \leq P_w^s(k, n) \leq \bar{P}_w \tag{E.16}$$
$$\forall k \in K, \ \forall n \in N,$$

Note that actual wind power production is limited by the available wind:

$$0 \le P_w^{sc}(k, n, m) \le \bar{P}_w^{sc}(k, m) \tag{E.17}$$
$$\forall\, k \in K, \ \forall\, n \in N, \ \forall\, m \in M$$

Transmission constraints h_{h+w}^t, h_h^t and h_w^t

The transmission constraints h_{h+w}^t valid for the coordinated study are:

$$P_w^{sc}(k, n, m) + \sum_{i \in I_c} \sum_{s \in S_i} P_{is}^{sc}(k, n, m) \le \bar{P}_{12} \tag{E.18}$$
$$\forall k \in K, \forall n \in N, \forall m \in M$$

In the uncoordinated case, the wind term shall be omitted in the constraints h_h^t for the hydro planning. Whereas, in the planning of the individual strategy of the wind producer the hydro term is still preserved in the h_w^t constraint. Thus, it defines that wind is allocated transmission capacity unused by the hydro.

Bibliography

[1] S. Aam, L. Holten, and O. Gjerde. Design of the measurement system for state estimation in the Norwegian high-voltage transmission network. In *Power Apparatus and Systems, IEEE Transactions on*, PAS 102(12):3769 – 3777, December 1983.

[2] A. Abur and A. Gomez Exposito. *Power System State Estimation: Theory and Implementation*. CRC Press, 1 edition, March 2004.

[3] A. Abur and G. M. Huang. *Power System State Estimation and Optimal Measurement Placement for Distributed Multi-Utility Operation*. PSERC Publication 02-45, November 2002.

[4] A. Abur and M. Kezunovic. *Enhanced State Estimation by Advanced Substation Monitoring*. PSERC Publication 02-48, November 2002.

[5] A. Abur, H. Kim and M. K. Celik. Identifying the Unknown Circuit Breaker Statuses in Power Networks. In *Power Systems, IEEE Transactions on*, 10(4):2029–2037, 1995.

[6] P. M Anderson. *Series compensation of power systems*. PBLSH! Inc in Encinitas, Calif., Apr 1996.

[7] J. Marquez Angarita and J. Garcia Usaola. Combining hydro-generation and wind energy: Biddings and operation on electricity spot markets. In *Electric Power Systems Research*, 77(5-6):393–400, April 2007.

[8] H.P. Asal, F. Oesch, N. Singh, D. Ebner, and S. Saly. Implementation of third generation of state estimation. In *PSCC*, pages 1031–1035, Graz, Austria, 1990.

[9] M. Assadian, R.J. Goddard, H.W. Hong, and D. French. Field operational experiences with on-line state estimator. In *Power Systems, IEEE Transactions on*, 9(1):50–58, 1994.

[10] A.G. Bakirtzis. Aumann-Shapley transmission congestion pricing. In *Power Engineering Review, IEEE*, 21(3):67–69, 2001.

[11] M. Bertran and X. Corbella. On the validation and analysis of a new method for power network connecticity determination. In *Power Apparatus and Systems, IEEE Transactions on*, PAS-101(2):316–324, Feb. 1982.

[12] J. Bialek. Tracing the flow of electricity. In *Generation, Transmission and Distribution, IEE Proceedings-*, 143:313–320, July 1996.

[13] M. Bockarjova, G. Andersson, and A. Sauhats. Statistical algorithm for power transmission lines distance protection. In *Probabilistic Methods Applied to Power Systems, 2006. PMAPS 2006. International Conference on*, pages 1–7, 2006.

[14] M. Bockarjova, A. Dolgicers, and A. Sauhats. Enhancing fault location performance on power transmission lines. In *Power Tech, 2007 IEEE Lausanne*, pages 1123–1128, 2007.

[15] M. Bockarjova, A. Sauhats, and G. Andersson. Statistical algorithms for fault location on power transmission lines. In *Power Tech, 2005 IEEE Russia*, pages 1–7, 2005.

[16] M. Bockarjova, M. Zima, and G. Andersson. On allocation of the transmission network losses using game theory. In *Electricity Market, 2008. EEM 2008. 5th International Conference on European*, pages 1–6, 2008.

[17] M. Bockarjova. Statistical approach in algorithms design and testing of power system protection, 2007. Thesis (Ph. D.)– Riga Technical University, Dept. of Electrical Engineering, 2007.

[18] P. Bonanomi. Phase angle measurements with synchronized Clocks-Principle and applications. In *Power Apparatus and Systems, IEEE Transactions on*, PAS-100(12):5036–5043, 1981.

[19] P. Bonanomi and G. Gramberg. Power system data validation and state calculation by network search techniques. In *Power Apparatus and Systems, IEEE Transactions on*, PAS-102(1):238–249, 1983.

[20] A. Bose and K.A. Clements. Real-time modeling of power networks. In *Proceedings of the IEEE*, 75(12):1607– 1622, 1987.

[21] K.-P. Brand, V. Lohmann, and W. Wimmer. *Substation Automation Handbook*. Utility Automation Consulting Lohmann, Bremgarten, Switzerland, 2003.

[22] S. Brattini and J. Finney. Metrics for PMU impact on power system state estimation. In *EIPP meeting*, Washington, DC, October 2005.

[23] S.P. Carullo and C.O. Nwankpa. Experimental validation of a model for an information-embedded power system. In *Power Delivery, IEEE Transactions on*, 20(3):1853–1863, 2005.

[24] E.D. Castronuovo and J.A.P. Lopes. On the optimization of the daily operation of a wind-hydro power plant. In *Power Systems, IEEE Transactions on*, 19(3):1599–1606, 2004.

[25] Jaewon Chang, G. N. Taranto, and J. H. Chow. Dynamic state estimation using a nonlinear observer for optimal series-capacitor switching control. In *International Journal of Electrical Power & Energy Systems*, 19(7):441–447, October 1997.

[26] R. D. Christie. Power systems test case archive. http://www.ee.washington.edu/research/pstca/.

[27] K.A. Clements, P.W. Davis, and K.D. Frey. Treatment of inequality constraints in power system state estimation. In *Power Systems, IEEE Transactions on*, 10(2):567–574, 1995.

[28] A. J. Conejo, J. M. Arroyo, N. Alguacil, and A. L. Guijarro. Transmission loss allocation: A comparison of different practical algorithms. In *Power Engineering Review, IEEE*, 22:66, 2002.

[29] Th. Van Cutsem and M. Pavella. Critical survey of hierarchical methods for state estimation of electric power systems. In *Power Apparatus and Systems, IEEE Transactions on*, 102:3415–3424, 1983.

[30] A.M.L. da Silva, and J.G. de Carvalho Costa. Transmission loss allocation: I. single energy market. In *Power Systems, IEEE Transactions on*, 18:1389–1394, 2003.

[31] M. S. Dorfman. *Introduction to Risk Management and Insurance*. Pearson/Prentice Hall, May 2007.

[32] D. Kalsson et al. System protection schemes in power networks. Task Force 38.02.19 187, CIGRE, June 2001.

[33] A.Gomez Exposito and A. de la Villa Jaen. Reduced substation models for generalized state estimation. In *Power Systems, IEEE Transactions on*, 16(4):839 –846, nov 2001.

[34] E. Faria, L.A. Barroso, R. Kelman, S. Granville, and M.V. Pereira. Allocation of Firm-Energy rights among hydro plants: An Aumann-Shapley approach. In *Power Systems, IEEE Transactions on*, 24(2):541–551, 2009.

[35] M.B.D.C. Filho, A.M.L. da Silva, and D.M. Falcao. Bibliography on power system state estimation (1968-1989). In *Power Systems, IEEE Transactions on*, 5(3):950–961, 1990.

[36] N. Flatabo, A. Calvaer, H.H.Happ, A. Johannesen, M. Ribbens-Pavella, and Y. Tamura. Advanced analytical tools in evaluationg power system dynamic and security performance - results of a questinnaire. Study Committee 38 28, CIGRE, March 1987.

[37] O.B. Fosso, A. Gjelsvik, A. Haugstad, B. Mo, and I. Wangensteen. Generation scheduling in a deregulated system. The Norwegian case. In *Power Systems, IEEE Transactions on*, 14(1):75–81, 1999.

[38] T.H. Fox, M.O. Mansour, E.H. Preston, J.D. Willson, and R.A. Wodyka. An approach to real time reactive monitoring for system security. In *IEEE Transactions on Power Apparatus and Systems*, PAS - 102(11):3687 – 3695, November 1983.

[39] F.D. Galiana, A.J. Conejo, and I. Kockar. Incremental transmission loss allocation under pool dispatch. In *Power Systems, IEEE Transactions on*, 17:26–33, 2002.

[40] D.J. Gaushell and H.T. Darlington. Supervisory control and data acquisition. In *Proceedings of the IEEE*, 75(12):1645– 1658, 1987.

[41] A. Ghassemian and D. French. Power system state estimator practical issues. In *Robust methods in State Estimation and Load Forecasting*, Paris, France, May 2006.

[42] F. Goderya, A. Metwally, and O. Mansour. Fast detection and identification of islands in power sysrtems. In *Power Apparatus and Systems, IEEE Transactions on*, PAS-99(1):217–221, February 1980.

[43] L. C. Haarla. State estimation ans load forecasting in Finland and in Sweden. In *Robust methods in State Estimation and Load Forecasting*, Paris, France, May 2006.

[44] I.A. Hiskens. Power system modeling for inverse problems. In *Circuits and Systems I: Regular Papers, IEEE Transactions on*, 51(3):539–551, 2004.

[45] I.A. Hiskens and M.A. Pai. Trajectory sensitivity analysis of hybrid systems. In *Circuits and Systems I: Fundamental Theory and Applications, IEEE Transactions on*, 47(2):204–220, 2000.

[46] I.A. Hiskens and P.J. Sokolowski. Systematic modeling and symbolically assisted simulation of power systems. In *Power Systems, IEEE Transactions on*, 16(2):229–234, 2001.

[47] L. Holten, A. Gjelsvik, S. Aam, F.F. Wu, and W.-H.E. Liu. Comparison of different methods for state estimation. In *Power Systems, IEEE Transactions on*, 3(4):1798–1806, 1988.

[48] H. E. House and P. D. Tuttle. Current-Carrying capacity of ACSR. In *Power Apparatus and Systems, Part III. Transactions of the American Institute of Electrical Engineers*, 77(3):1169–1173, 1958.

[49] Shih-Chieh Hsieh. Fair transmission loss allocation based on equivalent current injection and shapley value. In *Power Engineering Society General Meeting, 2006. IEEE*, page 6 pp., 2006.

[50] Shih-Chieh Hsieh and Hsin-Min Wang. Allocation of transmission losses based on cooperative game theory and current injection models. In *Industrial Technology, 2002. IEEE ICIT '02. 2002 IEEE International Conference on*, volume 2, pages 850–853 vol.2, 2002.

[51] IEEE. IEEE standard for calculating the current-temperature of bare overhead conductors. *Std 738-2006 (Revision of IEEE Std 738-1993)*, pages c1 –59, Jan. 2007.

[52] IEEE. IEEE standard requirements for instrument transformers. *Std C57.13-2008 (Revision of IEEE Std C57.13-1993)*, pages c1 –82, July 2008.

[53] N. Inoue, H. Daniels, R. Kilmer, and V. Echave. Implementation, testing and field installation of the Iberduero power system state estimator. In *Power Apparatus and Systems, IEEE Transactions on*, PAS 102(11):3541 – 3548, November 1983.

[54] M.R. Irving and M.J.H. Sterling. Substation data validation. In *Generation, Transmission and Distribution, IEE Proceedings C*, 129(3):119–122, May 1982.

[55] A. Jaderstom, J. Matevosyan, and L. Soder. Coordinated regulation of wind power and hydro power with separate ownership. In *Proceedings of Hydropower'05*, Stavanger, 2005.

[56] M. Junqueira, L. C. da Costa, L. A. Barroso, G. C. Oliveira, L. M. Thome, and M. V. Pereira. An Aumann-Shapley approach to allocate transmission service cost among network users in electricity markets. In *Power Systems, IEEE Transactions on*, 22:1532–1546, 2007.

[57] P. Kall and S. W. Wallace. *Stochastic Programming*. Wiley John & Sons, 1995.

[58] P.A. Kattuman, R.J. Green, and J.W. Bialek. A tracing method for pricing inter-area electricity trades. Cambridge Working Papers in Economics 0107, Faculty of Economics, University of Cambridge, June 2001.

[59] KEMA. Metrics for determining the impact of phasor measurements on power system state estimation. Eastern interconnection phasor project report, KEMA, March 2006.

[60] M. Kezunovic. Monitoring of power system topology in real-time. In *System Sciences, 2006. HICSS '06. Proceedings of the 39th Annual Hawaii International Conference on*, volume 10, page 244b, 2006.

[61] M. Kezunovic, A. Abur, A. Edris, and D. Sobajic. Data integration/exchange - Part 1: existing technical and business opportunities. In *Power and Energy Magazine, IEEE*, 2(2):14–19, 2004.

[62] M. Kezunovic, A. Abur, A.-T. Edris, and D. Sobajic. Data integration/exchange. Part 2: Future technical and business opportunities. In *Power and Energy Magazine, IEEE*, 2(3):24–29, 2004.

[63] D. S. Kirschen and G. Strbac. *Fundamentals of power system economics*. John Wiley and Sons, May 2004.

[64] H.J. Koglin and H.T. Neisius. Treatment of topological errors in substations. In *Proc. 10th Power Systems Computation Conference, Graz*, 129(3):1045–1053, 1990.

[65] H.J. Koglin, D. Oeding, and K.D. Schmitt. Identification of topological errors in state estimation. In *PSMC*, pages 140–144, Durham, 1986.

[66] G. A. Korn and Th. M. Korn. *Mathematical Handbook for Scientists and Engineers: Definitions, Theorems, and Formulas for Reference and Review*. Dover Publications, 2 revised edition, June 2000.

[67] M. Korpaas, J. O. G. Tande, K. Uhlen, E.S.Hause, and T. Gjengedal. Planning and operation of large wind farms in areas with limited power transfer capacity. In *Proceedings of 2006 EWEC*, Athens, March 2006.

[68] M. Korpaas, A. Holen, and R. Hildrum. Operation and sizing of energy storage for wind power plants in a market system. In *International Journal of Electrical Power & Energy Systems*, 25(8):606, 599, October 2003.

[69] Yu. Korshunov. *Mathematical Methods of Cybernetics*. Mir, 1990.

[70] S. Krau, G. Lafrance, and L. Lafond. Large scale wind farm integration: a comparison with a traditional hydro option. In *Proceedings EWEA Global Wind Power Conference*, Paris, April 2002.

[71] P. Kundur. *Power System Stability and Control*. McGraw-Hill Professional, 1994.

[72] S. Lefebvre, J. Prevost, E. Crainic, R. St-Arnaud, H. Horisberger, and B. Lambert. Practical experience with state estimation. In *Robust methods in Satet Estimation and Load Forecasting*, Paris, France, May 2006.

[73] W. A. Lewis and P. D. Tuttle. The resistance and reactance of aluminum conductors, steel reinforced. In *Power Apparatus and Systems, Part III. Transactions of the American Institute of Electrical Engineers*, 77(3):1189–1214, 1958.

[74] L.G.Labscker and E.B.Janovskaya. General methodology for the design of the decision optimality criteria in risk and uncertainty. In *Financial management, Vol. 5*, 2002.

[75] X.J. Lin, C.W. Yu, and C.Y. Chung. Pricing of reactive support ancillary services. In *Generation, Transmission and Distribution, IEE Proceedings-*, 152(5):616–622, 2005.

[76] E. Litvinov, Tongxin Zheng, G. Rosenwald, and P. Shamsollahi. Marginal loss modeling in LMP calculation. In *Power Systems, IEEE Transactions on*, 19:880–888, 2004.

[77] R. Lopez, R. Avila-Rosales, and J. Giri. Recent experiences and trends with state estimation in very large networks. In *Robust methods in State Estimation and Load Forecasting*, Paris, France, May 2006.

[78] R.L. Lugtu, D.F. Hackett, W.R. Mahoney, R.E. Pietropola, T.W. Langley, and C.K. Bush. The Altantic electric system control center. In *Power Apparatus and Systems, IEEE Transactions on*, PAS-102(11):3571 – 3575, November 1983.

[79] R.L. Lugtu, J. Markus, R.M Parker, K.D Snyder, S.J Wavrek, and B.W. Merrick. The Ohio Edison energy control center. In *Power Apparatus and Systems, IEEE Transactions on*, PAS-102(11):3577–3580, November 1983.

[80] PJM Training Materials: Locational marginal pricing. http://www.pjm.com/training/training-material.aspx.

[81] J. Matevosyan and L. Soder. Optimal daily planning for hydro power system coordinated with wind power in areas with limited export capability. In *Probabilistic Methods Applied to Power Systems, 2006. PMAPS 2006. International Conference on*, pages 1–8, 2006.

[82] J. Matevosyan. On coordination of wind and hydro power. In *7th The International Workshop on Large-Scale Integration of Wind*

Power into Power Systems as well as on Transmission Networks for Offshore Wind Farms, May 2008.

[83] J. Matevosyan, M. Olsson, and L. Soder. Hydropower planning coordinated with wind power in areas with congestion problems for trading on the spot and the regulating market. In *Electric Power Systems Research*, 79(1):39–48, 2009.

[84] A.P.S. Meliopoulos, G.J. Cokkinides, F. Galvan, and B. Fardanesh. GPS-synchronized data acquisition: Technology assessment and research issues. In *System Sciences, 2006. HICSS '06. Proceedings of the 39th Annual Hawaii International Conference on*, volume 10, page 244c, 2006.

[85] A.P.S. Meliopoulos, G.J. Cokkinides, M. Ingram, S. Bell, and S. Mathews. Visualization and animation of state estimation performance. In *System Sciences, 2005. HICSS '05. Proceedings of the 38th Annual Hawaii International Conference on*, page 55b, 2005.

[86] R. Minguez and A.J. Conejo. State estimation sensitivity analysis. In *Electrotechnical Conference, 2006. MELECON 2006. IEEE Mediterranean*, pages 956– 959, 2006.

[87] R. Minguez and A.J. Conejo. State estimation sensitivity analysis. In *Power Systems, IEEE Transactions on*, 22(3):1080–1091, 2007.

[88] H. Modir and R. A. Schlueter. A dynamic state estimator for power system dynamic security assessment. In *Automatica*, 20(2):189–199, March 1984.

[89] A. Monticelli. *State Estimation in Electric Power Systems: A Generalized Approach*. Springer, 1st edition, May 1999.

[90] A. Monticelli. Electric power system state estimation. In *Proceedings of the IEEE*, 88(2):262–282, 2000.

[91] M.Weibel, W.Sattinger, P.Rothermann, U.Steinegger, M.Zima, and G.Biedenbach. Overhead line temperature monitorig pilot project. In *CIGRE 2006 Session, SC B2-311, Paris*, August 27 - September 1, 2006.

[92] N. Nisan, T. Roughgarden, E.Tardos, and V. V. Vazirani. *Algorithmic Game Theory*. Cambridge University Press, September 2007.

[93] R. F. Nuqui. *State Estimation and Voltage Security Monitoring Using Synchronized Phasor Measurements*. PhD thesis, Virginia Polytechnic Institute and State University, July 2001.

[94] Th. J. Overbye. *Visualization of Power Systems and Components*. PSERC Publication 05-65, November 2005.

[95] J.-C. Peng, H. Jiang, and Y.-H. Song. A weakly conditioned imputation of an impedance-branch dissipation power. In *Power Systems, IEEE Transactions on*, 22:2124–2133, 2007.

[96] A.G. Phadke, J.S. Thorp, and M.G. Adamiak. A new measurement technique for tracking voltage phasors, local system frequency, and rate of change of frequency. In *Power Apparatus and Systems, IEEE Transactions on*, PAS-102(5):1025–1038, 1983.

[97] A. G. Phadke and J. S. Thorp. *Synchronized Phasor Measurements and Their Applications*. Springer, 2008.

[98] R. C. Pires, N. Dallocchio, A.V. Zampieri, F.A. Becon Lemos, and S. R. Ortiz Lopes. Orthogonal IRLS algorithm applied to equality constrained state estimation problem Brazilisa state utility experience. In *Robust methods in State Estimation and Load Forecasting*, Paris, France, May 2006.

[99] Naval Oceanography Portal. Sun or moon Altitude/Azimuth table: Locations worldwide naval oceanography portal. http://www.usno.navy.mil/USNO/astronomical-applications/ data-services/alt-az-world/?searchterm=sun%20position.

[100] M. Prais and A. Bose. A topology processor that tracks network modifications. In *Power Systems, IEEE Transactions on*, 3(3):992–998, 1988.

[101] ABB RTU560 Substation Automation (Power Protection & Automation Products). http://www.abb.com/product/ db0003db004281/ c12573e700330419c1256d8200401704.aspx.

[102] D. Rajicic. A method for determination whether a network is connected or split. In *Power Engineering Review, IEEE*, 21(7):65–66, 2001.

[103] Y. G. Rebours, D. S. Kirschen, M. Trotignon, and S. Rossignol. A survey of frequency and voltage control ancillary services Part

II: Economic Features. In *Power Systems, IEEE Transactions on*, 22(1):358–366, 2007.

[104] Ch. Rehtanz, A. Suranyi, J. Bertsch, and M. Zima. Verifying an Accuracy of a State Estimation. *http://www.freepatentsonline.com/ y2008/0262758.html*, (20080262758), October 2008.

[105] E. M. Reingold, N. Deo, and J. Nievergelt. *Combinatorial Algorithms Theory and Practice*. Prentice-Hall, Englewood Cliffs - N.J, 1977.

[106] R. E. Rosenthal. A GAMS users guide. http://www.gams.com/dd/docs/bigdocs/GAMSUsersGuide.pdf, 2008.

[107] P. Rousseaux, Th. Van Cutsem, and T. E. Dy Liacco. Whither dynamic state estimation? In *International Journal of Electrical Power & Energy Systems*, 12(2):104–116, April 1990.

[108] A.M. Sasson, S.T. Ehrmann, P. Lynch, and L.S. Van Slyck. Automatic power system network topology determination. In *IEEE Transactions on Power Apparatus and Systems*, PAS-92(2):610–618, 1973.

[109] A. Sauhats, M. Bockarjova, A. Dolgicers, and M. Silarajs. New method for complicated automation systems simulation test. In *Developments in Power System Protection, 2004. Eighth IEE International Conference on*, volume 1, pages 280–283 Vol.1, 2004.

[110] A. Sauhats and M. Danilova. Fault location algorithms for super high voltage power transmission lines. In *Power Tech Conference Proceedings, 2003 IEEE Bologna*, volume 3, page 6 pp. Vol.3, 2003.

[111] A. Sauhats, J. Inde, G. Vempers, and V. Neimane. On cogeneration strategies in the cities of North-Eastern europe. In *Power Tech, 2007 IEEE Lausanne*, pages 645–650, 2007.

[112] A. Sauhats, A. Jonins, V. Chuvychin, and M. Danilova. Fault location algorithms for power transmission lines based on Monte-Carlo method. In *Power Tech Proceedings, 2001 IEEE Porto*, volume 3, page 5 pp. vol.3, 2001.

[113] E. Scholtz, G.C. Verghese, and B.C. Lesieutre. Observer-based monitors for electromechanical dynamics in power networks. In *PSCC*, Liege, Belgium, August 2005.

[114] E. Scholtz. Observer-based monitors and distributed wave controllers for electromechanical disturbances in power systems. http://dspace.mit.edu/handle/1721.1/26723, 2004. Thesis (Ph. D.)–Massachusetts Institute of Technology, Dept. of Electrical Engineering and Computer Science, 2004.

[115] F.C. Schweppe. Power system Static-State estimation, Part III: implementation. In *Power Apparatus and Systems, IEEE Transactions on*, PAS-89(1):130–135, 1970.

[116] F.C. Schweppe and E.J. Handschin. Static state estimation in electric power systems. In *Proceedings of the IEEE*, 62(7):972–982, 1974.

[117] F.C. Schweppe and R.D. Masiello. A tracking static state estimator. In *Power Apparatus and Systems, IEEE Transactions on*, PAS-90(3):1025–1033, 1971.

[118] F.C. Schweppe and D.B. Rom. Power system Static-State estimation, Part II: Approximate model. In *Power Apparatus and Systems, IEEE Transactions on*, PAS-89(1):125–130, 1970.

[119] F.C. Schweppe and J. Wildes. Power system Static-State estimation, Part I: Exact model. In *Power Apparatus and Systems, IEEE Transactions on*, PAS-89(1):120–125, 1970.

[120] ABB OMU Combined Current/Voltage Transformers (Instrument Transformers & Sensors). http://www.abb.com/product/db0003db002618/ c12573e7003302adc1256f07002e59e0.aspx.

[121] V. Shah, John R. Gilbert, and S. Reinhardt. High performance graph algorithms from parallel sparse matrices, online: http://acts.nersc.gov/ events/para06/shah.pdf, 2006.

[122] N. R. Shivakumar and A. Jain. A review of power system dynamic state estimation techniques. In *Power System Technology and IEEE Power India Conference, 2008. POWERCON 2008. Joint International Conference on*, pages 1–6, 2008.

[123] N. Singh. *Detection and Identification of Topological Errors in Online Power System Analysis*. PhD thesis, Diss.ETH, 1989.

[124] N. Singh. State estimation: Reality check and practical consideration. In *Robust methods for power system state estimation and load forecasting: state of the art and prospects, Workshop, Paris La Defence, France.*, May 29-30, 2006.

[125] N. Singh and F. Oesch. Practical experience with rule-based online topology error detection. In *Power Systems, IEEE Transactions on*, 9(2):841–847, 1994.

[126] I. W. Slutsker and J. M. Scudder. Network observability analysis through measurement Jacobian matrix reduction. In *Power Apparatus and Systems, IEEE Transactions on*, PWRS-2(2), May 1987.

[127] I.W. Slutsker. Bad data identification in power system state estimation based on measurement compensation and linear residual calculation. In *Power Systems, IEEE Transactions on*, 4(1):53–60, 1989.

[128] I.W. Slutsker, S. Mokhtari, L.A. Jaques, J.M.G. Provost, M.B. Perez, J.B. Sierra, F.G. Gonzalez, and J.M.M. Figueroa. Implementation of phasor measurements in state estimator at Sevillana de Electricidad. In *Power Industry Computer Application Conference, 1995. Conference Proceedings., 1995 IEEE*, pages 392–398, 1995.

[129] M.M. Smith, R.S. Powell, M.R. Irving, and M.J.H. Sterling. Robust algorithm for state estimation in electrical networks. In *Generation, Transmission and Distribution, IEE Proceedings*, 138(4):283–288, 1991.

[130] Du Songhuai, Zhou Xinghua, Mo Lu, and Xue Hui. A novel nucleolus-based loss allocation method in bilateral electricity markets. In *Power Systems, IEEE Transactions on*, 21:28–33, 2006.

[131] J.C.S. Souza, A.M. Leite da Silva, and A.P. Alves de Silva. Online topology determination and bad data suppression in power system operation using artificial neural networks. In *Power Systems, IEEE Transactions on*, 13(3):796–803, 1998.

[132] A.K. Subramanian and J. Wilbur. Power system security functions of the energy control center at the Orange and Rockland utilities. In *Power Apparatus and Systems, IEEE Transactions on*, PAS - 102(12):3825 – 3833, December 1983.

[133] N. Vempati, I.W. Slutsker, and W.F. Tinney. Enhancement to Givens rotations for power system state estimation. In *Power Systems, IEEE Transactions on*, 6(2):842–849, 1991.

[134] K. O. Vogstad. Utilizing the complementary characteristics of wind power and hydropower through coordinated hydro production scheduling using EMPS model. In *Proceedings of Nordic Wind Energy Conference*, Trondheim, March 2008.

[135] K. O. Vogstad, H. Holttinen, A. Botterud, and J. O. G. Tande. System benefits of coordinating wind power and hydropower in a deregulated market. In *Proceedings of Wind Power for the 21st century*, Kasel, 2000.

[136] F.F. Wu. From congestion management, reliability to market power: Pay no congestion charge. In *Proceedings of Bulk Power System Dynamics and Control IV Conference (IREP)*, Cortina d'Ampezzo, August 2004.

[137] F.F. Wu and W.-H.E. Liu. Detection of topology errors by state estimation [power systems]. In *Power Systems, IEEE Transactions on*, 4(1):176–183, 1989.

[138] Bei Xu, C. Yuksel, A. Abur, and E. Akleman. 3D visualization of power system state estimation. In *Electrotechnical Conference, 2006. MELECON 2006. IEEE Mediterranean*, pages 943– 947, 2006.

[139] O. R. Saavedra Y. P. Molina, R. B. Prada. Allocation of transmission loss cost using Game theory. In *Power Tech Proceedings, 2007 IEEE Lausanne*, page 6 pp., 2007.

[140] P.D. Yehsakul and I. Dabbaghchi. A topology-based algorithm for tracking network connectivity. In *Power Systems, IEEE Transactions on*, 10(1):339–346, 1995.

[141] P. Zarco and A.G. Exposito. Power system parameter estimation: A survey. In *Power Systems, IEEE Transactions on*, 15(1):216–222, 2000.

[142] B.M. Zhang and K.L. Lo. A recursive measurement error estimation identification method for bad data analysis in power system state estimation. In *Power Systems, IEEE Transactions on*, 6(1):191–198, 1991.

[143] B.M. Zhang, S.Y. Wang, N.D. Xiang, M.Z. Zhu, Y.M. Deng, M.L. Xu, and J.M. Jiang. A state estimator with real-time implementation in the Northeast China power system. In *Advances in Power System Control, Operation and Management, 1991. APSCOM-91., 1991 International Conference on*, pages 560–565 vol.2, 1991.

[144] S. Zhong and A. Abur. Combined state estimation and measurement calibration. In *Power Systems, IEEE Transactions on*, 20(1):458–465, 2005.

[145] M. Zima, M. Zima-Bockarjova, and G. Andersson. Liberalization of the electricity sector in Switzerland. In *Proceedings, 8th International Conference on Control of Power Systems*, June 11-13, 2008.

[146] M. Zima and Ch. Rehtanz. Electric power transmission network state estimation. *http://www.freepatentsonline.com/EP1324455B1.html*, (EP1324455), February 2005.

Curriculum Vitae

EDUCATION

2005 - 2010	Swiss Federal Institute of Technology (ETH), Zurich, Switzerland; PhD studies in Electric Power Systems
2002 - 2007	Riga Technical university (RTU), Riga, Latvia; PhD studies in Electric Power Engineering
1996 - 2002	Riga Technical university, Riga, Latvia; BSc, Engineer and MSc studies in Electric Power Engineering
1999 (01-06)	Royal Institute of technology (KTH), Stockholm, Sweden; guest studies in Electrical Engineering

EXPERIENCE

2010 - present	ABB Corporate Research Center, Dättwil, Switzerland, Utility Solutions
2005 - 2010	ETH Zurich, Assistant at the Power Systems Laboratory;
2004 - 2005	ETH Zurich, guest student at Power Systems Laboratory, scolar of Swiss Federal Commission for scholarships for foreign students FCS;
2000 - 2004	Latvenergo (energy utility), Latvia, R&D planning engineer.